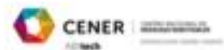
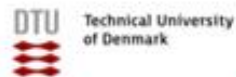




## OFFSHORE DEMONSTRATION BLADE

Final report



## Document History

Revision	Date	Prepared by	Checked by	Approved by	Revision History
0	28 Aug 2019	Contributing Partners	Paul Livingstone	ODB Partners	First Created

## Contents

Background.....	4
1 Work Package 1 – Project Management.....	5
1.1 Startup of project.....	5
1.2 Press release .....	5
1.3 Project Management.....	6
1.4 Project communication.....	6
2 Work Package 2 – Technology Maturing .....	8
2.1 Low drag vortex generator design .....	8
2.2 Erosion Metallic protective insert: FEM modelling & blade integration analysis.....	16
2.3 FEM structural model: X-Stiffener.....	22
2.4 Support for maturing the X-Stiffener .....	25
2.5 Erosion Sensor: modelling & testing .....	31
2.6 Cross Sectional Shear Distortion Sensor: modelling & testing .....	35
2.7 Advanced Hybrid Polymer (AHP) coating solution: modelling, polymer design and properties modulation .....	40
2.8 Process design for erosion coating.....	60
2.9 Retrofittable add-ons: modelling .....	62
3 Work Package 3 – Validation tests .....	66
3.1 Coating & metallic insert small scale tests: Material & subcomponent tests.....	66
3.2 Wind Tunnel Test for Low Drag VGs and Metallic Leading Edge Protection .....	68
3.3 Erosion tests.....	71
3.4 Blade shear deformation measurements.....	73
3.5 Planning and construction of test rigs .....	77
3.6 Sub-component testing of the X-Stiffener.....	78
4 Work Package 4 – Wind turbine integration .....	86
4.1 Manufacturing & installation instruction: Low drag vortex generators.....	86
4.2 Manufacturing & installation instruction: metallic protective insert kit .....	87
4.3 Manufacturing & installation instruction: Shear distortion measurement .....	87
4.4 Manufacturing & installation instruction: X-Stiffener .....	87
4.5 Manufacturing & installation instruction: Erosion Sensor.....	91
4.6 Manufacturing & installation instruction: Cross Sectional Shear Distortion Sensor for the X-stiffener (CSSDS) .....	92

---

4.7	Manufacturing & repair instruction: Aerox coating O&M solution .....	92
4.8	Manufacturing & work instruction: Aerox coating O&M solution .....	92
4.9	Manufacturing & installation instruction: Aerodynamic add-ons for Siemens Gamesa turbine .....	93
4.10	Installation procedure definition & review .....	94
5	Work Package 5 – Installation, service and decommissioning .....	95
5.1	Product installation: Low drag vortex generators .....	95
5.2	Product installation: metallic protective insert kit .....	95
5.3	Product installation: X-Stiffener .....	95
5.4	Product installation: Cross Sectional Shear Distortion Sensor for the X-Stiffener .....	95
5.5	Product installation: Erosion Sensor .....	97
5.6	Application of Aerox coating .....	97
5.7	Support to on-site installation activities .....	97
5.8	Installation of aerodynamic add-ons at the Siemens Gamesa turbine .....	98
5.9	Decommissioning of system .....	99
6	Work Package 6 – Data analysis .....	100
6.1	Power curve analyses .....	100
6.2	Blade shear distortion data analysis (pre X-stiffener installation) .....	107
6.3	Blade shear distortion data analysis (post X-stiffener installation) .....	111
6.4	Blade CSSDS data analysis .....	112
6.5	Erosion sensor measurement analyses .....	112
6.6	Coating performance analysis .....	112
6.7	Add-ons performance analysis .....	119
7	Work Package 7 – Dissemination and exploitation .....	121
7.1	Kick-off seminar .....	121
7.2	Mid-term Seminar and Report .....	121
7.3	Closing and final reporting to national funding bodies .....	121

Annex A – Aerox O&M Coating Solution Preparation Method **Fejl! Bogmærke er ikke defineret.**

## Background

---

The large-scale deployment of offshore wind provides economically viable, secure, low carbon energy sources that meet the EU's climate change targets for 2030.

The EU-wide target of 27% renewable contribution of final energy consumption in the EU as a whole by 2030 requires technological innovations capable of providing a significant breakthrough in lowering the Levelised Cost of Energy (LCOE).

In offshore wind, Operations and Maintenance (O&M) costs represent 16-23% of LCOE (sources: Tavner, Offshore Wind Turbine Reliability; & BVG Associates). Rotor O&M represents a large part of this cost, specifically issues around blade erosion and blade structural integrity. Furthermore, rotor aerodynamic performance is a key component to reduce LCOE, with an estimated 1% increase in Annual Energy Production (AEP) equating to 1% reduction in LCOE.

The Offshore Demonstration Blade (ODB) project aims to reduce the LCOE of offshore wind by up to 4.7% by demonstrating a set of blade technologies aimed at increasing the rotor energy performance and reducing O&M costs.

The ODB project will demonstrate the following novel technologies:

- aerodynamic low drag add-ons;
- leading edge insert for erosion protection;
- structural stiffener to prevent damage due to shear distortion;
- fibre optic sensors to monitor and validate structural stiffener performance;
- fibre optic sensors to detect leading edge erosion and top coating performance;
- High-performance hybrid coating for leading edge protection;
- Aerodynamic next-generation blade add-ons that are 100% retrofittable increase AEP (decreasing LCOE).

**For ease of cross-reference this Final Report has been structured into sections that correspond to the tasks identified in the original bid document, with leaders of each sub section identified.**

# 1 Work Package 1 – Project Management

## 1.1 Startup of project

Leader: ODSL

The Offshore Demonstration Blade (“ODB”) project is an international collaboration aimed at demonstrating seven novel blade retrofit technologies that have the potential to reduce the Levelised Cost of Energy (“LCOE”) of offshore wind by up to 4.7%.

The ODB project is supported by funding from the DemoWind 2 programme, a European Research Area Network (ERA-NET) COFUND programme. DemoWind 2 is an ERA-NET Cofund Action programme supported by the European Union’s Horizon 2020 Framework Programme. The DemoWind 2 programme aims to facilitate the cost reduction of innovative technologies to accelerate their commercial deployment by connecting European offshore wind demonstration opportunities and supporting knowledge exchange and collaborative working between existing and new European partnerships.

The ODB project is being delivered by a consortium of ten project partners from four European countries. The ODB consortium is formed of the following organisations:

- Aerox Advanced Polymers (“AEROX”)
- Bladena ApS
- Centro Nacional De Energias Renovables (“CENER”)
- Universidad CEU Cardenal Herrera (“CEU”)
- Dansk IngeniørService A/S (“DIS”)
- Technical University of Denmark (“DTU”)
- Offshore Renewable Energy Catapult Limited (“ODSL”)
- Siemens Gamesa Renewable Energy
- TNO
- Total Wind

## 1.2 Press release

Leader: DIS

Press releases for national and international media was prepared by DIS and ODSL for approval by the project partners as communicable project milestones are reached. A press release announcing the commencement of the ODB project was issued on 8<sup>th</sup> November 2017 detailing the purpose and goals of the project. This was issued some 10 months after the formal project kick off meeting, with the delay being due to delays in the Spanish partners receiving confirmation of their funding from their national authorities.

### 1.3 Project Management

Leader: ODSL

The ODB consortium formally came into being on 10<sup>th</sup> July 2016 with the signing of the ODB Consortium Agreement by all ten partners in the project. The Consortium Agreement was negotiated and agreed between all partners and was based upon DESCA - Horizon 2020 Model Consortium Agreement (Version 1.2, March 2016) with project specific amendments. The two-year ODB project will be coordinated by the ODSL with DIS leading on project communication and dissemination.

Frequent progress meetings have been held with all partners to review the consortium action list, provide progress updates to all partners, coordinate activities between different technologies, and to ensure all partners are aware of upcoming key dates.

The General Assembly is the decision-making body of the consortium with powers defined in the consortium agreement. It meets at least twice a year with the 2017 General Assemblies held at partner's facilities in Denmark and in the UK. The first General Assembly of 2018 was held in March at the CEU facility in Valencia, Spain. The final face to face project meeting was held in June 2019 with all project partners present. This meeting coincided with the project's Final Dissemination Event.

### 1.4 Project communication

Leader: DIS

The Communication Plan sets out the communications management principles for the ODB project. The plan covers key messages, communication responsibilities and lines of communication between all project partners.

DIS is responsible for Work Package 7 – Dissemination and Exploitation – and will therefore have the lead on coordinating external project communication activities. However, all communications activity must be approved by ODB partners. Also, all 10 project partners are committed to maximising the potential impact of disseminating the outputs of the project to relevant stakeholders.

The Plan sets out the key messages, activities and timetable for external communication in relation to project communications. The outputs from the Plan will communicate the successful demonstration of the novel blade technologies that have the potential to lower the Levelised Cost of Energy (LCOE) by up to 4.7%. The plan is a live document and as such project partners will update DIS on external messaging references and opportunities.

The objectives of all communication activities should be:

- To demonstrate that the novel technologies demonstrated represent a step change in improving rotor energy performance and reducing O&M costs.
- To demonstrate that the technology has been successfully tested and if deployed commercially has the potential to reduce the LCOE of European offshore wind by 4.7%.

The communication deliverables are:

Summary of Deliverables			
Deliverable number	Deliverable name	Work package number	Lead Partner
D1.2	Final version project & communication plan	WP1	ODSL
D7.2	Midterm report	WP7	DIS
D7.3	Final Project report	WP7	DIS
	Press Release		DIS
	Website launch		DIS
	Exhibition		DIS
	Workshop		DIS

*Table 1 - Communications Deliverables*

The main target audiences for communications activities are detailed in the table below.

Target group	Description
Owner/Operators, Offshore Wind Supply Chain	Offshore wind project developers, Original equipment manufacturers
National and EU funding bodies	National funding bodies and EU commission
Public authorities	National & EU Authorities, especially those responsible for site authorization
Investors	Project financiers, insurance companies, institutional investors
Associations	Wind Energy associations at national and EU level Environmental associations
Medias	National and international medias, trade press

*Table 2 - Communications Target Audiences*

All key messages are target to the audiences/target groups, with an objective of the message.

Project outputs will be shared through a variety of communication channels.

## 2 Work Package 2 – Technology Maturing

### 2.1 Low drag vortex generator design

Leader: CENER

Important Note:

-----

CENER received the confirmation from MINECO (Spanish national funding body) about the funding to be received by the end of October 2017. In addition, the budget was considerably reduced from the budget requested by CENER.

For CENER, MINECO does not fund researcher's personnel costs, only the ones derived from new hiring, so a new researcher joined CENER team on November 29<sup>th</sup> 2017.

Even though the budget, time and resources were reduced, CENER has advanced in the design of the low drag vortex generator.

-----

Vortex generators are devices that are added to the wind turbine blades in order to delay separation. They work producing vortices that mix the high energy upper parts of the boundary layer with the lower parts, re-energizing the boundary layer and delaying separation.

The conventional vortex generators (rectangular or delta shaped) are very useful delaying separation but they produce a drag penalty to the blades. The objective of this project is to design low drag vortex generators that add a drag to the blade surface smaller than the one added by conventional vortex generators.

The activities performed are summarized as:

1. CFD computations of conventional vortex generators mounted on a flat plate and comparison with experiments from previous projects to validate the tools.
2. CFD computations of new shaped vortex generators on a flat plate.
3. CFD computations of vortex generators (conventional and designed) mounted in airfoil sections.
4. CFD computations of the Levenmouth wind turbine (3D) in order to understand how the flow behaves in the blade and how it could be improved with the use of vortex generators.

These activities are described in detail being in the sections below, with due consideration to confidentiality issues.

#### 2.1.1 CFD computations of conventional vortex generators

Conventional vortex generators have been computed using the open source CFD code OpenFoam. The version used is 4.0. The conventional vortex generators have a height of 5 mm and a length of 12.5 mm in order to be compared with the experimental campaign performed

in the AVATAR project. Meshes modelling a pair of rectangular VGs are calculated, they are shown below in Figure 1.

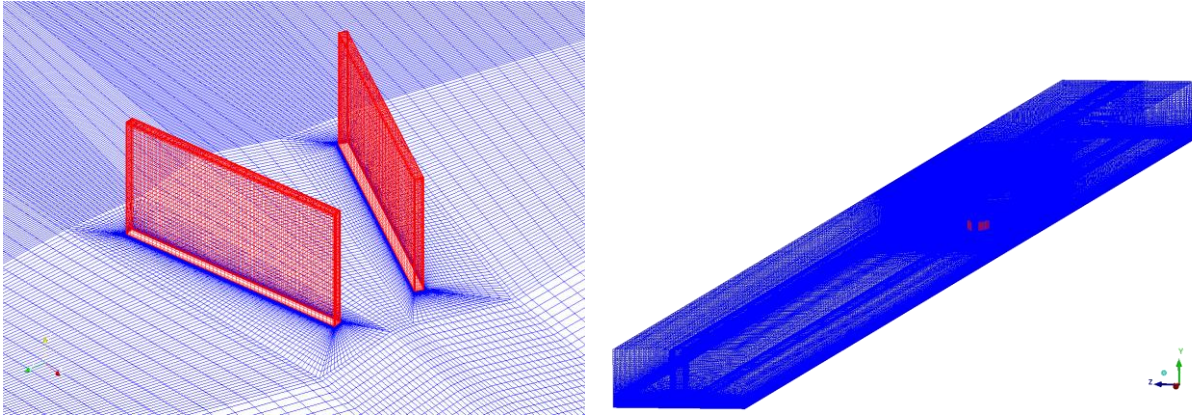


*Figure 1- Mesh for the vortex generators pair. 12 million cells.*

The meshes have 12 million nodes, and were calculated using the KOmega SST model for a Reynolds number of 5100.

The velocity profiles for this case are plotted in the some lines located in different planes after the VG pair and compared with the experimental campaign from AVATAR (Figure 2). The results were satisfactory and the CFD produce good comparisons.

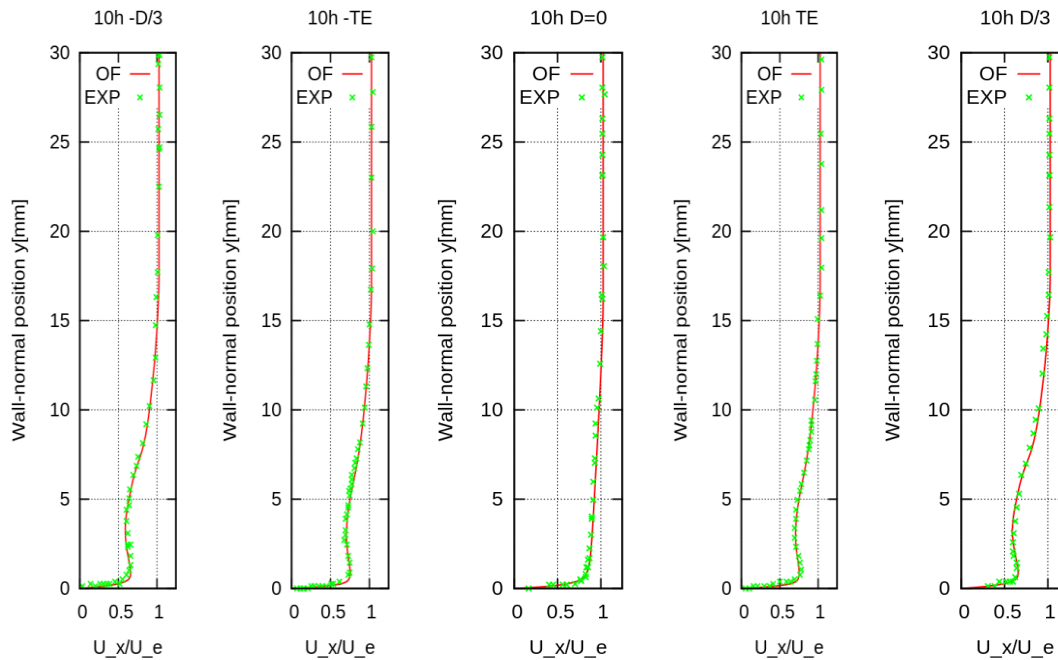


Figure 2 -Velocity profiles in the plane 10h after the vortex generator pair in the middle of the vortex generators, in the trailing edge of each one TE, and in one third of the vortex generator trailing edge separation (0mm, 6.25mm and 10 mm respectively)

The planes are shown in Figure 3 and as can be seen the vortex are fully developed right after the VG location. Some other results are obtained, such as peak vorticity evolution, vortex lateral and vertical paths and will be included in future reports.

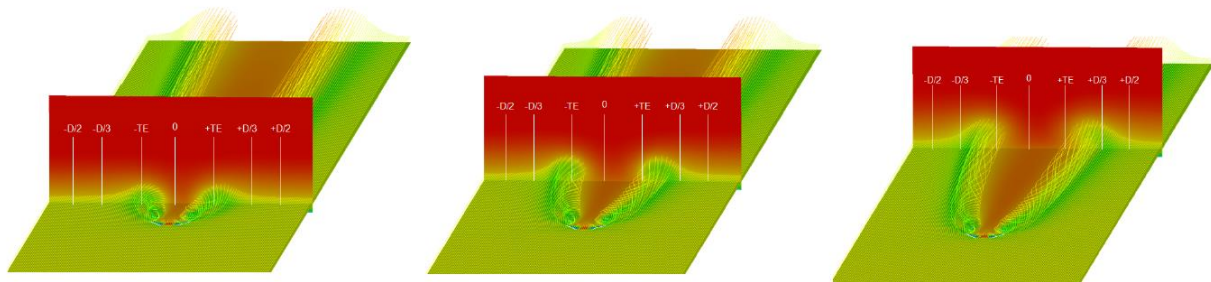


Figure 3 - Flow field in three planes after the vortex generators (planes at 10h-25h & 50h being h the vortex generator height)

### 2.1.2 Design of low drag vortex generators

In the ODB project CENER designed Low drag vortex generators. The main objective of the designs was to reduce the drag added to the surface when the vortex generators were installed. In addition an increase in the efficiency of the blade section was also a requirement for the designs.

Several vortex generators shapes were designed and computed, the following figure show two examples of their shape.

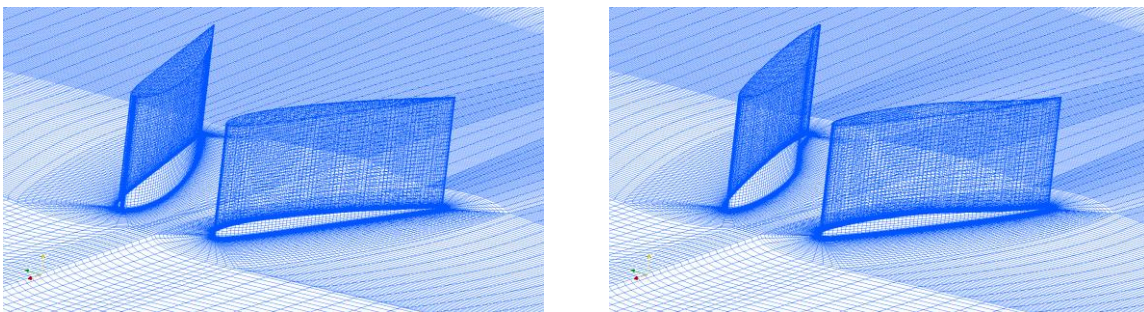
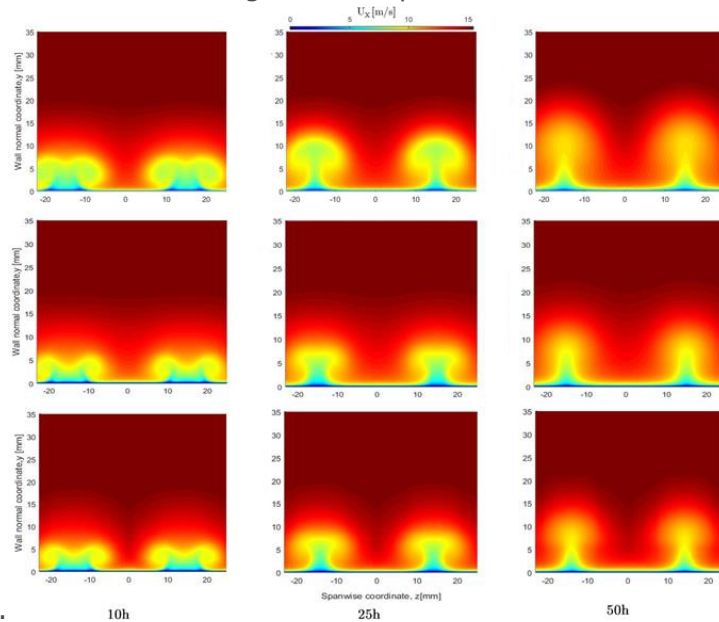


Figure . Vortex generators shapes designed during the ODB project.

These VG shapes are compared in order to evaluate the vortex generator cross section effect over the production of vortices. The following figures show velocity contours for three planes after the vortex generator pair for three different geometries: rectangular, delta and airfoil

shaped. As can be seen the different vortex generators produce different vortices and effects



over the flow.

*Figure 4 - Velocity fields in three planes right after a vortex generators mounted on a flat plate (10h, 25h and 50h) for three different vortex generator shapes (top rectangular, middle delta and low airfoil shaped)*

Several vortex generators shapes were compared and finally one was selected to be the most suitable to be installed in the 7 MW Levenmouth wind turbine. The VG shape is based on a symmetric airfoil. This VG was 3D printed to be tested in the wind tunnel and in the wind turbine. CENER created the manufacturing plan of the VGs to be sent to the manufacturer. The vortex generator shape is shown in the following figure.

Vortex generators geometry. Designed by CENER in the ODB project.

### 2.1.3 Within the project, CENER also defined the support plate for the VG pair to be installed both in the wind turbine and the wind tunnel. CFD of vortex generators mounted in airfoil sections

In the first project period, CFD computations of conventional vortex generators mounted on airfoils are performed. The objective of these computations is to evaluate how the different shaped vortex generators contribute to delay separation.

The first computations are being performed on conventional VGs (rectangular and delta shaped) mounted in a DU97W300 airfoil to be compared with the experiments from the AVATAR project in which CENER participated.

In this case the meshes model only a pair of VGs, have a total number of cells of 12 million and are computed using the KOmega SST turbulence model. The meshes and some visualization of the flow are shown in the Figure 5 and Figure 6.

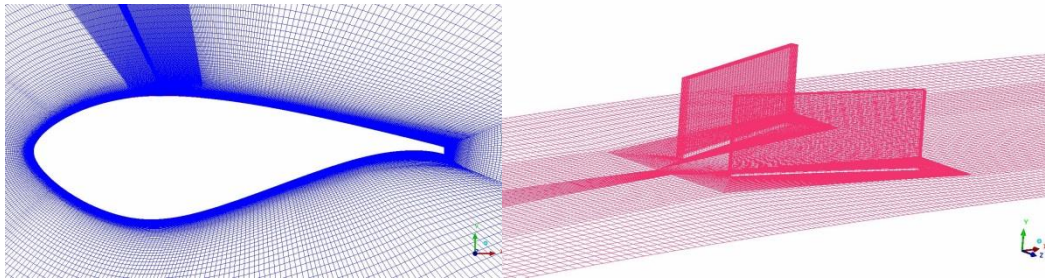


Figure 5 - Mesh used for the computations of the vortex generators mounted in the DU97W300 airfoil.

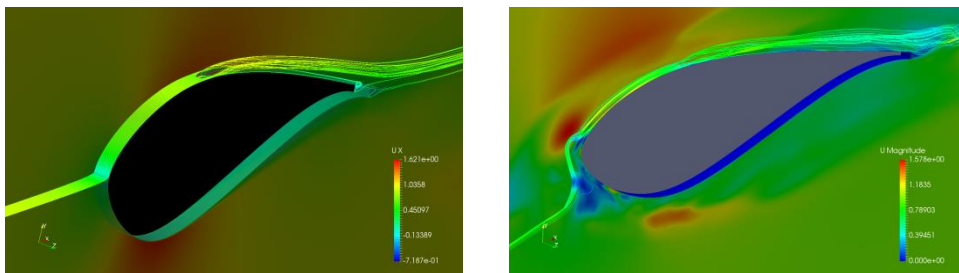


Figure 6 - DU97W300 airfoil flow visualization with a rectangular pair of VGs mounted. Left AOA=0° and right AOA=12°.

#### 2.1.4 CFD computations on the Levenmouth Blade

During the first period of the project, CENER worked in creating the mesh of the Levenmouth Wind Turbine blade in order to perform 3D CFD computations to evaluate the flow in the blade and the best areas to place the vortex generators. Due to confidentiality reasons (NDA between ODSL and CENER) images of the blade mesh are not provided.

In addition, pseudo 2D computations of blade sections with the vortex generators integrated were done to evaluate computationally the effect of using this type of add-ons. The computations also included the leading edge protection system with the aim of evaluate the capability of the VGs of mitigate its aerodynamic effect.

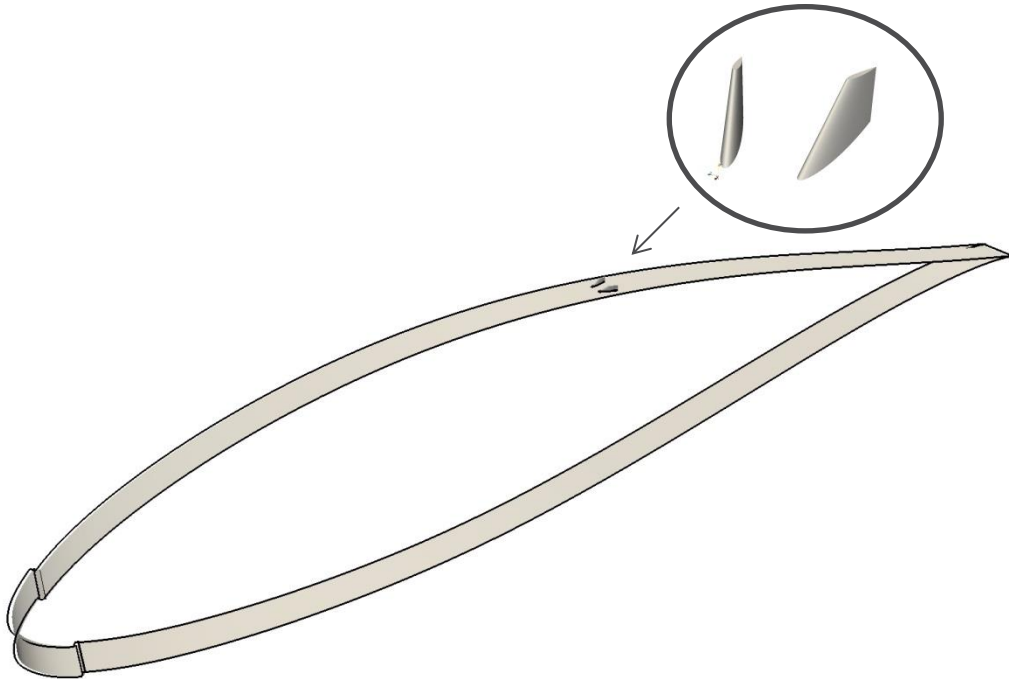
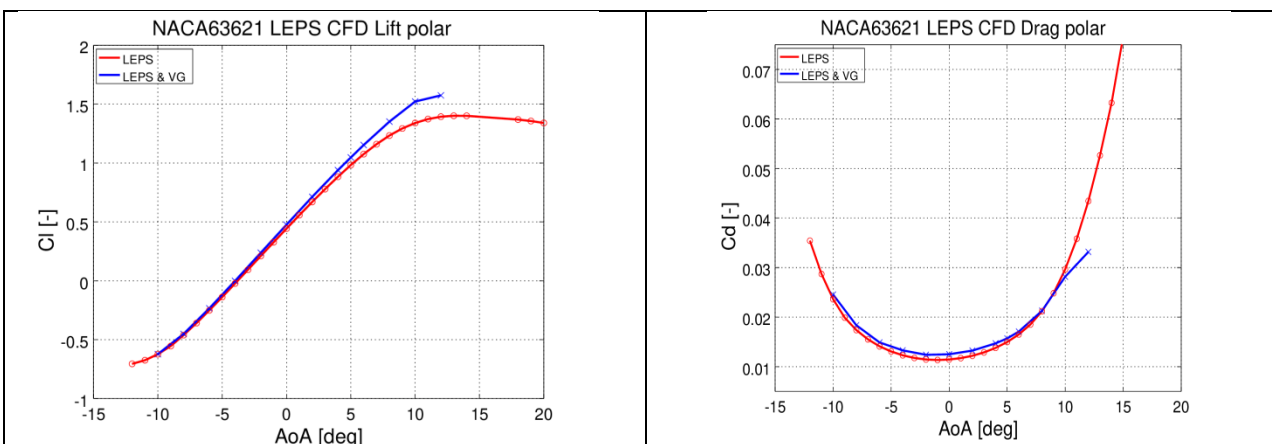


Figure 7 – Blade section studied with the leading edge erosion protections system and the low drag vortex generators.

The aerodynamic polar curves computed using OpenFoam v4 are shown next. The comparisons show the flow behaviour with leading edge protection system with and without VGs. When the VGs are included both lift and efficiency (lift divided by drag) increase and so the vortex generators mitigate the aerodynamic problems derived from the use of a leading edge protection system.



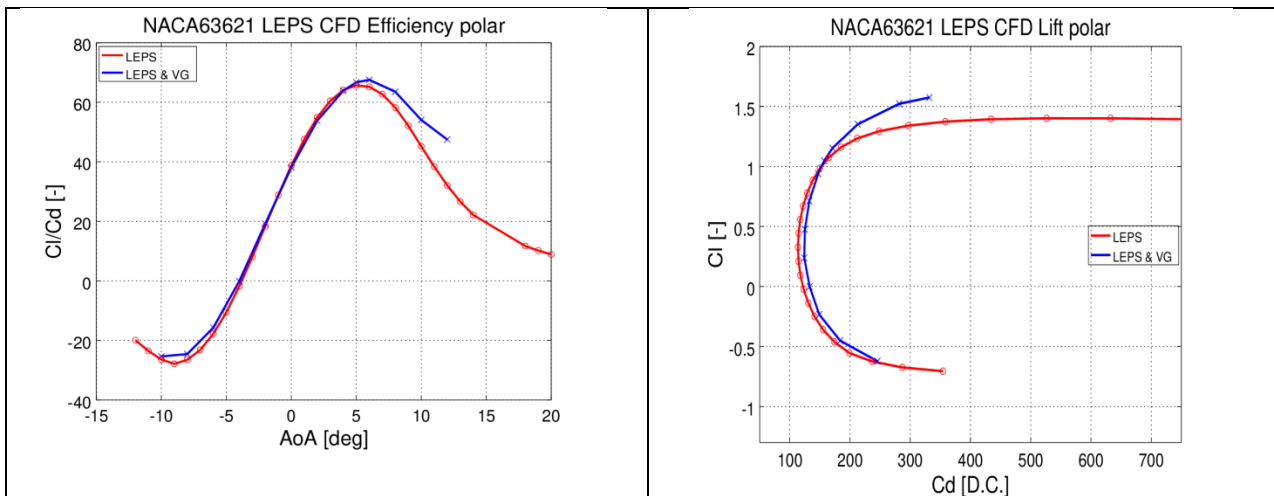


Figure 8 – CFD simulations of the Levenmouth wind turbine section with the leading edge protection system with and without VGs.

Some figures with flow visualization of the calculations are shown next:

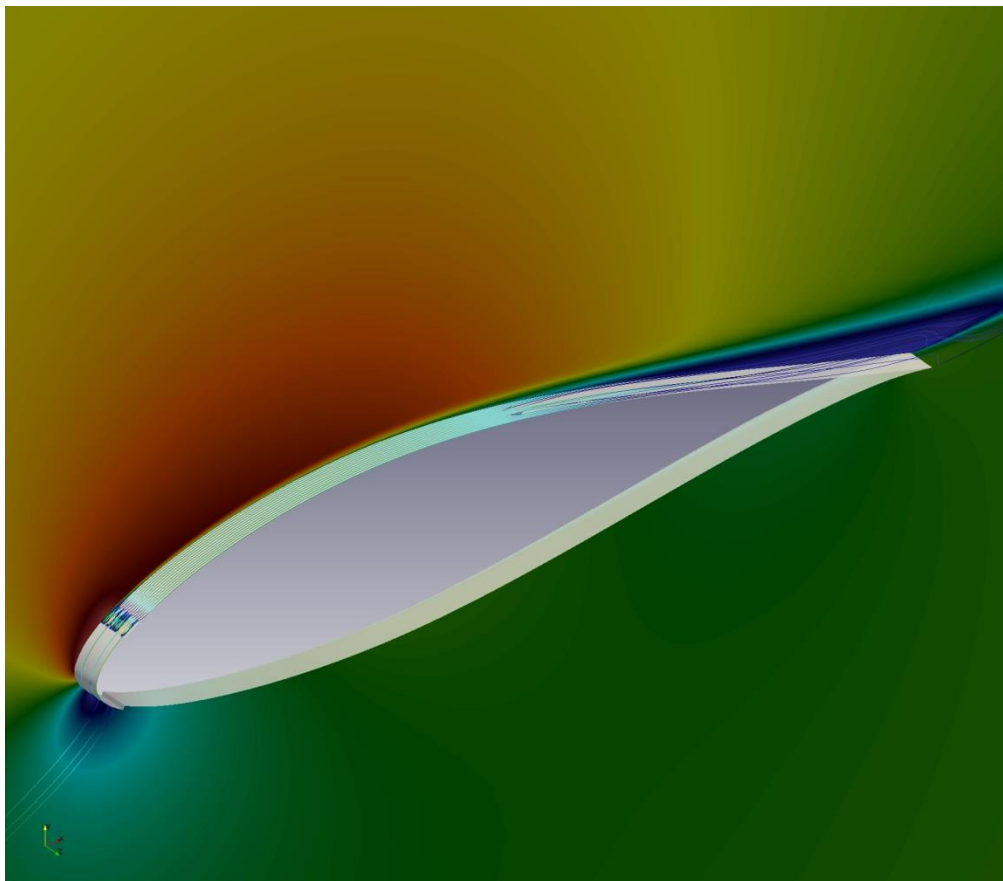


Figure 9 – Flow visualization from computations in the blade section with LEPS and VGs.

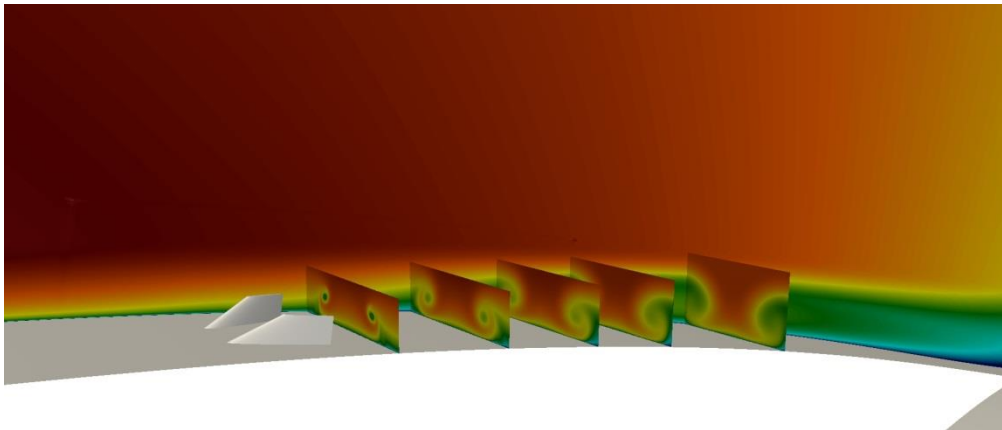


Figure 10 – Vortices after the VGs in the computations from the blade section with LEPS and VGs.

## 2.2 Erosion Metallic protective insert: FEM modelling & blade integration analysis

Leader: ODSL

### 2.2.1 Introduction

The current three bladed, upwind design of wind turbine has evolved to suit its environment. Onshore, the tip speed of turbines is limited by the amount of noise the turbine can generate, and turbines are considered to be more visually appealing if they rotate more slowly. This has driven the adoption of three bladed turbines as the dominant turbine type used by the industry. There are also fatigue issues which require the use of a teeter-hub to implement two-bladed downwind turbines but overall these do not add to the cost of energy.

Onshore, this combination of factors has meant that leading edge erosion has not been a huge problem for the industry because it only starts to be an issue at higher tip speeds. Offshore, with the noise and aesthetic considerations removed, erosion becomes the limiting factor on tip speed. There are considerable benefits to moving to higher tip speeds – two bladed turbines are more viable, the blades will become more slender (thus reducing the amount of material required in their construction) and the higher rotational speed means that the turbine torque is lower, which reduces the cost of both the drivetrain and the structural elements of the turbine. However, erosion currently limits tip speed to around 90m/s. In the helicopter industry, tip speeds of over 200m/s are not uncommon, and the problem of erosion has been addressed with the use of extremely hard electroformed nickel strips which protect the leading edge.

This work package aims to demonstrate that the use of electroformed nickel plates is feasible for wind turbine leading edge protection. The integration method for adding the metallic leading-edge erosion protection tiles has followed a simulation based approach up until the time of writing. The tiles will be adhesively bonded onto the leading edge, with an additional mechanical fixing to act as a redundant method of attaching the tiles to the blade.

The following elements have been considered during the development of the leading-edge erosion protection system:

- Business case and potential cost savings arising from increasing blade tip speed
- Tile geometry requirements
- Adhesive stresses under extreme blade loads for baseline geometry
- Clashing of tiles under extreme blade loading
- Fatigue of nickel tiles
- Effect of the tiles on blade loading
- Loading of mechanical fixing
- Design of mechanical fixing
- Design of adhesive test rig
- Integration of tiles into the turbine lightning system

All of these steps are considered in more detail in the project deliverables.

### 2.2.2 Business Case and Potential Cost Savings from Increased Tip Speed

Leading edge erosion is responsible for significant energy yield losses in offshore wind. State of the art PU coatings require typically maintenance every 1-4 years. According to the analysis provided below, the Levelised Cost of Erosion for a 10MW wind turbine would be in the range of 2% - 3% of the NPV of the energy yield, considering current operations & maintenance strategy (periodic repairs on wind turbine blades). It is estimated that a solution providing lifetime erosion protection implemented in a 10MW wind turbine would reduce the levelised cost of erosion compared to the current operation & maintenance strategy from 3% down to 1%. This means a 2% reduction in the cost of energy.

In addition to the O&M cost savings that can be obtained using current blade designs, if the strips allow substantially higher tip speeds to be achieved then additional cost savings can be realised.

If the limitation imposed by leading edge erosion was removed and tip speeds were increased, then considerable reductions in blade mass could be achieved because of the resultant decrease in blade planform area. Using the blade of the ORE Catapult 7MW research turbine at Levenmouth as a baseline, the estimated blade mass could be reduced by 6Te (a 17% reduction) and the nacelle mass could be reduced by 90Te (a 22% reduction). Assuming that cost is approximately proportional to mass these savings could amount to a 4% reduction in the levelised cost of energy.

It was therefore concluded that the cost reductions from very high tip speeds were worth pursuing further.

### 2.2.3 Tile Geometry Requirements

The tile geometry was chosen on the basis of the typical chordwise extent of existing leading-edge erosion protection. The spanwise length of the tiles was chosen on the basis that they would be installed by rope access and it should therefore be possible to hold and manipulate the tiles with only one hand (a 500mm length was chosen as a compromise between ease of handling and number of tiles). Finally, the thickness of the tiles was chosen to be similar to what is used on helicopters as this is a proven application (which is towards the thinner end of

what is possible using the electroforming process, leading to an additional benefit of lower adhesive stresses). This led to the following tile parameters:

- The tiles extend about 3% of the chord length on both pressure and suction side
- The tiles are 500mm in length
- The tiles are at least 0.3mm thick

#### 2.2.4 Blade Displacement Load Cases

It was determined that the stress in the adhesive would be affected by the following parameters:

1. Tile geometry and stiffness (thickness, chordwise extent on each side of the blade, spanwise length, and Young's Modulus)
2. Blade bending stiffness and axial stiffness
3. Blade bending and axial loading
4. Distance of the leading edge from the blade neutral axis

The tile geometry can be easily generated for any section of the blade, the blade stiffness properties and distance of the leading edge from the neutral axis are available in the Bladed model of the turbine, and the extreme blade loads at each section are available from the blade design report. A parametric FE model of the blade was created which aims to recreate the curvature of the blade and the strain at the leading edge under extreme loads to check the Von Mises stress in the adhesive.

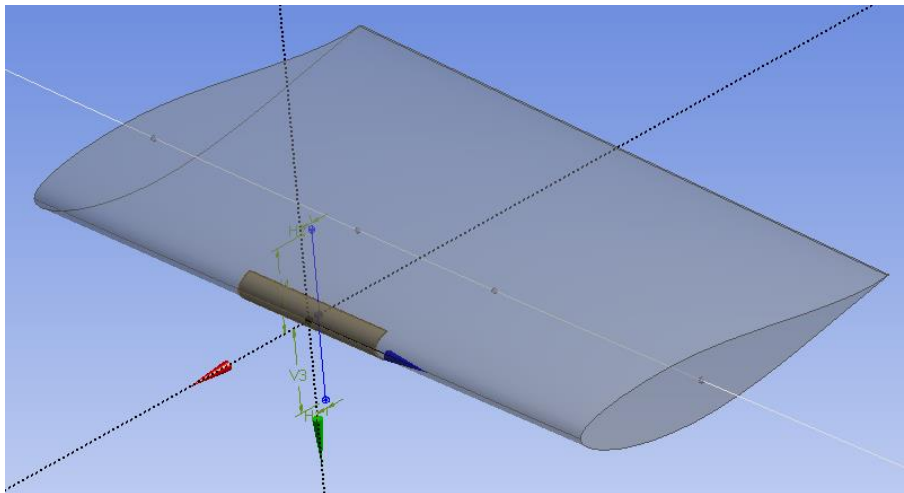


*Figure 11 - Parametric FE model of blade/adhesive/tile system*

This model determined that the section at 77m from the root would be the most critical section. However, there is an existing lightning receptor at 74m from the root, and this section was almost as critical as the 77m section in terms of adhesive stress, so it was chosen as the section at which tiles would be installed.

### 2.2.5 Clashing of tiles under extreme loading

Clashing of the tiles under extreme loading was checked using a CAD model of the blade, and it was concluded that a strip separation of 2mm would be sufficient to prevent clashing.

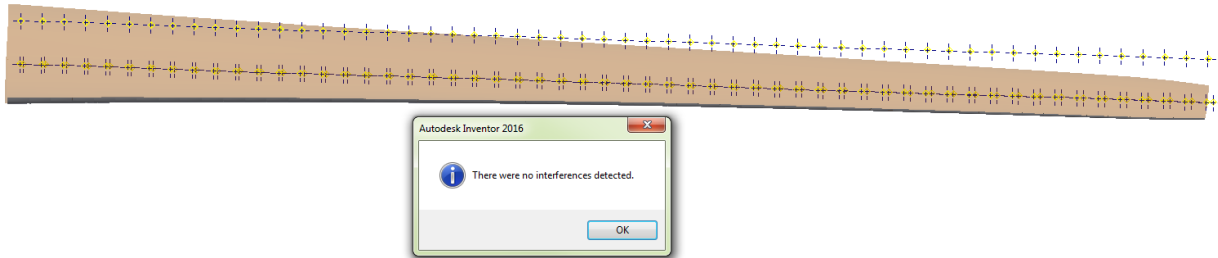


Figure 12 - Clash detection under the critical edge max load case

### 2.2.6 Choice of Adhesive

The leading-edge erosion protection plates will be installed at height, which rules out the use of adhesives which are reliant on hot pressure bonding (which is how the erosion shields are bonded to helicopter blades). Cold bonded adhesives were then selected based on their datasheet bond strength to fibre reinforced plastic and steel (which was considered to have similar bonding properties to nickel), their weather resistance and the suitability of the application process. After this qualification stage, 3M DP490 was found to be the best choice and using the datasheet tensile properties it was checked in the model described above.

### 2.2.7 Aerodynamic Analysis

The effect of the nickel plates on turbine performance was assessed using the wind turbine simulation tool Bladed. Aerodynamic polars were generated for the case where the nickel strips are attached to the leading edge of the blade using FLUENT – a comparison between the unmodified and modified polars is shown in Figure 13.

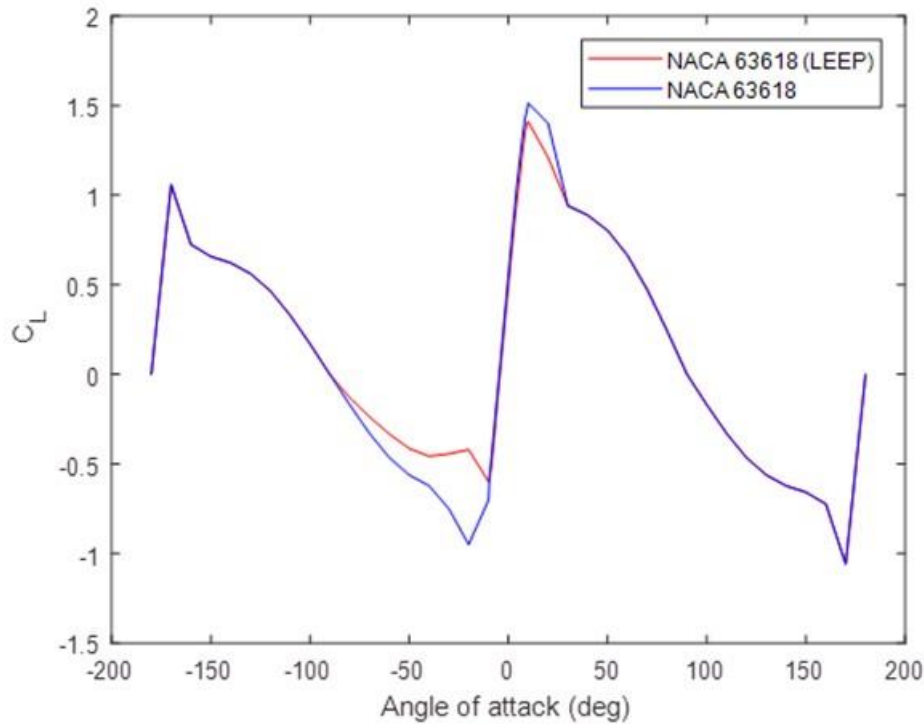
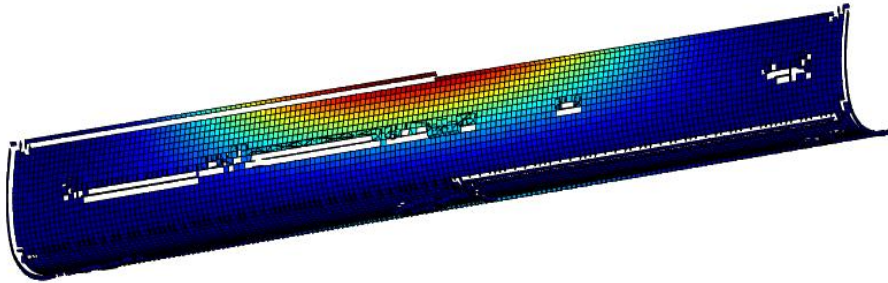


Figure 13 - Plot of lift coefficient for unmodified and modified aerofoils

These were then applied to the blade model in Bladed between the 73.5m station and the 74.5m station and the loads were compared to those with an unmodified blade. It was found that the blade root extreme and fatigue loads were not greatly affected, and neither were the tower top and bottom extreme loads. However, the tower top and bottom design equivalent loads increased. This will be further investigated.

### 2.2.8 Fatigue of Nickel Plates

Using the parametric model described earlier, the strain in the z (axial) direction of the nickel strip was assessed due to a unit  $M_x$ ,  $M_y$  and  $F_z$  load was assessed. The axial strain due to any combination of these loads can then be obtained by superposition. ORE Catapult has in-house wind turbine blade fatigue analysis software certified by DNV-GL, and this was used to do a fatigue analysis on the nickel strip.



*Figure 14 - Plot of Palmgren-Miner damage sum at each point on critical tile*

Figure 14 shows a map of where the worst damage occurred on the critical tile. At the most damaged location, the maximum strain cycle amplitude was lower than the endurance limit of the worst performing nickel found in the literature by a factor of 3, so it was concluded that fatigue is unlikely to be a problem for the strips.

### 2.2.9 Design of Redundant Mechanical Fixing

The extreme inertial loading generated by a tile at the tip were calculated using Bladed, and the extreme aerodynamic loading was calculated using FLUENT at 0° and 24° angles of attack. The redundant mechanical fixing will consist of a 'Bighead' stud bonded onto the blade surface (with the bond isolated from the main bond to prevent crack propagation between the two). Small scale testing on this adhesive joint is scheduled to be performed in the next quarter.

### 2.2.10 Design of Flexural Test Rig

The adhesive modelling performed during this feasibility study was rather simplistic, and was aimed at comparing adhesives against each other in terms of suitability rather than stating with any degree of certainty that the adhesive would survive in the field. The reason for this is the complex loading regime that the tiles experience – the state of being bent about both axes means that the adhesive experiences a combination of Mode 1, Mode 2 and Mode 3 stressing (see Figure 15). The correct way to analyse this system would be to use a fracture mechanics approach with cohesive zone elements representing the nickel-adhesive and adhesive-blade interfaces. However, these models require a substantial amount of characterisation data, which is not available for this specific combination of materials.

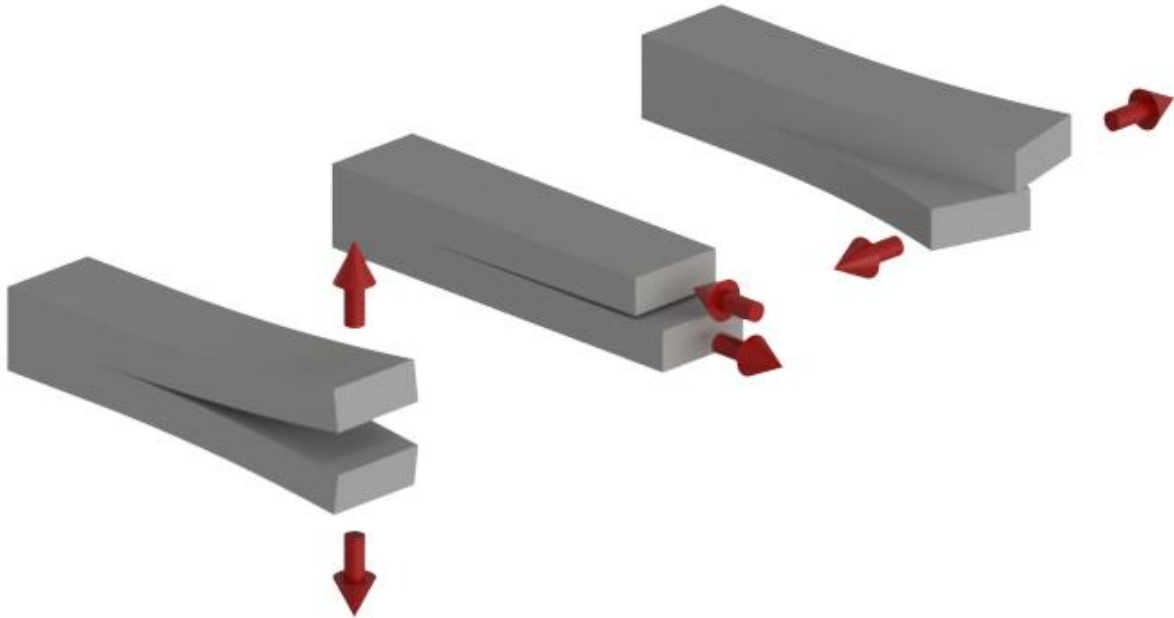


*Figure 15 - Modes of crack growth - Mode 1, Mode 2 and Mode 3*

In order to reduce risk, a simple test rig has been created which can recreate the curvature and strain conditions experienced on the blade on simple tubular specimens with a similar radius to the leading edge at the critical section. The design and manufacture of this test rig is detailed in the report on Milestone 1.

## 2.3 FEM structural model: X-Stiffener

Leader: Bladena

The FEM blade model of the Levenmouth turbine with 83.5m blades was developed based on information received from Catapult. During a two-day workshop at Catapult facilities in Blyth, relevant information regarding the 83.5m blade was shared with Bladena.

The developed FEM model incorporates the global geometric blade characteristics such as length, max. chord position and size, relative thicknesses of the aerodynamic profiles, shear webs position in the blade relative to the trailing edge, etc. Local characteristics such as layup thickness and composition in critical areas such as the trailing edge in max chord region are as well incorporated.

A fine mesh in critical areas ensures the validity of the obtained deformations. The FEM blade model was used to simulate different expected loading scenarios during normal operation conditions. Focus is put on understanding the cross-sectional shear distortion blade behaviour.

Cross sectional shear distortion is post-processed for both main box of the blade as well as the rear box. Figure 16 illustrates the nomenclature used in post-processing.

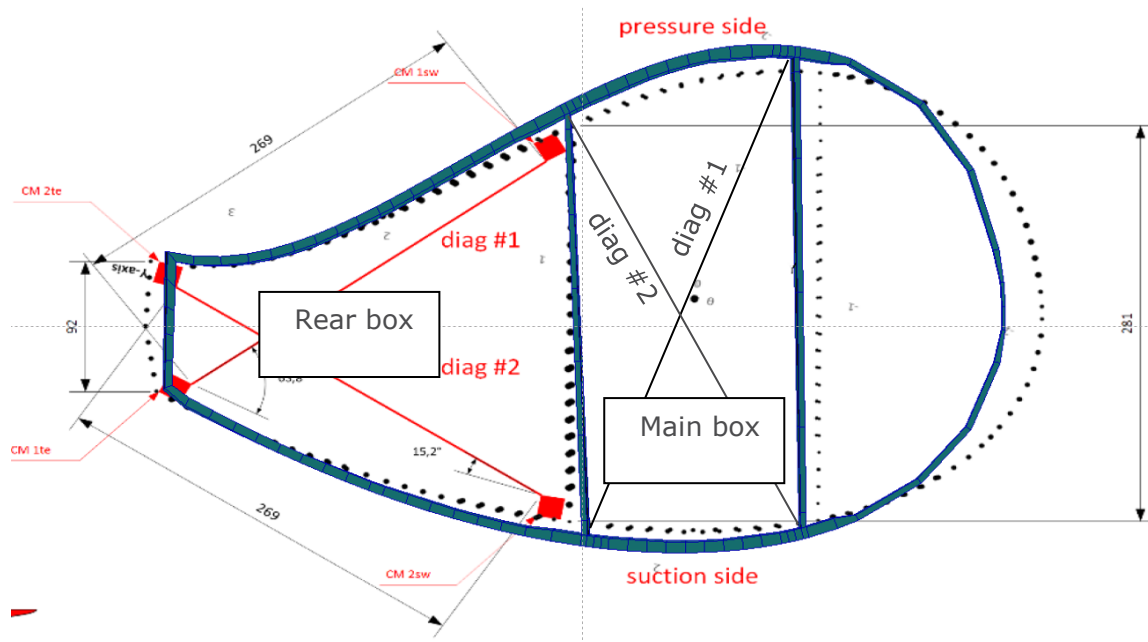


Figure 16: 12m radial position cross section with details on the main and rear boxes

Cross sectional shear distortion is shown in Figure 17 and Figure 18.

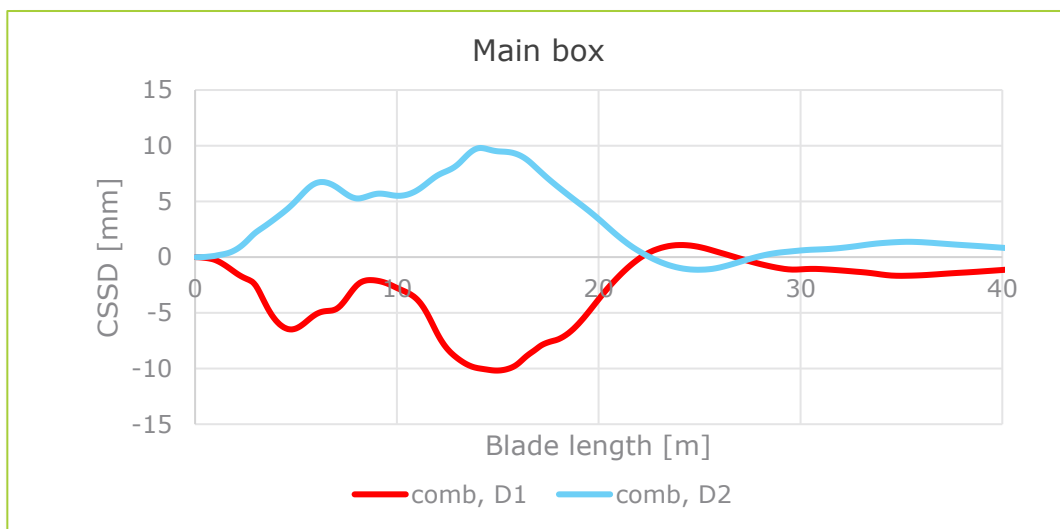


Figure 17: Cross-sectional Shear Distortion in the main box.



Figure 18: Cross-sectional Shear Distortion in the rear box

This information is later used when the positioning of the X-Stiffener in the blade is decided.

The X-Stiffener is modelled as a bar finite element with properties allowing only tension to be taken into consideration. The bar2 element is fixed in the blade using an RBE3 MPC, thus distributing the load on an area similar to the attached corner brackets in the real blade.

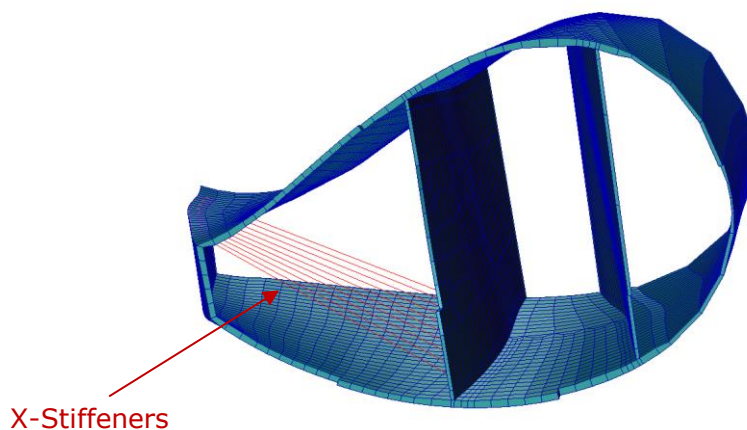


Figure 19: Modelling of X-Stiffeners in the blade

The impact of the X-Stiffener is assessed by comparing the reduction of the local deformation (cross sectional shear distortion) before and after the X-Stiffener was installed.

In Figure 20 cross sectional shear distortion is post processed in the model with the X-Stiffener and the diagonal 2 is used as a comparison base.

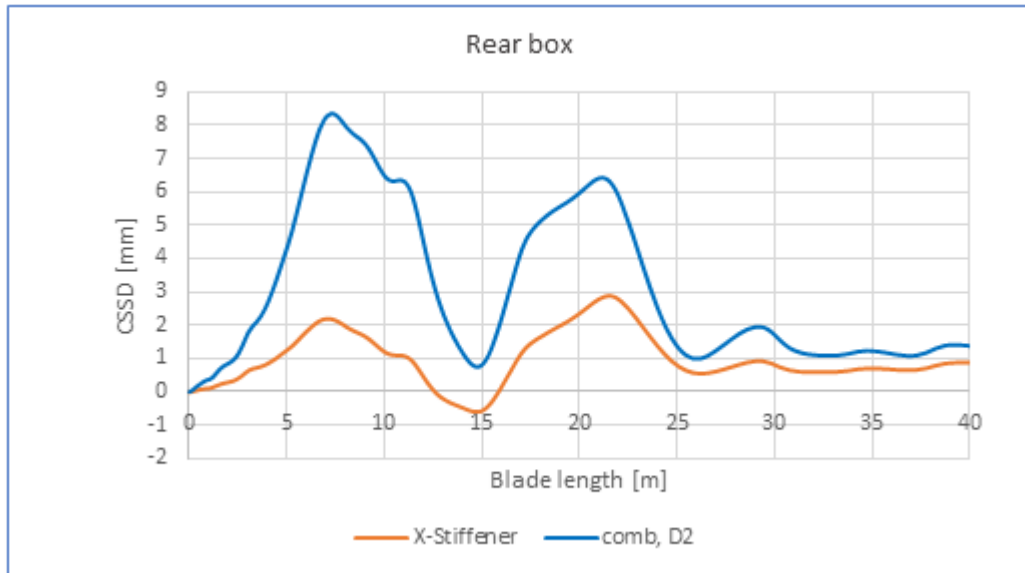


Figure 20: Comparison of cross sectional shear distortion. With red with X-Stiffener; with blue without.

The impact of introducing a connection between the two opposite corners is noted. When the X-Stiffener is used, the cross sectional shear distortion magnitude is reduced with more than 70%.

•

## 2.4 Support for maturing the X-Stiffener

Leader: Bladena

Initial research showed that a simple maturing of the X-Stiffener™ product was insufficient and therefore much more extensive product development have been carried out by DIS, through management and support from Bladena. In **Fejl! Henvisningskilde ikke fundet.** you see the old X-Stiffener™ that was designed for the geometry of an SSP34m blade (Box spar design), but due to the complex geometry of the Levenmouth 83,5m turbine the design was changed to accommodate this.

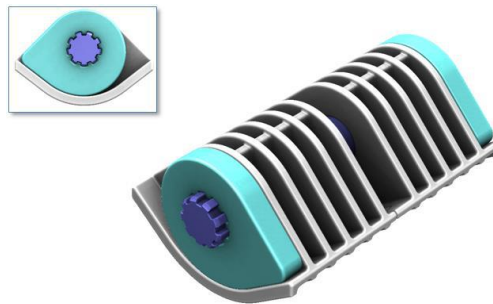


Figure 21 – Old X-Stiffener™ design before project start

In **Fejl! Henvisningskilde ikke fundet.** is shown a new adaptable X-Stiffener™ design that has been improved in the way that it can accommodate the different corner types of the Levenmouth turbine, with varying angles and radius including the high force estimations from task 2.3.



Figure 22 – New adaptable X-Stiffener™ design

The new design as undertaken different load analysis etc. and materials are currently being tested in combination with the initially chosen adhesive to finalize the size of the corner mounts. Next step is to get correct prototypes made of the corner mount to test the attachment of the full bracket into a constructed test piece simulating the actual blade geometry. These test pieces are not available from any other blades and are therefore to be manufactured, this will be done by the beginning of 2018.

Initial testing of the new corner mounts shown in **Fejl! Henvisningskilde ikke fundet.** resulted in high peeling stresses in the Bondline due to high loads experienced during operation of the turbine. Therefore, the development process needed to be revised and a change in materials and design needed to be conducted. In the beginning of 2018, materials were investigated in collaboration with DIS and SIKA DANMARK A/S to test the adhesion to different materials in connection with the specified adhesive (SikaForce 7818 L7 – Approved for internal wind turbine blade repairs), see Figure 23. Final material was decided to be PUR 1150 Solid, as it proved excellent strength for high loads including excellent adhesion to the specified adhesive. This material ensured optimal connection between corner mount and blade panel, this way, a controlled failure mode was obtainable.



Figure 23 – Adhesion testing for different materials in connection with specified adhesive using SIKA DANMARK facilities in collaboration with DIS & Bladena

To transfer high loads optimally from the cross reinforcement to the blade panel/glass fibre corner, through the PUR 1150 Solid. It was decided to use a fiberglass rod of ECR glass with epoxy resin moulded into the PUR 1150 Solid corner mount. With this process, any slack that could potentially interfere with optimal load transfer was avoided, see Figure 24.

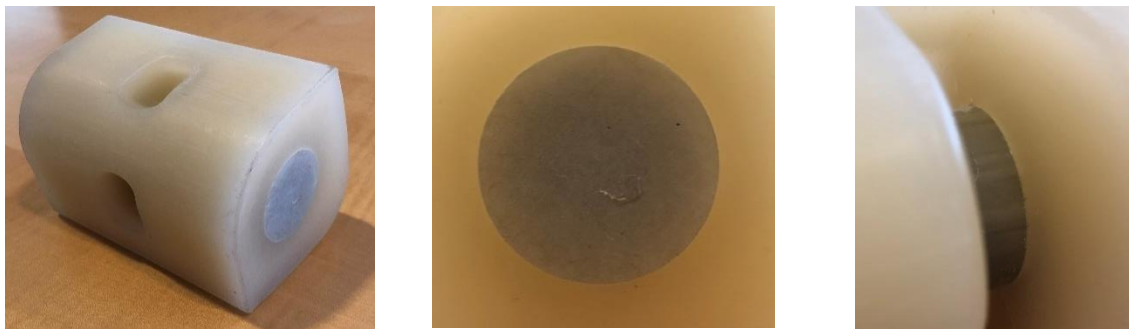


Figure 24 – New corner mount moulded by Tinby A/S showing final design where PUR 1150 Solid is moulded around a Ø30mm ECR fiberglass rod for optimal load transfer

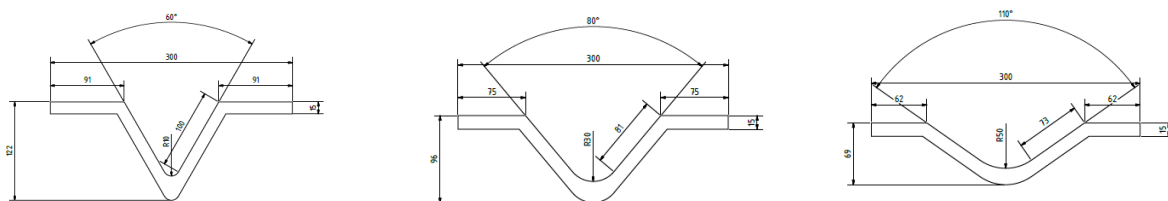
To account for the complex geometry the corner mounts need to handle, three different lower moulds have been produced using the same upper mould part. As shown below in Figure 25, first corner mount will be used for angles between 60°-80°, second mount will be used for angles between 80°-110° and third mount is for 110°-140° angles. The design/shape of the corner mount ensures that sufficient Bondline surface is obtained in angles from 60° to 140° blade angles using a linear approach to the inside radius of the blade.



Figure 25 – Photo showing the 3 different corner mounts produced to cover angles between 60° & 140°

Calculations for the corner mount connections have been in correlation with standard procedure used in the wind industry where adhesive bond lines should not exceed 5 mm of thickness. Therefore, the area of the connection to the blade panel is designed for  $1_{-0}^{+4}$  mm bond line thickness, and areas exceeding this is not included in the calculations.

To control the failure mode of the full X-Stiffener™ assembly, testing of the corner mounts have been conducted on “worst case” specially made glass fibre corners. These glass fibre corners have been produced in angles of 60°, 80° and 110° to mimic the angles in between each corner mount, see Figure 26. As an example, the bracket covering 60°-80° have been tested in glass fibre corners of 60° and again at 80°.



*Figure 26 – Drawings of specially produced glass fibre corners to mimic “worst case” scenarios for testing of adhesion to corner mounts*

After careful consideration and testing performed at DTU (See more in section 3.6), we have reached a strength of approx. 2 MPa. That is the connection to pure glass fibre, the connection to sandwich panel will be minimum 1,2 MPa. From adhesion coupon testing the strength to the glass fibre was tested for 12+ MPa, and the adhesion to the PUR was 15+ MPa. We believe after thorough examination of the test performed on the glass fibre corners, that the clamping method and design of specimen has led to high peeling stresses in the Bondline due to bending of the glass fibre corner. The size of the specimen has led to these results, where it is believed that this high local deformation would not be possible in the full blade, hence; these peeling stresses would not be present in full scale, and a strength closer to the 12 MPa is still valid. From these findings, and to make sure there is no blade risk involved, we have moved on with a safety factor of 4+. We have taken a worst case saying if the bracket is only 50% attached to the blade and gone down to 0,5 MPa strength. That results in a maximum force in each blade corner of approx. 600 kg. Therefore, the locking mechanism for the X-Stiffener™ has been tested and validated to ensure the rope will loosen at a maximum load of 600 kg, hence; no blade risk is involved.

For connecting the corner mounts, different fibre rope types have been investigated to give us the optimal strength properties to ensure proper connection for full blade life time by using non-conductive materials. This resulted in a Ø8 mm Dyneema® DM20 (Provided by DYNAMICA Ropes ApS) rope, pre-stretched at high temperatures to remove as much elongation as possible. As this rope type have a specified maximum load capability of 6.900 kg, we are working below 10% of the strength, this is also to ensure proper tension through product lifetime. The rope is chosen for its high strength, low elongation and very good ability to handle creep together with the extremely high strength to weight ratio (6,9 ton → 3,5kg/100m).

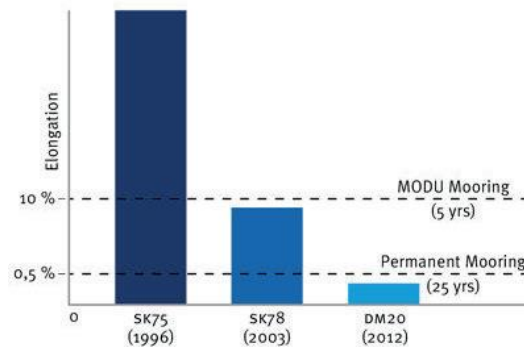


Figure 27 – Elongation performance of the rope used for the X-Stiffener™ product

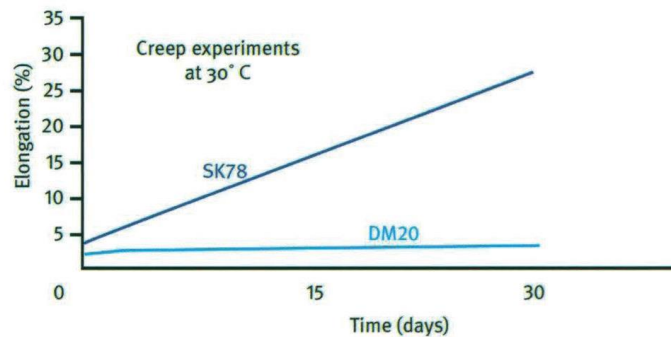


Figure 28 – Creep performance of the rope used for the X-Stiffener™ product

To lock the X-Stiffener™ connection, a friction-based approach was decided so that the maximum breaking load could be managed precisely. Testing of the length of the overlap in relation to the strength have been performed at DTU together with Bladerna to investigate the possibilities. By using a heavy-duty glue-lined shrinkwrap from 3M-DANMARK, and proper rope surface preparations, only 11 cm overlap is necessary to obtain a maximum load of 600 kg.



Figure 29 – Photo showing the locking mechanism for the X-Stiffener™ product

Risk management have been carried out throughout the development process by using a Failure Mode and Effect Analysis (FMEA) tool to deal with all possible failure modes. Bladerna`s current FMEA is covering: Design, Installation and operation. Below in Figure 30 is shown the rating scheme for the FMEA that shows the content and reasoning for different values implemented in the FMEA.

Value	Severity of Failure	Probability of Occurrence	
			Failure
1	Customer will not notice the adverse effect or it is insignificant	Remote probability of occurrence	≤1 in 100,000
2	Customer will probably experience a slight effect after a long time	Low failure rate with supporting documentation	1 in 10,000
3	Customer will experience a slight effect	Low failure rate without supporting documentation	1 in 2000
4	Customer will experience a reduction in performance. Repair will be needed eventually	Occasional failures	1 in 1000
5	Warranty repair or significant manufacturing or assembly complaint. Overall function of system is partly lost.	Relatively moderate failure rate with supporting documentation	1 in 500
6	High degree of customer dissatisfaction due to component failure without complete loss of function.	Moderate failure rate without supporting documentation	1 in 200
7	Function of complete system is lost. Very high degree of dissatisfaction due to loss of function. No impact on safety or governmental regulations	Relatively high failure rate with supporting documentation	1 in 100
8	Effect can result in unsafe situations. Severe damage to the overall system	High failure rate without supporting documentation	1 in 50
9	Effect will cause damage to the complete system and its surroundings. Dangerous situations will occur	Failure is almost certain based on warranty data or significant DV-test	1 in 20
10	Effect can cause highly dangerous and life-threatening situations. Heavy damage to machinery.	Assured of failure based on warranty data or significant DV-testing	≥1 in 10

Figure 30 – Rating scheme for FMEA used to manage the development for the X-Stiffener™ product

In Figure 31 it is shown how the different values are calculated into three different severity categories from green (No noticeable risk) to red (High risk for severe failure). Where the X-Stiffener™ development initially contained mostly green, but also some yellow rated failure modes. These yellow rated failure modes have been used to further development and improve that part of the product to make sure all failure modes by the end of the project and before final installation is rated as green (No noticeable risk).

Failure mode and effect analysis (FMEA)											
Color Chart for Assessment											
P = Probability (chance) of Occurrence S = Severity of failure R = Risk Priority Number (P x S)											
		Probability of Occurrence									
		1	2	3	4	5	6	7	8	9	10
Severity of Failure	1	1	2	3	4	5	6	7	8	9	10
	2	2	4	6	8	10	12	14	16	18	20
	3	3	6	9	12	15	18	21	24	27	30
	4	4	8	12	16	20	24	28	32	36	40
	5	5	10	15	20	25	30	35	40	45	50
	6	6	12	18	24	30	36	42	48	54	60
	7	7	14	21	28	35	42	49	56	63	70
	8	8	16	24	32	40	48	56	64	72	80
	9	9	18	27	36	45	54	63	72	81	90
	10	10	20	30	40	50	60	70	80	90	100

Figure 31 – Failure mode category calculation scheme

This structured and documented approach to the development process has led to the final approval by Catapult for installation on the 7MW Levenmouth turbine.

Initially planned for installation around August/September 2018, but due to complications with the turbine, the installation window was pushed to November 2018. The cold weather around

that time made the curing of the adhesive difficult, and it was decided to push the installation until the temperature was approx. 10°C and above. Therefore, final installation was conducted by GEV in May 2019 with supervision and assistance from Bladena (See Figure 32).

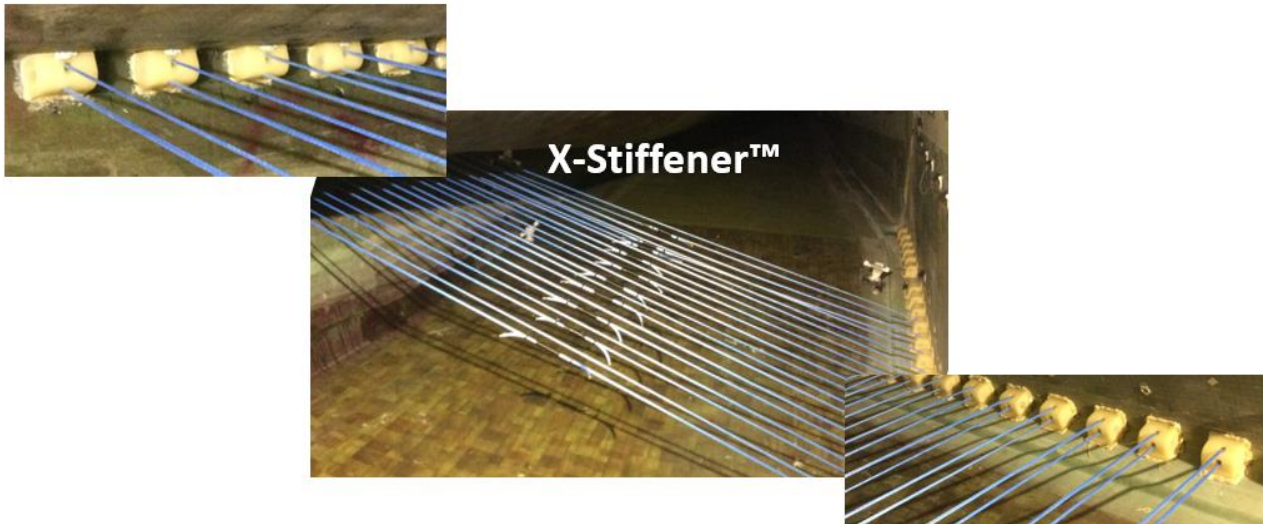


Figure 32 – Final installation of the X-Stiffener™ in the 7MW Levenmouth turbine

The solution and the initial planning were to install the X-Stiffener™ in both diagonals in the rear box of the blade, but from the measurements obtained one diagonal showed to be dominant. This diagonal was therefore reinforced by the X-Stiffener™ with 10 connections around max chord with a spacing of approx. 20 cm to distribute the loads properly.

For more information regarding the installation procedure etc. see **Fejl! Henvisningskilde ikke fundet. Fejl! Henvisningskilde ikke fundet. Fejl! Henvisningskilde ikke fundet..**

## 2.5 Erosion Sensor: modelling & testing

Leader: TNO

TNO and Siemens Gamesa have held some meetings in order to clarify some important points to be taken into account in the erosion sensor. Some points that need to be clarify in a near future are, for instance, adherence, feasibility study of its integration from the structural and aerodynamic point of view as holes are required to pass the fibre through the blade and could appear steps due to the sensor, compatibility with lightning protection system (LPS), communication protocol, alarms, etc. In this sense, Siemens Gamesa has offered its support to TNO in order to try to study some of the points in the next months.

### 2.5.1 Principle of erosion sensor

The main principle opted for measuring erosion is based on humidity sensing. In previous projects, TNO successfully developed a humidity sensor based on optical fibre technology. More

specifically, Fibre Bragg Grating based fibres (FBGs) with a moisture responsive coating were used for this purpose. During the current project, the integration of these fibres in leading edge protection (LEP) coatings of windmill blades is investigated.

The mechanism of erosion detection using humidity sensors is based on a difference in response to the externally changing humidity conditions. For a non-eroded coating, a slow response of the sensor is expected, since moisture transport through a high quality coating progresses slowly. For an eroded coating, suffering from weight loss (thickness reduction) and / or microcracks, moisture transport is much faster, leading to a fast sensor response.

### 2.5.2 Feasibility studies

In order to study this principle for LEP coatings, two main questions needed to be answered:

Is the mechanical stability of the fibres in the LEP coating sufficient to perform measure erosion? Especially so, since significant droplet impact forces act on the coating (and the fibre).

Are the formulation, moisture transport and mechanical properties compatible with the moisture sensing fibres to function as an erosion sensor?

To determine the mechanical stability, TNO supplied erosion sensor fibres to Aerox. The fibres were in integrated various testing coupons and submitted to rain erosion testing. In addition, the mechanical properties of the fibres were shared with CEU, who used these data to run mechanical simulations.

Initially, humidity test were done with TNO fabricated PUR coatings to study the proof of principle. Next, the functionality of the rain erosion sensor inside the AEROX LEP coating was studied. In order to do so, various test samples were prepared at Aerox in collaboration with TNO (Figure 33), after which humidity test were done at TNO with these samples. Finally, rain droplet impact was simulated experimentally at TNO, to relate the droplet impact energy to the response of the fibres incorporated in the Aerox samples.



*Figure 33 - Incorporation of TNO sensor fibres in Aerox coatings at Aerox laboratories (Valencia, Spain).*

### 2.5.3 Results

The rain erosion tests, analysed by Aerox, as well as the simulations done at CEU, indicated that the top part of the blade, is not a good position for the fibre from a mechanical point of view (denoted as position 1 in **Fejl! Henvisningskilde ikke fundet.**). Large mechanical stress is exerted on the fibres incorporated in the top part of the blade, possibly leading to failure of the fibre. In addition, the erosion of the AHP LEP coating was significantly accelerated in presence of the fibre (at position 1). This is probably due to the mismatch in mechanical properties between the AHP LEP coating (rubber-like) and the fibre (stiff, glass-like).

Because this issue was anticipated for at the start of the project, other fibre positions were studied as well, shown in **Fejl! Henvisningskilde ikke fundet.**

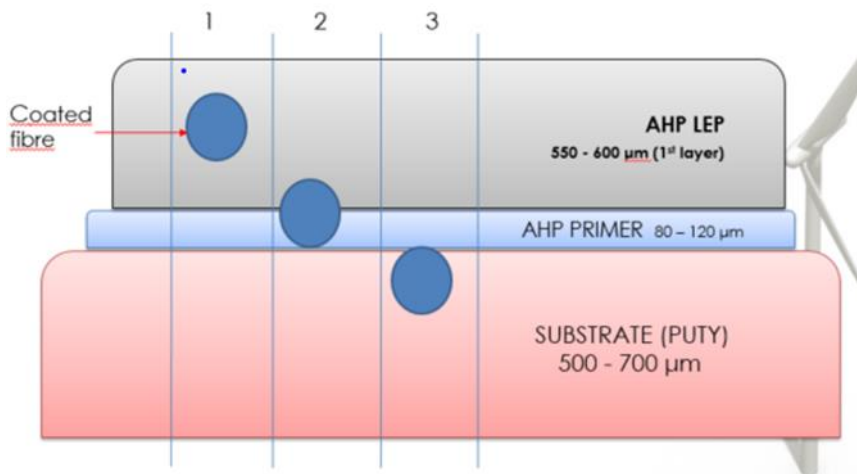


Figure 34 - Fibre positions denoted as 1 (LEP), 2 (primer) and 3 (putty) tested with rain erosion tests (Aerox), mechanical simulations (CEU), humidity (TNO) and rain droplet impact experiments (TNO). Figure courtesy Aerox.

In the figure below the accelerated rain erosion results are shown when embedding a fibre at position 2 and 3. A comparison has been made when no fibre was embedded as well.

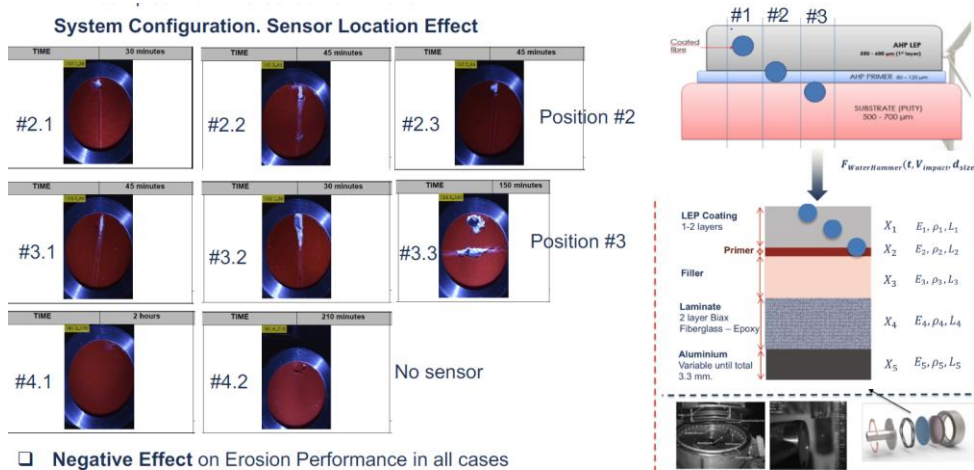


Figure 35: Test runs on the accelerated rain droplet erosion test setup analysing the effect of fibre optic sensor location.

Although erosion is accelerated at position# 2, it does allow for erosion sensing based on humidity signals. In addition, this position is more likely to ensure the fibre does not break during droplet impact and it allows for tracking the number and (low) energy of droplet impact(s).

The initial humidity test with TNO fabricated PUR coatings indicated that the principle of erosion sensing in PUR coatings was feasible. Depending on the thickness of the coating present, humidity signals differed due to a difference in moisture transport, implying that the erosion measurement is possible with this approach. Next, the fibres incorporated in the Aerox coatings at positions 1, 2 and 3 were tested. From an erosion sensing point of view, fibre positions 1 and 2 were favoured, measuring humidity inside of the AHP LEP and primer coatings (**Fejl! Henvisningskilde ikke fundet.**). Position 3 was less favourable, probably because moisture transport over various interfaces occurs at a much slower rate and because the swelling and shrinking mechanism is hampered when the sensor is at position number 3.

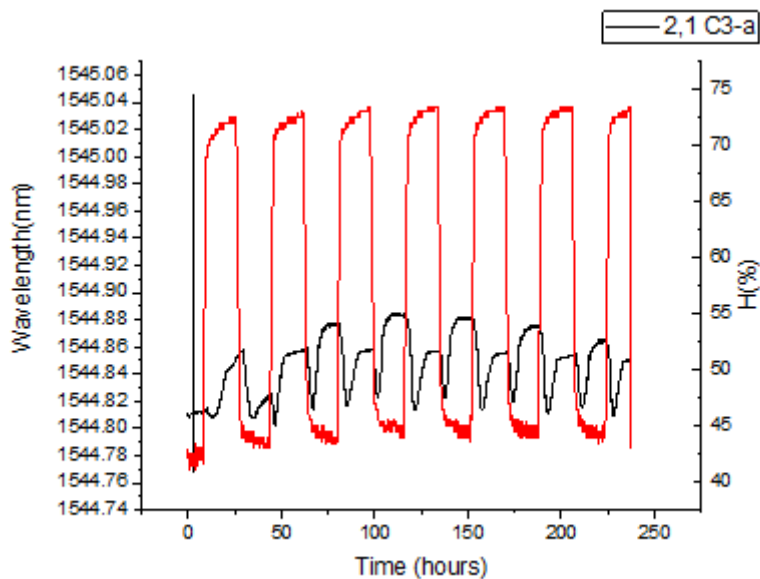


Figure 36 - Fibre response (black line) incorporated in Aerox coatings at position 2 (primer) while varying the humidity (red line) between 45 and 75% relative humidity.

Based on the mechanical stability and functional sensing aspects studied during this feasibility study, it can be concluded that this principle is feasible for erosion testing. However, care should be taken at which position the erosion sensor fibres are placed inside the coating on the wind turbine blade. For mechanical stability, the deeper the fibre is embedded, the better the mechanical stability of both fibre and LEP coating.

Finally, the droplet impact experiments indicated that the number of impacts as well as the energy of the impact can be related to the fibre response for low energy impact (comparable to small rain droplets with speeds up to  $125 \text{ m}\cdot\text{s}^{-1}$ ). For high energy impact the number of droplets could be measured, but the energy of the impact could not be related to the fibre response because of a threshold behaviour encountered.

#### 2.5.4 Conclusion

Based on the mechanical stability and functional sensing aspects studied during this feasibility study, it can be concluded that this principle is feasible for erosion sensing.

During this study, the best position to place the erosion sensor was found to be in the AHP primer layer, position nr. 2 of **Fejl! Henvisningskilde ikke fundet.**. At that position it does allow for erosion sensing based on humidity signals. Representative tests in the laboratory made clear that the sensor has a negative impact on the life-time of the Aerox LEP coating. For that reason it was decided not to install the erosion sensor in the Levenmouth Demonstration Turbine (LDT).and spent the remaining budget on running experiments and models to evaluate trade-off to steer development in future.

## 2.6 Cross Sectional Shear Distortion Sensor: modelling & testing

Leader: TNO

### 2.6.1 Modelling Approach

Cross sectional shear distortion is an indicator for the deformations a wind turbine blade experiences during operation. In the context of this project it is measured as the length change of the two diagonals of the rear box of blade #3 at certain distances from the blade root (specified as radius e.g. R14 in meters) of the Levenmouth Demonstration Turbine (LDT). While initially the main box of this blade was envisaged, it became apparent that this structure was too narrow for the installation of the Cross Sectional Shear Distortion Sensor (CSSDS) during the first inspection of the blade's interior. The radii of interest are R12, R14 and R16 at which the diagonal length change is expected to be less than 30 mm by the work package partners. For illustration, the cross section at R14 is depicted in Figure 37. While the dimensions of the cross sections differ with only up to 50 cm, their shape changes rather significantly. This results in a more complex design and installation procedure of the CSSDS than originally anticipated.

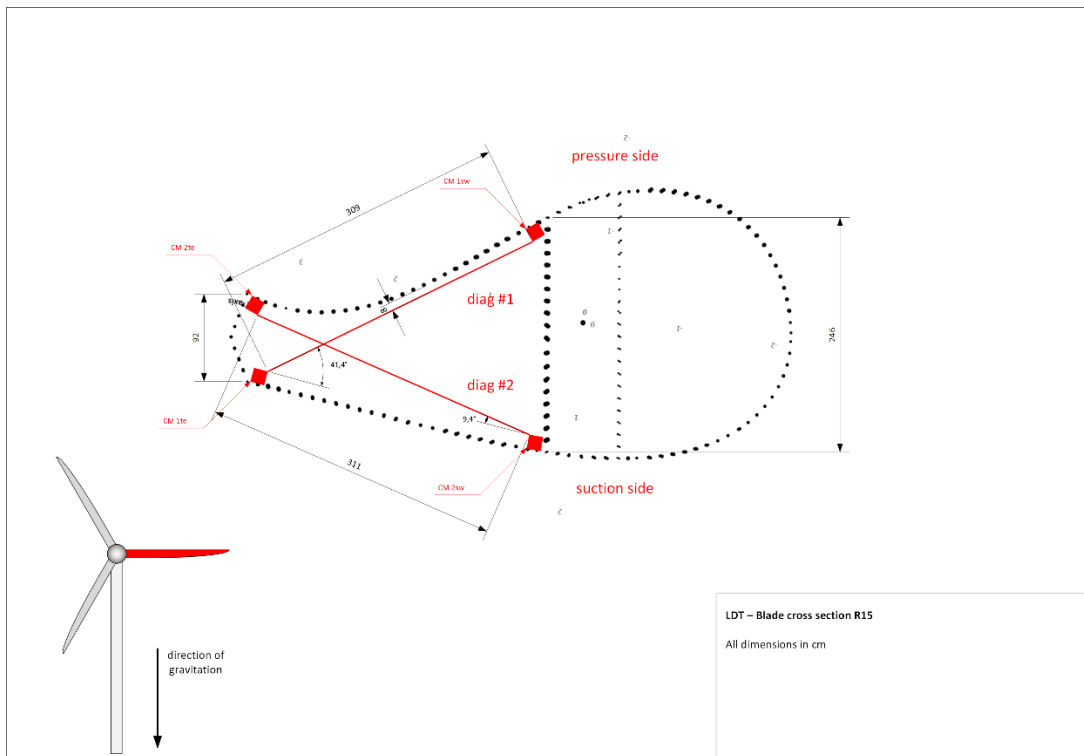


Figure 37 - Cross section R14 of LDT

To determine the length of the cross sectional diagonals, TNO developed the CSSDS based on its Fibre Bragg Grating (FBG) technology. The CSSDS schematic design and interfaces are depicted in Figure 38. The sensor transfers mechanical strain (i.e. the length change of the diagonals) into an optical response of an optical fibre (i.e. the sensing fibre) that can easily be measured by off the shelf electronics placed inside the hub. Therefore, the sensing fibres have to be strained along the identified diagonals and attached to the blade interior (suction and pressure side surfaces). This attachment is realised by the so called Fibre Corner Mounts (FCM). Once the mechanical strain is translated into an optical signal that propagates along the optical fibre from the measured cross section, it can be measured by the interrogator and measurement PC that are placed inside the wind turbine's hub. There, the measurement data is processed, aggregated and send to TNO using ethernet or a 4G connection.

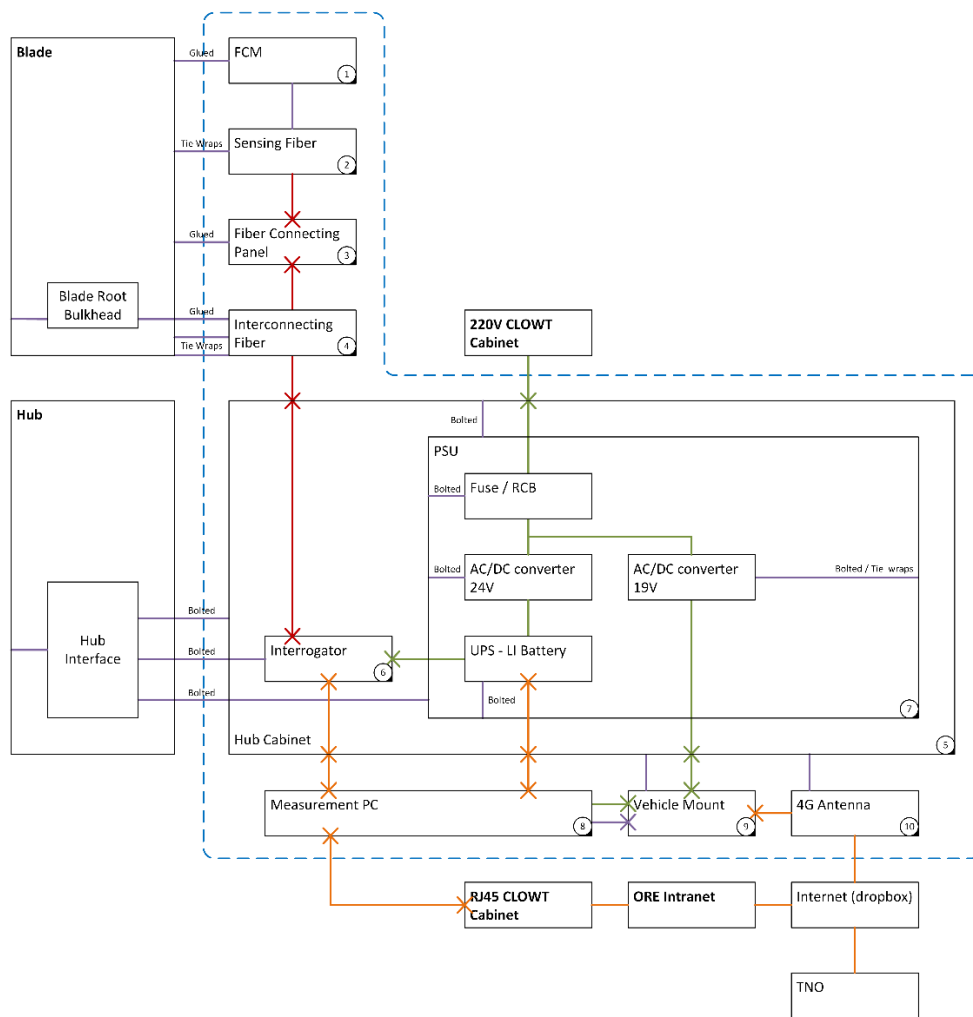


Figure 38 – CSSDS schematic design & interfaces

The CSSDS is designed such, that it can measure the diagonal length change of the specified cross sections with an accuracy and precision of below 0.5 mm over a period of operation of 12 months. Also it has to be able to be installed and decommissioned by trained TotalWind technicians and comply to the requirements of ODSL.

The two most complex components that had to be developed for the CSSDS are the Fibre Corner Mount (FCM) and the Hub Cabinet (HC) and are therefore briefly discussed subsequently.

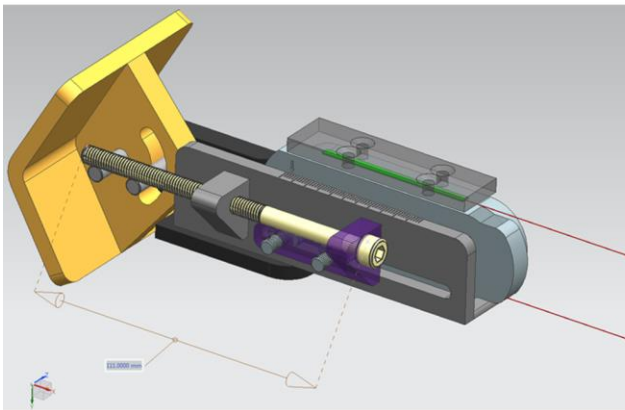
### 2.6.2 Fibre Corner Mount

The main purpose of the FCM is to transfer rear box deformation into the sensing optical fibre to pick up upon the strain along the diagonals. Therefore it has to:

- Provide a robust and rigid interface to the blade surface

- Clamp the sensing optical fibre without slip and not exceeding the minimal bend radius of 15 mm
- Apply a well-defined pre tension to the fibre, such that the fibre can also measure compression of the rear box diagonals
- Be able to be installed simply and safely by the TotalWind technicians

One FCM is placed in each of the 4 corners of the 3 designated cross sections of the rear box as depicted in Figure 37 symbolized by red cubes. Figure 39 shows the first concept and the final design of the FCM, illustrating the development necessary to transform the requirements into actual functionality.



**TNO** innovation  
for life

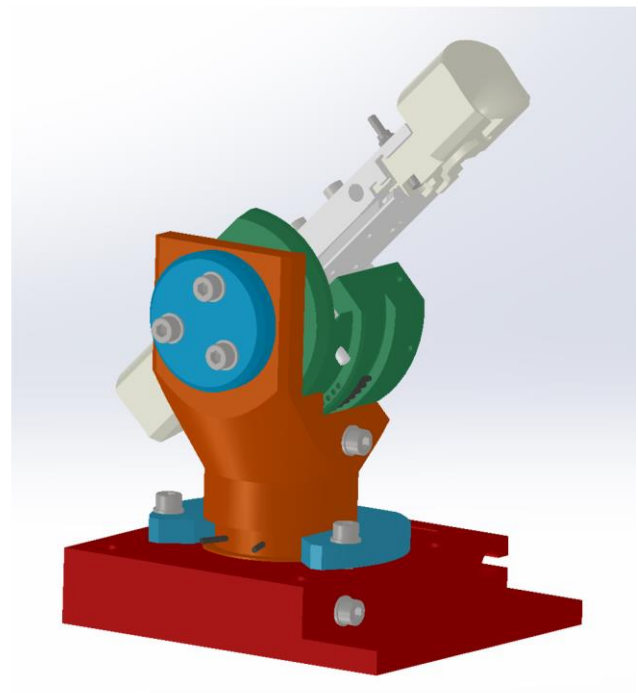


*Figure 39 - FCM first concept (left) and final design (right)*

### 2.6.3 Hub Cabinet

While the FCM is required to translate the diagonal strain into an optical signal that propagates inside the optical fibres, an optical interrogator is needed to convert it into an electronic signal that can easily be processed. To provide the interrogator with a suitable environment, mechanical protection and to enable an uninterrupted operation for at least 12 h, even when the power to the hub cabinet is cut, the HC was developed. The HC also holds the measurement PC that manages the data created by the interrogator. In order to be able to install the HC with the weight and volume constraints imposed by the wind turbine, the HC had to be broken up into 3 sub-assemblies, the power supply unit sub-assembly, the interrogator sub-assembly and the cabinet with the measurement PC installed. They are depicted in Figure 40. The HC also provides the external interfaces to the other components of the CSSDS, as well as to the wind turbine. The HC is going to be installed inside the hub of LDT and mounted onto the hub interface provided by ODSL.

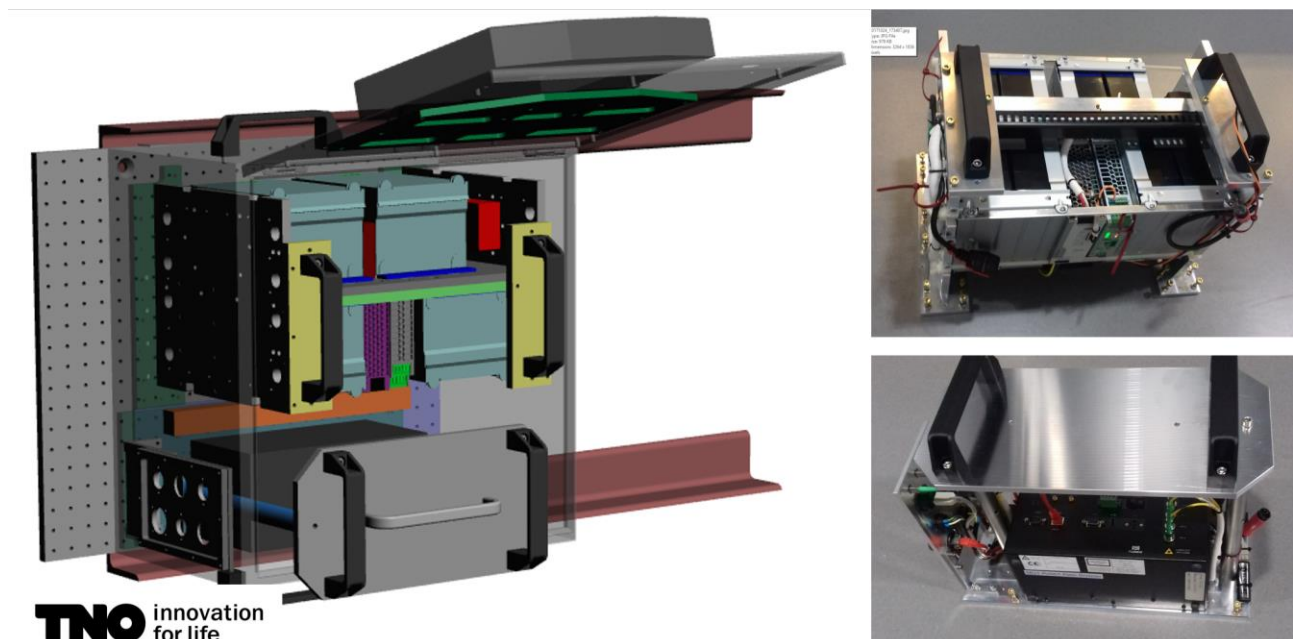
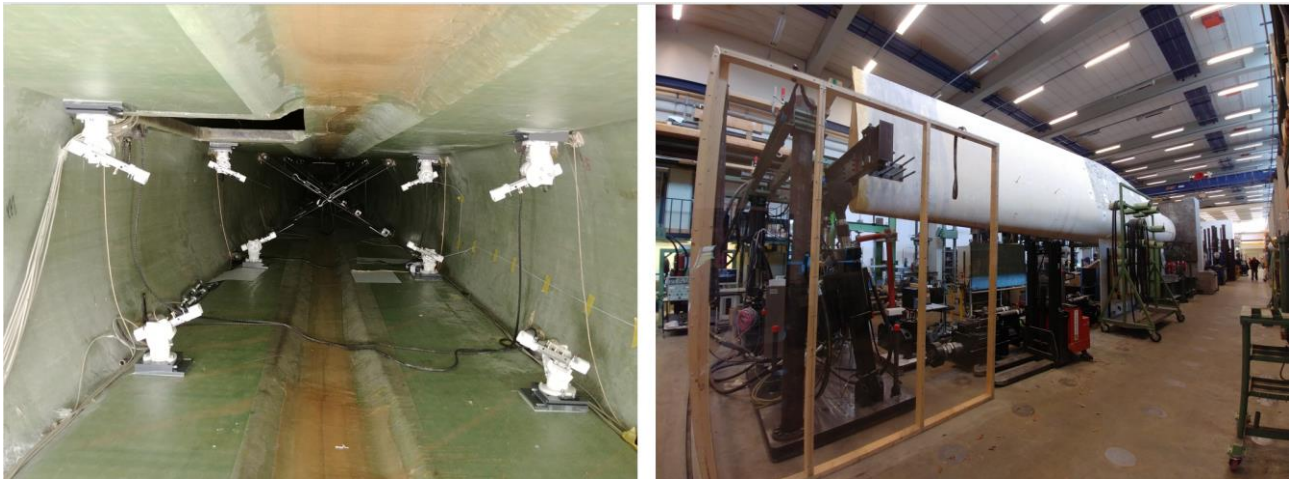


Figure 40 - Hub Cabinet (left), power supply unit sub-assembly (top right) and the interrogator sub-assembly (bottom right)

### 2.6.4 DTU Test Integration

The CSSDS sensor is developed by TNO, and had to be installed by blade technicians in a wind turbine that is managed by ORE Catapult and its contractors. The separation of tasks and responsibilities inherent to this construction and the fact that it will be a first time right installation form a risk for the installation and operation of the CSSDS that is mitigated by a test integration of the CSSDS into the blade test rig at DTU. There the complete CSSDS system was installed with two cross sections of the blade equipped in November 2017. The test

integration (see Figure 41) resulted in an improved installation manual, training of the blade technicians and confidence to be able to integrate the CSSDS successfully into LDT with the estimated effort.



*Figure 41 - CSSDS test integration at DTU, installed FCMs inside the blade (left) and test rig (right)*

## 2.7 Advanced Hybrid Polymer (AHP) coating solution: modelling, polymer design and properties modulation

Leader: Aerox

### 2.7.1 Refinement of the formulation of the AHP polymer

The work started with the AEROX AHP Technology and a first formulation of the AEROX AHP leading edge protection (designated "LEN 9"). AEROX AHP Technology is based on the precise combination of two thermoset polymers with different rheological, thermal, chemical and physical properties, allowing the creation of high-performance materials with extraordinary erosion resistance.

AEROX AHP Leading Edge Protection ("LEP") system consists of a 2-component polyurea-polyurethane coating which is extremely easy to apply with excellent erosion resistance. Once the product is applied on the leading edge of the blade, it creates a protective multilayer system (together with the composite material of the blade and the commonly used putty) which absorbs and dissipates the energy of the impacts of the raindrops.

AEROX AHP LEP system can be applied either at the blade manufacturer premises or in field. The coating solution was designed with three application methodologies to fit the requirements of each OEM and/or blade manufacturer (spray, paint roller and filling knife) (See Figure 42).



*Figure 42 - Application methodologies on wind blades. Left: spray. Centre: roller. Right: filling knife.*

The formulation of the AHP polymer was adjusted to both environments Levenmouth conditions (service) and Siemens Gamesa production conditions (service and plant). Viscoelasticity and mechanic response to impacts were defined, simulated and tested in order to select the most adequate formulation.

Four additional formulations were created (LEN 22, LEN 23, LEN 30 and LEN 39) modifying viscosity, amount of pigment, and additives in order to modify the elasticity, hardness, energy absorption capacity, application window (moisture and temperature) with the objective of finding the best formulation for service and plant applications.

Simulations carried out by CEU, shown in Figure 43, compared the behaviour of the different LEP polymers under the effect of the raindrop impacts in comparison to AEROX's Gel Coat. It was observed that the capability of the coating to transfer wave energy in the multi-layered system can influence the erosion damage. Stress reflections oscillate repeatedly through the coating and substrate structure until dampened out by the materials' properties, to reduce the energy of the initial shockwave. These LEP elastomer material coatings (LEN9 and LEN22) were formulated with low macroscopic elastic modulus, high ultimate strain and high resilience that reduce the stress at the impact surface and dampen the stress waves, ensuring the rapid recovery time of the material and the energy is dissipated quickly (depending on the dynamic properties and the thickness). It is important to remark from Table 3 that the transmitted stress waves were reduced significantly from the liquid to the coating and, on the other hand, amplified from the coating layer to the substrate, which in fact was not a problem due to the higher mechanical capabilities of the laminate. These materials store energies at a reasonably low level of stress (at a value lower than the fracture strain) but needed to be defined considering the appropriate adhesion between the coating and the substrate and their relative impedances (See Table 3).

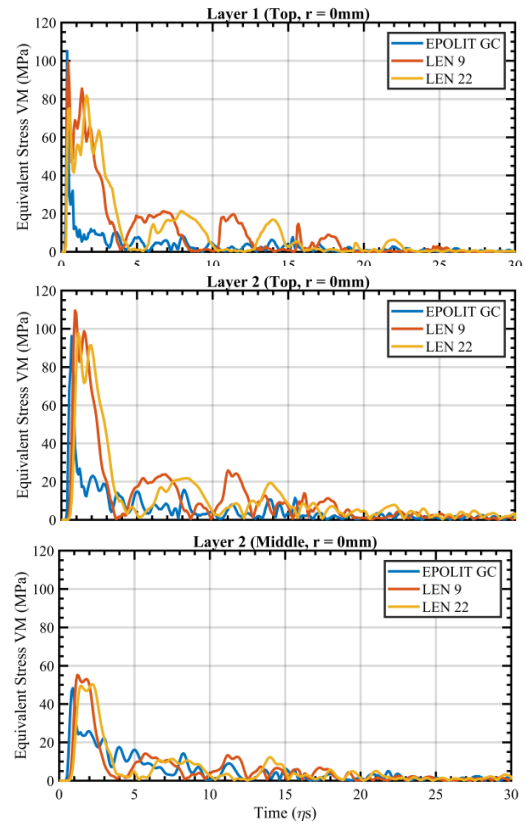
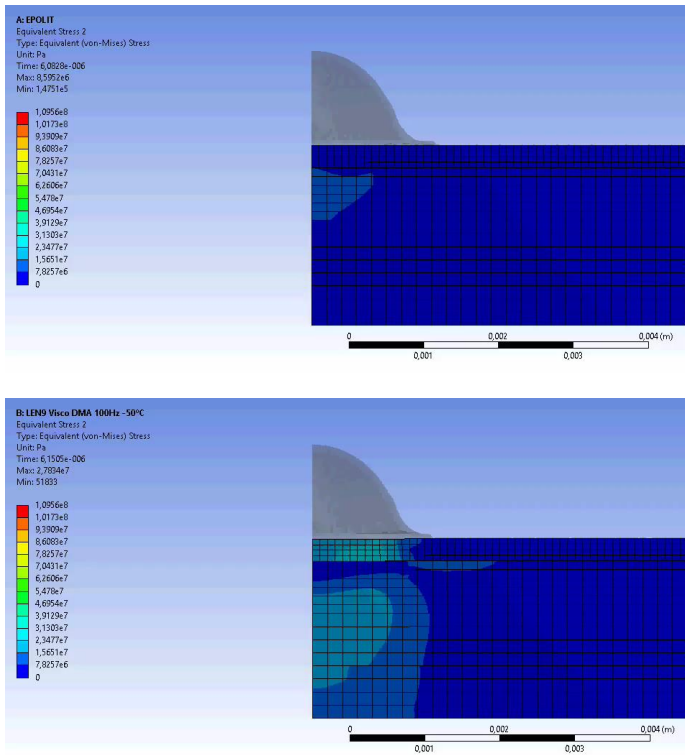


Figure 43 - Simulation of the stress developed through the thickness by different polymers (Epolit GC, LEN9, LEN22). Example of obtained results for tested coupons configurations.

Material Combination: Coating-Substrate	Z <sub>L</sub> (Kg/m <sup>2</sup> s)	Z <sub>C</sub> (Kg/m <sup>2</sup> s)	Z <sub>S</sub> (Kg/m <sup>2</sup> s)	$\frac{\sigma_{R_{LC}}}{\sigma_{I_{LC}}}$	$\frac{\sigma_{T_{LC}}}{\sigma_{I_{LC}}}$	$\frac{\sigma_{R_{CS}}}{\sigma_{I_{CS}}}$	$\frac{\sigma_{T_{CS}}}{\sigma_{I_{CS}}}$
LEP-GFRP	1482000,00	92870,88	5648008,50	0,882	0,118	-0,968	1,968
Gel Coat-GFRP	1482000,00	3041052,45	5648008,50	-0,345	1,345	-0,300	1,300

Table 3 - Impedance properties of selected candidate materials. Reflected and Transmitted waves as a function of the Incident stress at surface (Liquid-Coating) and at interface (Coating-Substrate)

The five polymers, were also tested in the RET rig at University of Limerick. Several samples of each formulation were tested. Figure 44 shows an example of the maximum resistance reached by different samples. LEN 30 offered better performance than any other formulation tested.

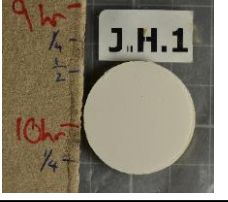
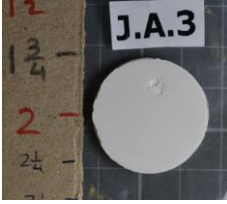
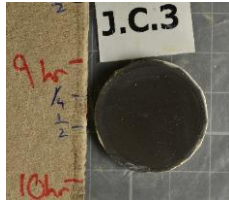
LEN 9 (Reference)	LEN 22	LEN 23	LEN 30	LEN 39
				
2,5 hours	5,5 hours	8,5 hours	7,5 hours	10 hours
				
2 hours	3 hours	9,5 hours	15 hours	5,5 hours

Figure 44 - Results of RETs performed on 5 AHP polymer formulations.

The selection of the polymer was made taking into account the average resistance of each formulation and the ability to be sanded and adapted to a cartridge format (See Figure 45).

The selected formulation was that labelled as LEN30. The repair and application methods are described in full in Annex A.

	LEN 9	LEN 22	LEN 23	LEN 30	LEN 39
SANDING?	✓	✓	✗	✓	✓
CARTRIDGE FORMAT?	✓	✗	✗	✓	✗
RAIN EROSION RESISTANCE	2 hours	4 hours	8 hours	9 hours	7 hours

Figure 45 - Formulation selection criteria.

### 2.7.2 Modulation of the adhesion of the coating

During the rain erosion tests performed some samples showed delamination failure. This was interpreted as lack of adhesion between the LEP and the putty/porefiller (See J.C.1 in Figure 44).

In order to improve the adhesion, an intermediate layer of AHP Primer (Aerox AHP PR) was applied. The objective of the primer was to avoid delamination and to control the fast growth of the eroded zone once the erosion is initiated.

Pull-off tests (Figure 46) showed a change in the failure mechanism from adhesion failure without using primer to cohesive failure when the primer is applied. Peeling tests showed the increase of energy required to separate the coating from the filler when using primer compared to samples without primer.

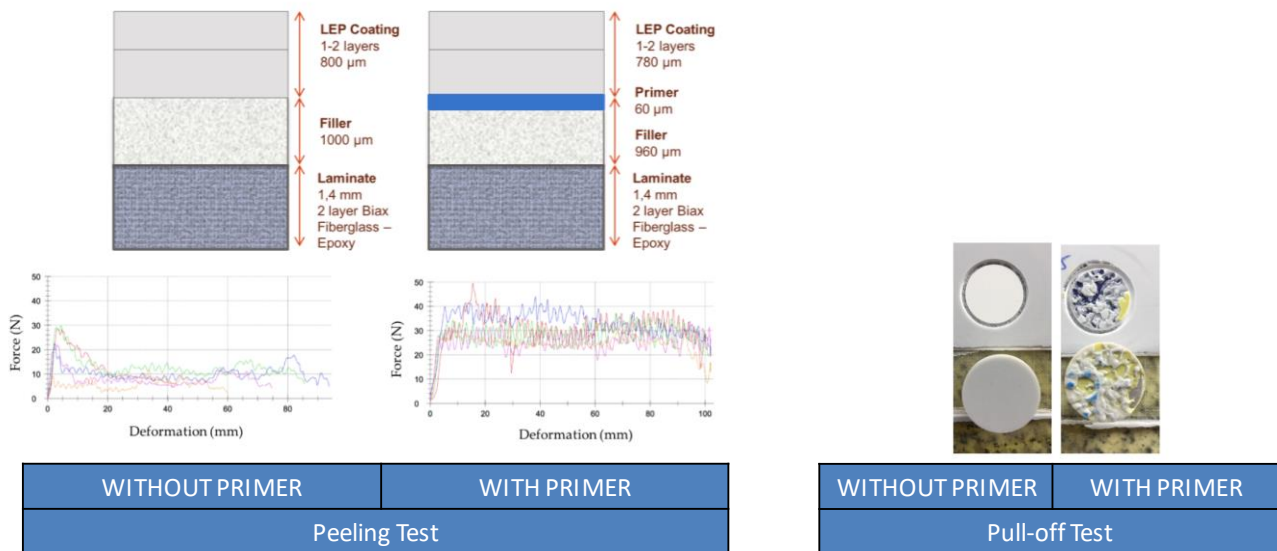
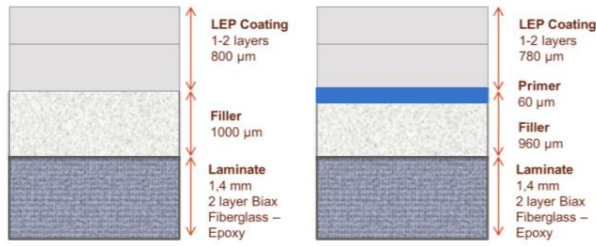


Figure 46 - Pull-off and peeling tests.

Nanoindentation tests were used in order to characterise each layer of the LEP configuration (LEP – PRIMER – FILLER). Indentation modulus and hardness of each layer were obtained as showed in Figure 47.

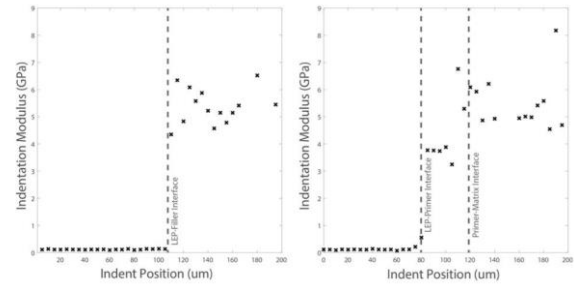


Material Combination: Coating-Substrate	$Z_L$ (kg/m <sup>2</sup> s)	$Z_C$ (kg/m <sup>2</sup> s)	$Z_S$ (kg/m <sup>2</sup> s)	$\frac{\sigma_{R1C}}{\sigma_{LC}}$	$\frac{\sigma_{T1C}}{\sigma_{LC}}$	$\frac{\sigma_{R2C}}{\sigma_{CS}}$	$\frac{\sigma_{T2C}}{\sigma_{CS}}$
LEP-GFRP	1,48M	0,09M	5,65M	0,882	0,118	-0,968	1,968
LEP-Filler	1,48M	0,09M	2,83M	0,882	0,118	-0,936	1,936
LEP-Primer	1,48M	0,09M	2,28M	0,882	0,118	-0,922	1,922
Primer-Filler*	2,28M	2,83M				-0,107	1,107

(\* the relative acoustic properties are not considered on the liquid-coating surface and the primer acts as a first substrate layer instead of the coating layer and the filler as the second substrate layer)

Bulk properties obtained for LEP configuration materials with nanoindentation testing.

Material	Indentation Modulus	Hardness
LEP	21.37±0.45 MPa	6.39±0.8 MPa
Primer	3.66±0.29 GPa	130.75±47 MPa
Filler	8.76±0.87 GPa	167.37±14.17 MPa



WITHOUT PRIMER      WITH PRIMER  
Nanoindentation Testing

Figure 47 - Left: Impedance properties of LEP candidate materials. Reflected and Transmitted waves as a function of the Incident stress at surface (Liquid-Coating) and at interface (Coating-Substrate ; Right: Nanoindentation testing showing interface properties variation due to intermediate primer layer.

The relative acoustic properties were quantified for the different combinations of material candidates for the multi-layered system. It could be observed that the filler layer inclusion and even the primer layer did not negatively influence the reflected and the transmitted waves to the LEP compared to the direct application of the LEP over the GFRP laminate. Moreover, considering the primer layer as a first substrate layer over the subsequent filler layer, there was a reduced value for the reflected and transmitted stress waves. These results correlate well with the similar erosion incubation time observed in both configurations (with and without a primer) in the rain erosion testing summarised in Figure 48 and Figure 49 for the LEP configuration.

Simulations of the stresses caused in the multilayer system depending whether the primer is applied or not, showed differences in the maximum values reached in each case. Maximum stresses were reduced when the primer was applied. Simulation results were confirmed with rain erosion tests carried out on fast degradation coatings with and without primer.

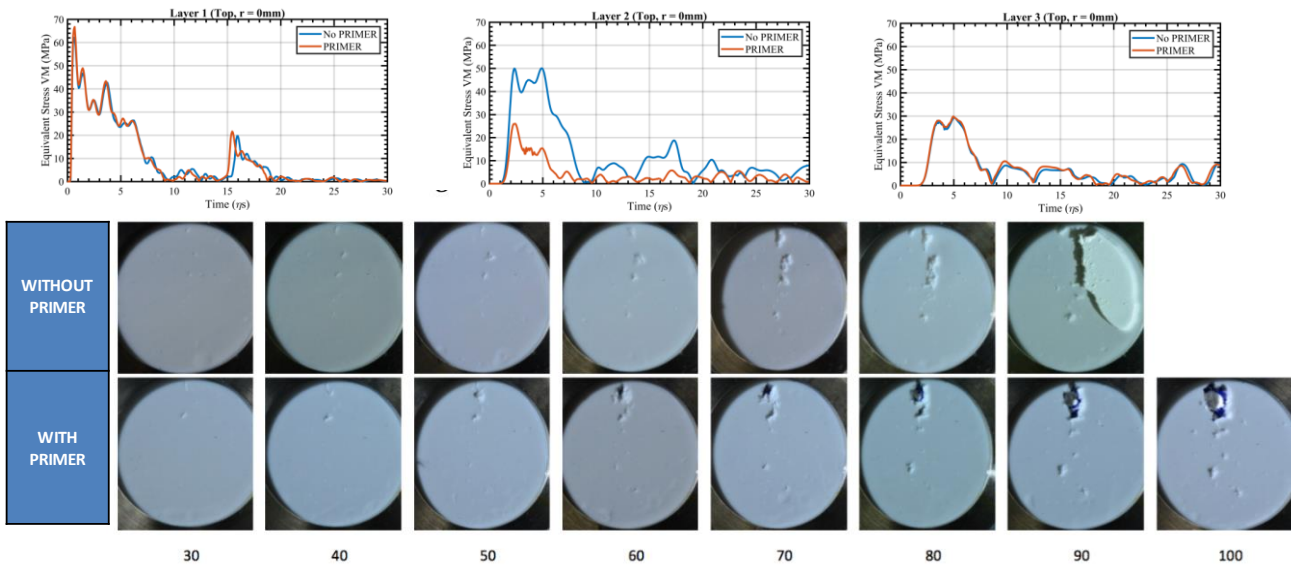


Figure 48 - Simulation of the stresses absorbed with and without primer.

Finally, rain erosion tests were carried out in order to evaluate the influence of the primer on the resistance of the coating system (Figure 49). In the meantime, application processes were improved, reaching around 15 hours in average with LEN 30 at Rain Erosion Tests. It was observed that the primer slightly reduced the resistance (from 15 to 14 hours). However, the degradation of the coating was progressive from the erosion initiation spot. This is unlike what happened when the primer was not used, when fast delamination was observed from the moment when the first damage occurred.

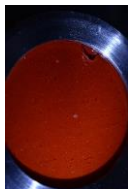
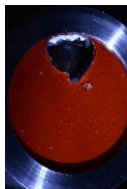
WITHOUT PRIMER			
	17 hours	15 hours	
WITH PRIMER			
	14 hours	8 hours	14 hours

Figure 49 - Evaluation of the influence of the primer on the overall resistance.

### 2.7.3 Definition of Plant Application (Siemens Gamesa Plant)

The definition of the plant application in Siemens Gamesa’s premises was carried out applying AEROX AHP LEP System (AEROX AHP LEP 910 and AEROX AHP LEP 920). There were made 5 different application as described in Table 4.

APPLICATION	PRODUCT	METHOD OF APPLICATION
#1	AHP LEP 910	1 layer by roller.
#2	AHP LEP 920	1 layer by filling knife
#3	AHP LEP 920	2 layers wet on wet by filling knife
#4	AHP LEP 920	1 layer by filling knife, sanding + 1 layer by filling knife.

*Table 4 - Test applications (Siemens Gamesa plant)*

The application was carried out by Siemens Gamesa Plant operators, as shown in Figure 50.



*Figure 50 - AHP LEP Service System application (Siemens Gamesa plant)*

The conclusions extracted from the tests were:

- A primer is required to ensure the good adhesion of the coating when applied both ways.
- The finish surface of the roller application was not good enough and had to be improved.
- The application by filling knife was faster and offered the best finishing surface. Therefore, it was preferred by Siemens Gamesa plant.

GAMESA Plant	
LEP by Filling Knife	Comments
	<ul style="list-style-type: none"> <li><input type="checkbox"/> Adhesion Primer: <ul style="list-style-type: none"> <li><input type="checkbox"/> Needed to ensure a good adhesión in ANY CONDITION of application.</li> </ul> </li> <li><input type="checkbox"/> LEP by roller: <ul style="list-style-type: none"> <li><input type="checkbox"/> Finish Surface needed to be improved.</li> </ul> </li> <li><input type="checkbox"/> LEP by filling knife <ul style="list-style-type: none"> <li><input type="checkbox"/> Great Finish</li> <li><input type="checkbox"/> Quick application</li> <li><input type="checkbox"/> Best application for Plant.</li> </ul> </li> </ul>

Figure 51 – Siemens Gamesa plant application results.

#### 2.7.4 Definition of Service Application (Siemens Gamesa Service)

The definition of the service application in Siemens Gamesa’s premises was carried out applying AEROX AHP LEP Service System (AEROX AHP PR 108, AEROX AHP LEP 910 and AEROX AHP LEP 920).

There were made 5 different application as described in Table 5.

APPLICATION	PRODUCT	METHOD OF APPLICATION
#1	AHP PR 108 Service	1 layer by roller
	AHP LEP 910 Service	2 layers wet on wet by roller
#2	AHP PR 108 Service	1 layer by roller
	AHP LEP 920 Service	1 layer by filling knife
#3	AHP PR 108 Service	1 layer by roller
	AHP LEP 920 Service as Filler	1 layer by filling knife
	AHP LEP 920 Service as LEP	1 layer by filling knife
#4	AHP LEP 920 Service	2 layers wet on wet by roller
#5	AHP LEP 920 Service	1 layer on the sides and 1 layer on the central zone of LEP

Table 5 - Test applications (Siemens Gamesa service).

The application was carried out by Siemens Gamesa Service operators, at the service training site in Pamplona (Spain), as shown in Figure 52.



Figure 52 - AHP LEP Service System application (Siemens Gamesa service).

Table 6 summarises the results from this testing. Full details of the test methodology is described in Annex A.

AHP LEP VERSION	ADVANTADGES	DISADVANTADGES
<b>AHP PR 108 Service</b>	<ul style="list-style-type: none"> <li>- Lower probability of wrong mixing ratio due to cartridge format.</li> <li>- Reduction in intermediate stocks.</li> <li>- Less disposables - Offer another method to control thickness</li> <li>- Ensure better adhesion of AHP LEP</li> <li>- Not necessary wait until cure to apply the next layer</li> </ul>	<ul style="list-style-type: none"> <li>- Application on blade directly</li> </ul>
<b>AHP LEP 910 Service</b>	<ul style="list-style-type: none"> <li>- Lower probability of wrong mixing ratio due to cartridge format.</li> <li>- Reduction in intermediate stocks.</li> <li>- Time of LEP stage.</li> <li>- Roughness of process</li> </ul>	<ul style="list-style-type: none"> <li>- Levelling</li> <li>- Application of 2 layers.</li> </ul>

	<ul style="list-style-type: none"> <li>- Easy to apply for non-experienced operators</li> </ul>	
<b>AHP LEP 920 Service</b>	<ul style="list-style-type: none"> <li>- Lower probability of wrong mixing ratio due to cartridge format.</li> <li>- Reduction in intermediate stocks.</li> <li>- Same disposables than filler.</li> <li>- More than 500 µm in one hand.</li> <li>- Time of LEP stage.</li> <li>- Fast curing</li> <li>- Great Finish</li> <li>- Good feedback of operators.</li> <li>- Levelling</li> <li>- Application on blade directly</li> </ul>	<ul style="list-style-type: none"> <li>- Confirm the application #5 as roughness method of application.</li> </ul>

*Table 6 - Feedback from Siemens Gamesa's technicians.*

Regarding the application methods, the conclusions extracted from the tests were:

- The primer was not suitable to be applied directly on the blade and had to be previously put in a container.
- It would be interesting if the rheology of the primer could be modified in order to use it as porefiller.
- The roller application offered deficient finish surface and should be improved. At the same time, roller application was the easiest way and was suitable for non-experienced operators.
- The application by filling knife offered the best finish surface as well as the fastest method. However it required practice by the operators.

GAMESA Service			
PRIMER	LEP by Roller	LEP by Filling Knife	Comments
			<ul style="list-style-type: none"> <li><input type="checkbox"/> Adhesion Primer: <ul style="list-style-type: none"> <li><input type="checkbox"/> Not Suitable to be applied directly on the blade → Use of container.</li> <li><input type="checkbox"/> Modify the rheology to use as porefiller.</li> </ul> </li> <li><input type="checkbox"/> LEP by roller: <ul style="list-style-type: none"> <li><input type="checkbox"/> Application method suitable for non-experienced operators</li> <li><input type="checkbox"/> Finish Surface needed to be improved</li> </ul> </li> <li><input type="checkbox"/> LEP by filling knife <ul style="list-style-type: none"> <li><input type="checkbox"/> Great Finish</li> <li><input type="checkbox"/> Quick application</li> <li><input checked="" type="checkbox"/> <b>Recommended application</b></li> </ul> </li> </ul>

*Figure 53 – Siemens Gamesa service application results.*

### 2.7.5 Definition of Service Application (TotalWind)

The definition of the service application was carried out applying Aerox AHP LEP Service System at Total Wind's premises (AEROX AHP PR 108, AEROX AHP LEP 910 and AEROX AHP LEP 920).

There were made 5 different applications as described in Table 7.

APPLICATION	PRODUCT	METHOD OF APPLICATION
#1	AHP LEP 910 Service	2 layers wet on wet by roller.
#2	AHP LEP 920 Service	1 layer by filling knife
#3	AHP LEP 920 Service	1 layer on the sides and 1 layer on the central zone of LEP
#4	AHP LEP 910 Service	2 layers wet on wet by roller and spread the final layer with a brush
#5	AHP LEP 920 Service	1 layer by filling knife trying to improve the transition zone.
#6	AHP LEP 920 Service	1 layer on the sides and 1 layer on the central zone of LEP trying to improve the transition zone.

*Table 7. Test applications (TotalWind).*

The application was carried out by Total Wind operators, at Total Wind facilities in Brande (Denmark).

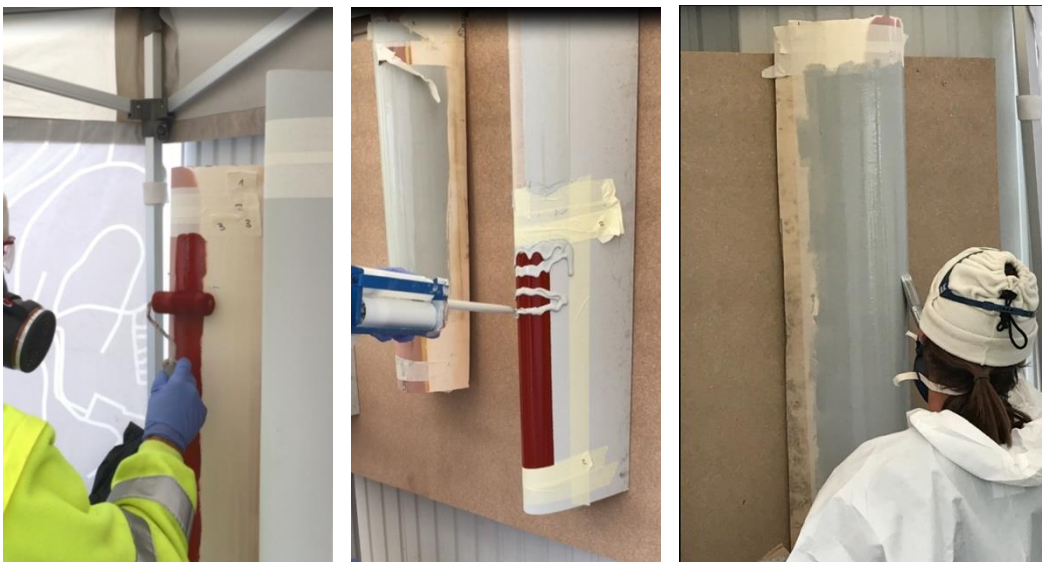


*Figure 54 - AHP LEP Service System application (Total Wind).*

Table 8 summarises the results of this testing. Full details on the application methods are described in Annex A.

AHP LEP VERSION	ADVANTADGES	DISADVANTADGES
<b>AHP PR 108 Service</b>	<ul style="list-style-type: none"> <li>- Lower probability of wrong mixing ratio due to cartridge format.</li> <li>- Reduction in intermediate stocks.</li> <li>- Less disposables</li> <li>- Offer another method to control thickness</li> <li>- Ensure better adhesion of AHP LEP</li> <li>- Not necessary wait until cure to apply the next layer</li> <li>- Could be used as porefiller using a filling knife.</li> </ul>	<ul style="list-style-type: none"> <li>- Surface appearance could be better.</li> </ul>
<b>AHP LEP 910 Service</b>	<ul style="list-style-type: none"> <li>- Lower probability of wrong mixing ratio due to cartridge format.</li> <li>- Reduction in intermediate stocks.</li> <li>- Time of LEP stage.</li> <li>- Roughness of process</li> <li>- Same disposables than AHP PR 108</li> <li>- Fast curing</li> <li>- Easy to apply for non-experienced operators</li> <li>- Suitable for application by rope</li> <li>- Application on blade directly</li> </ul>	<ul style="list-style-type: none"> <li>- Necessity of use a brush to get a smooth surface.</li> <li>- Application of 2 layers.</li> </ul>
<b>AHP LEP 920 Service</b>	<ul style="list-style-type: none"> <li>- Lower probability of wrong mixing ratio due to cartridge format.</li> <li>- Reduction in intermediate stocks.</li> <li>- Same disposables than filler.</li> <li>- More than 500 µm in one hand.</li> <li>- Time of LEP stage.</li> </ul>	<ul style="list-style-type: none"> <li>- Application by spatula might be incompatible with rope application</li> </ul>

	<ul style="list-style-type: none"> <li>- Great Finish</li> <li>- Good feedback of operators.</li> <li>- Levelling</li> <li>- Application on blade directly</li> </ul>	
--	---	--

*Table 8 - Feedback from TotalWind's technicians.*

Regarding the application methods, the conclusions extracted from the tests were:

- Total Wind preferred the primer in the same colour as LEP.
- As the product is to be applied using rope access, the operator has only one free hand to work. Therefore, TotalWind selected the application method that utilised the roller.
- In order to improve the finishing surface, a brush was used to level the finish.
- Application by filling knife was the fastest way. However, it was not suitable for operators undertaking rope access.

TOTAL WIND			
PRIMER	LEP by Roller	LEP by Filling Knife	Comments
			<ul style="list-style-type: none"> <li><input type="checkbox"/> Adhesion Primer: <ul style="list-style-type: none"> <li><input type="checkbox"/> The primer is spread in a container instead of be applied on the blade.</li> <li><input type="checkbox"/> Change the colour to Grey as LEP</li> </ul> </li> <li><input type="checkbox"/> LEP by roller: <ul style="list-style-type: none"> <li><input type="checkbox"/> Suitable application by rope access.</li> <li><input type="checkbox"/> Needed to levelling the Surface with a brush.</li> <li><input type="checkbox"/> <b>Recommended application.</b></li> </ul> </li> <li><input type="checkbox"/> LEP by filling knife <ul style="list-style-type: none"> <li><input type="checkbox"/> Not suitable to be applied by rope Access due to the operator needs to have a free hand.</li> <li><input type="checkbox"/> Quick application</li> </ul> </li> </ul>

*Figure 55 - Total Wind service application results.*

### 2.7.6 Definition of repairing procedure

Repairing of an eroded zone must ensure a transition zone without edges (<0.4mm). The repair procedure developed by Aerox, which offers a good transition between non-repaired and repaired zone, is summarised below. Further details can be seen in section 4.7 with full details provided in Annex A.

1. Sanding of the zone to be repaired until the putty/porefiller.
2. Sanding of a transition zone of at least 5 cm between the eroded and non-eroded surface. The sanding must reach the primer in the edge in contact with the zone to be repaired.
3. Application of one layer of primer covering both eroded and transition zones and a layer of LEP covering the eroded zone.

Application of a second layer of LEP covering both eroded and transition zones.

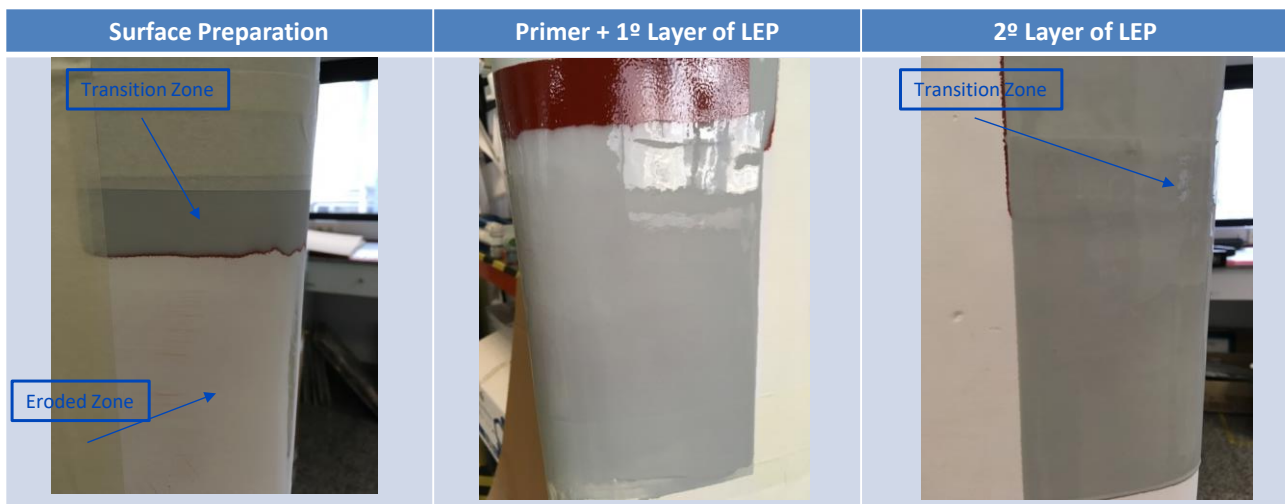


*Figure 56 - AEROX AHP LEP repairing procedure.*

### 2.7.7 Numerical Simulation Approach: Service Application and Manufacturing concerns that influence leading edge protection erosion performance in wind turbine blades

Under impingement, the blade composite structure is affected by the shock wave caused by the collapsing water droplet on impact, and the elastic and viscoelastic responses of the materials, surface preparation, coating application and the interactions between them. The capability of the LEP coating to transfer wave energy can influence the erosion damage. Stress reflections oscillate repeatedly through the coating and structure until damped by the material properties to reduce the energy of the initial shockwave. By matching delamination resistance between the coating and the blade structure, coating life time under repeated impacts can be extended.

### 2.7.7.1 Effect of thickness variation through the multilayer system

In a first study, the LEP thickness variation due to the application method was analysed in order to define its influence on erosion and its capability to attenuate the stress through the thickness, see Figure 8 and 9.

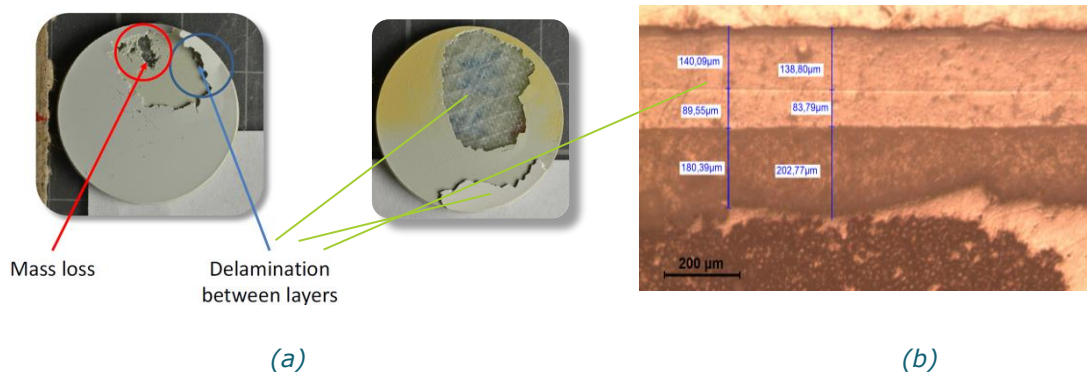
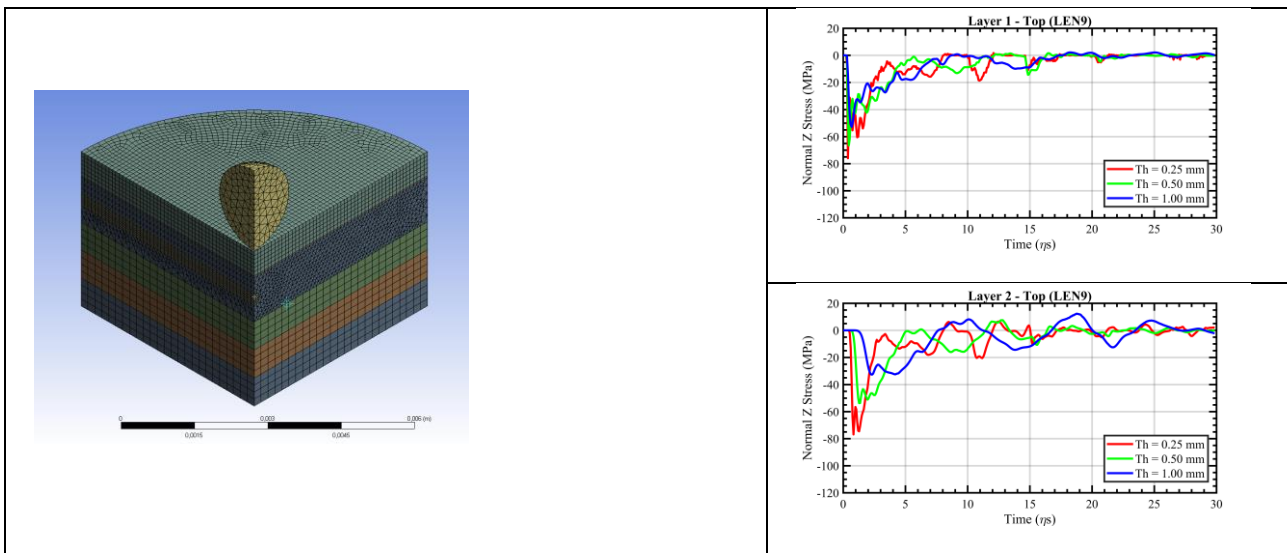


Figure 57 - (a) Rain erosion testing specimens. Erosion failure due to mass loss on surface and interface delamination. (b) Multilayer system microscopy. Two coating layers with different thickness depending on the application method, define an interface that tend to delaminate upon impingement.



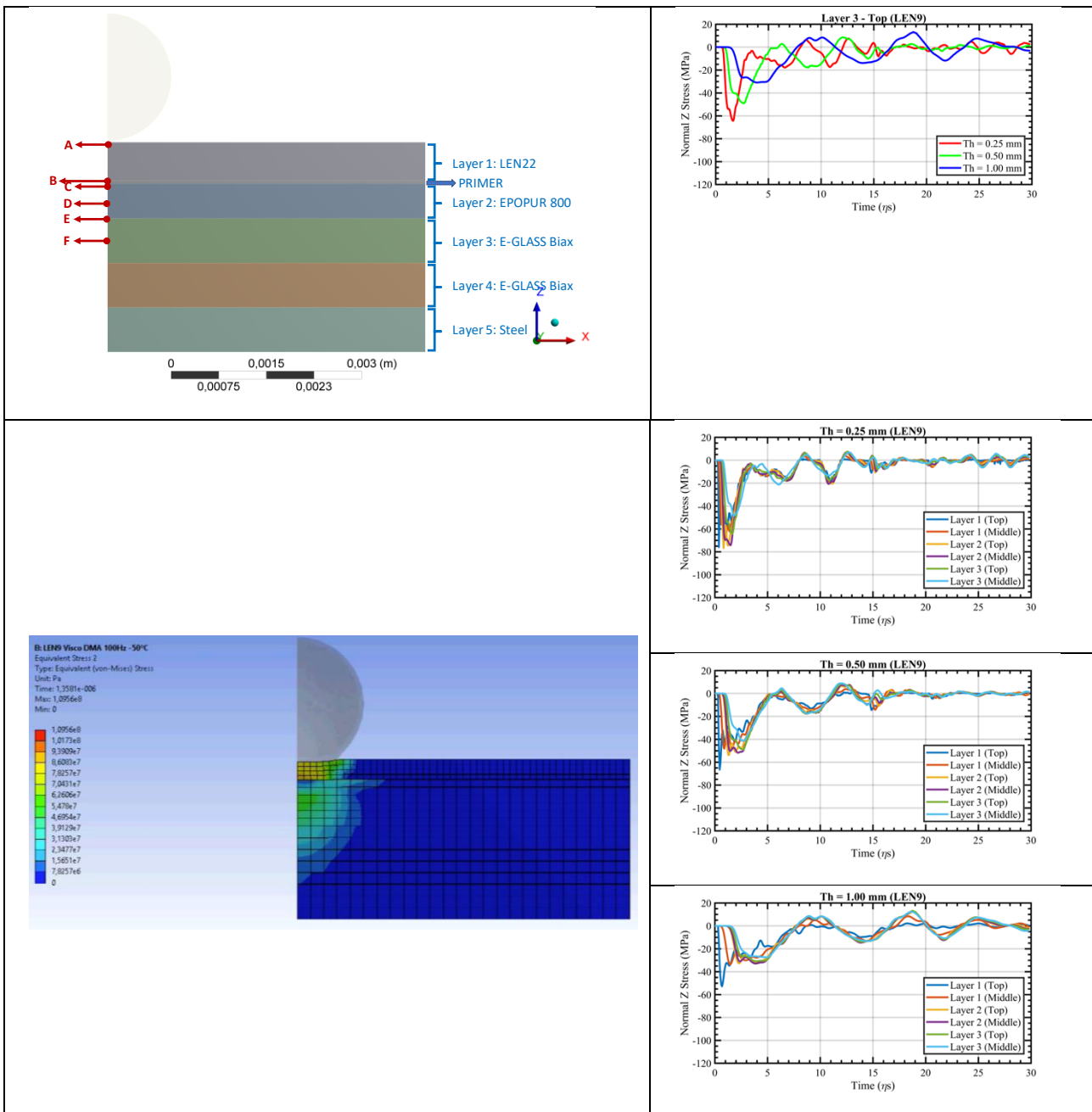


Figure 58 - AEROX AHP LEP single impact simulations with LEP layer thickness variation for the blade multilayer configuration system.

### 2.7.7.2 Process design for erosion coating. Modelling manufacturing factors that affect Interface coating-laminate relation with mass loss in erosion.

Destructive mechanical testing was also undertaken. Pull-off strength testing of the samples showed the failure in the composite laminate and hence the capability of the coating to assure the required target strength. A specially-developed peeling test for interface coating-laminate adhesion response quantification showed that these testing results correlated with the rain erosion tests, as shown in Figure 59 and Figure 60.



Figure 59 - (a) Rain erosion testing specimens. Erosion failure due to mass loss on surface and interface delamination for coupons depending on Primer application, Sanding and no sanding processing (b).

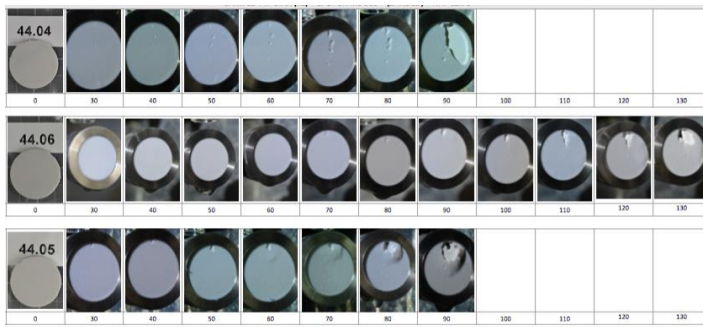


Figure 60 - (a) Rain erosion testing failure evolution due with sanding processing.

The objective of the work was to assess the coating-laminate interface through numerical modelling, correlating the manufacturing coating application factors (curing, sanding, spray, roller, trowel, etc.) with the material's resistance to rain erosion damage through mass loss measurements in the Whirling Arm Rain Erosion Rig (WARER) at the University of Limerick.

The coating-laminate adhesion and erosion is affected by the repetitive shock wave caused by the collapsing water droplet on impact. In order to assess the mechanical response of the multilayer interfaces, it was defined the Cohesive Zone Modelling (CZM) between layers to be incorporated in the numerical modelling of the rain droplet impact. The proposed methodology states the CZM input parameters with both physical Pull-off and Peeling testing of manufactured specimens and their numerical modelling. The approach allows one to account for the effect of the surface preparation and coating application and the interactions between them with the multilayer system. This methodology has been studied with the coating curing conditions, but can be extended to any other coating surface application process like sanding, spray, roller, trowel, primer, etc. (further work on its development).

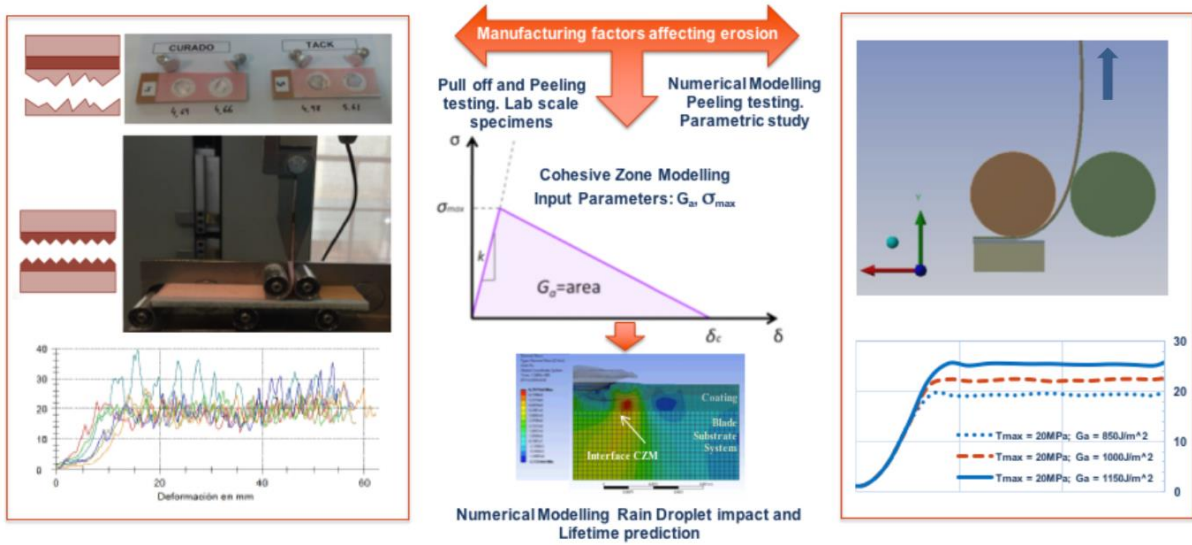


Figure 61 - Proposed methodology for the modelling of manufacturing factors that affect erosion. Input parameters for Cohesive Zone Modelling are determined with Peeling testing and its simulation.

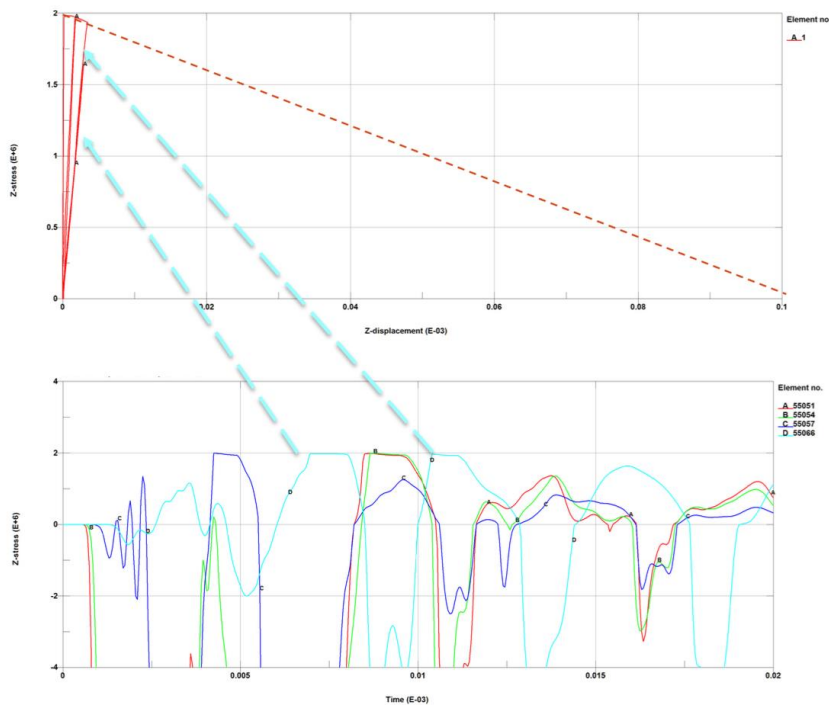


Figure 62 - Stress vs Strain evolution for repeated impacts at interface layer. Cohesive Zone Modelling determined with Peeling testing and its numerical simulation.  $G_a$  Adhesive fracture energy loss estimation

## 2.8 Process design for erosion coating

Leader: Siemens Gamesa

Regarding the Aerox solution, Siemens Gamesa carried out a preliminary study of the possible application process in factory and in field.

Siemens Gamesa and Aerox carried out a preliminary validation of the possible application process (**Fejl! Henvisningskilde ikke fundet.**). Although the applicability is good, some improvements are needed in order to facilitate the correct finish and optimal time duration of the application in field.

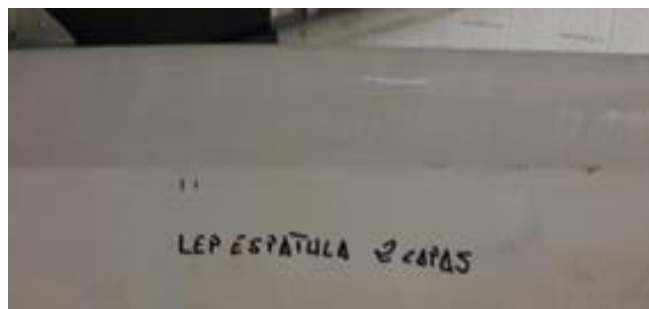


Figure 63 - Real Blade tip applied with Aerox solution

Recommendations were identified in order to reduce the complexity of the process and increase its robustness. Moreover, it was needed to review the need to sand the LEP as well as the need to define and optimize the process for the transition area. In addition, some optimization should be carried out related to the viscosity, colour or brightness.

Optimizations were done by Aerox of their LEP and new process tests were carried out on a real leading-edge airfoil piece of ca. 7m. Different application methods and thicknesses were tried on the same airfoil. One layer of Aerox LEP was coated by spatula on the airfoil with a thickness in the range 300-700µm of wet film thickness. Sagging was observed when the wet film thickness was above ca. 450-500µm, but the levelling and smoothness of the surface was adequate when the thickness was below this range.



Figure: process tests on 7m leading-edge airfoil with Aerox LEP solution



## 2.9 Retrofittable add-ons: modelling

Leader: Siemens Gamesa

### 2.9.1 Aim

The aim of this section is to show the preliminary results obtained from aerodynamic and acoustic measurements conducted in the Virginia Tech Stability Wind Tunnel in June 2017. Background Aerodynamic noise produced by current wind turbines is critical due to environmental aspect and local regulations.

There are several procedures to get a better performance relating to noise produced by wind turbines. At the same time, it is important not to get any penalization on energy production to keep the wind farm in optimal production conditions and not to affect to the economic benefit of the wind farm.

Serrations are proposed as the geometrical solutions to reduce noise emissions. The advantages of this system are that it can be used on current wind farms without bigger modifications, are relatively cheap to install and can achieve important noise reductions.

### 2.9.2 Design and Definition

Prior to defining the test matrix for the wind tunnel test, a design process was completed and design parameters have been fixed.

The most important parameters in its design are:

- Ratio: Relationship between length and extension.
- Angle: Angle between the aerodynamic profile and the device (see **Fejl!**  
**Henvisningskilde ikke fundet.**)

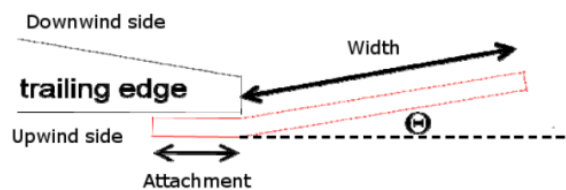


Figure 64 - Definition of Angle

- Location: Pressure or suction side.
- Length. In relation to the rope of the aerodynamic profile.

All these parameters are taken into account when making a first aerodynamic design. This is later analysed in a wind tunnel testing campaign. It is therefore important that the design of the testing campaign considers all these parameters.

The definition of these parameters depends on the aerodynamic airfoil geometry on which they will later be located. Additionally, the positioning on the blade does not cover the entire length

but only its last part, towards the tip. Therefore, it is not necessary to analyse all sections of the blade, but only those where these devices will be placed.

Along the entire length of where the devices will be placed different sections are considered, taking into account the design factors that have been previously identified.

This makes the design process iterative, and different alternatives are considered until finding the optimal solution. This solution must be then be validated.

The first iterations worked on the definition of how many different sections of the blade needed to be defined, so that they covered the entire length where the devices were placed. **Fejl! Henvisningskilde ikke fundet.** shows the chord vs the radius of the blade and identifies three separate sections (identified by the horizontal lines) of the blade which will have different designs of VG installed. This ensures the design of the retrofittable add-ons is appropriate for its position on the blade.

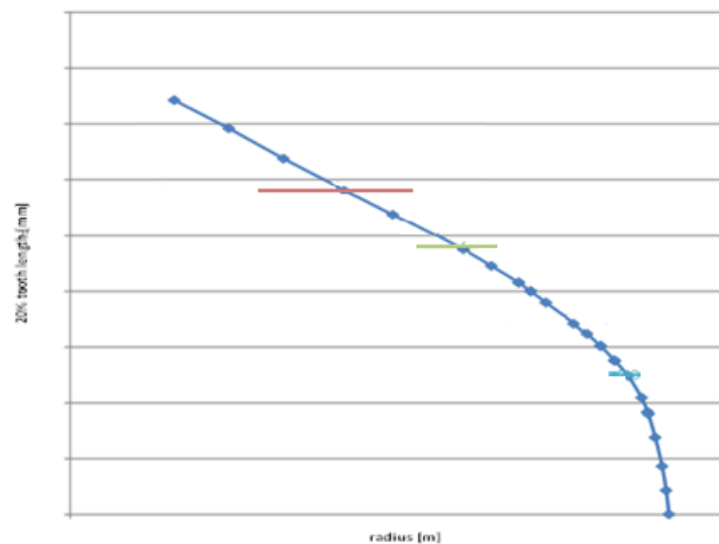


Figure 65 – Graph showing the chord vs distance from the hub

Once the main sections or blocks of devices have been identified, the next step is to adapt these sections to obtain the number of panels and their geometry.

The geometric definition of these panels is very important to their subsequent manufacture and future assembly in the wind turbine

### 2.9.3 Test Configurations

Once the design of the aerodynamic airfoil geometry of the validation wind turbine is confirmed the next phase of the project consists of evaluating these designs in a wind tunnel test campaign. The target of this test is verifying those design parameters already mentioned, and then selecting the optimal designs that can be taken on in a validation field test.

This project phase is very important, since it will allow us, with a relatively low cost, to evaluate different designs.

The test matrix includes the following parameters:

- Configuration: If it is clean or dirty
- Device: If it is placed or not to measure the effect it introduces
- Location: If it is in the suction or pressure area
- Angle: Different angles are tested to analyse their effect

As a result of all the combinations, we have a matrix that involves 20 different tests, divided into 6 main areas that will be carried out in the wind tunnel (**Fejl! Henvisningskilde ikke fundet.**).

No. of Tests	Configuration	Device	Location	Angle	Target
2	Clean/Dirty	No	—	—	Airfoil with no device
3	Clean	Yes	Suction	3 angles	Suction Area
5	Clean	Yes	Pressure	5 angles	Pressure Area
2	Clean	Yes	Pressure	1 angles	Material
3	Clean	Yes	Pressure	3 angles	Ratio
5	Clean/Dirty	Yes/No	Pressure/Suction		Best design

Table 9 - Wind Tunnel Test Matrix

To perform these tests, the wind tunnel of the Technological University of Virginia was selected. Among the reasons for this choice are the technical characteristics of the tunnel and availability to perform the tests.

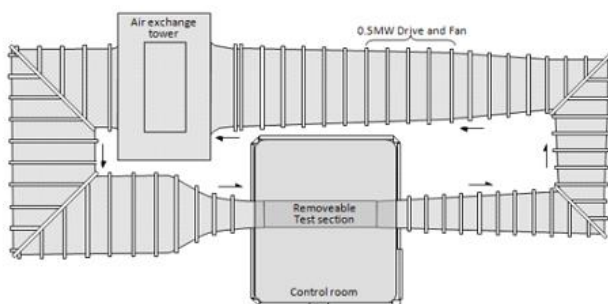


Figure 66 - Technological University of Virginia Wind Tunnel

To perform the tests, in addition to manufacturing the devices, an aerodynamic airfoil had to be manufactured that replicated the same aerodynamic airfoil of the wind turbine blade that will later be used for field validation. This is shown below in **Fejl! Henvisningskilde ikke**

fundet.. The design of the vortex generator serrations is shown in **Fejl! Henvisningskilde ikke fundet.**

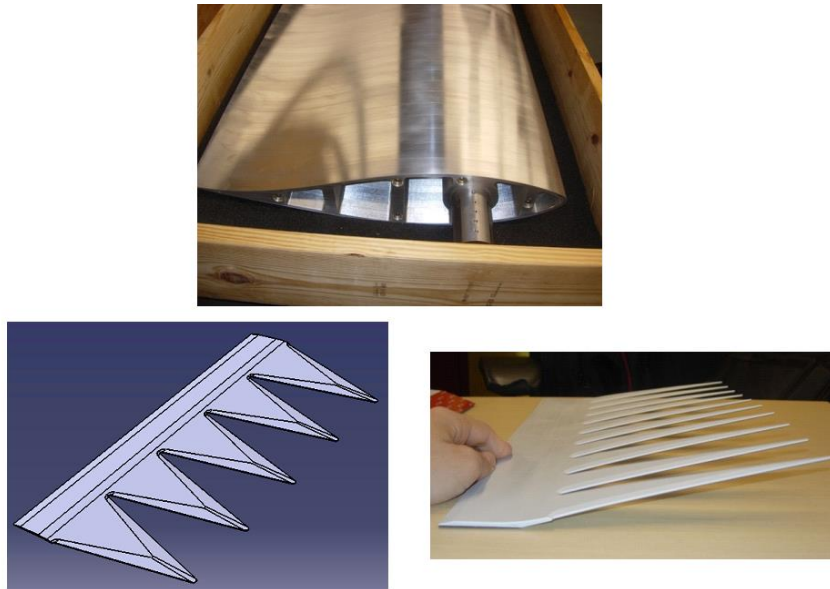


Figure 67 - Airfoil model and serrations

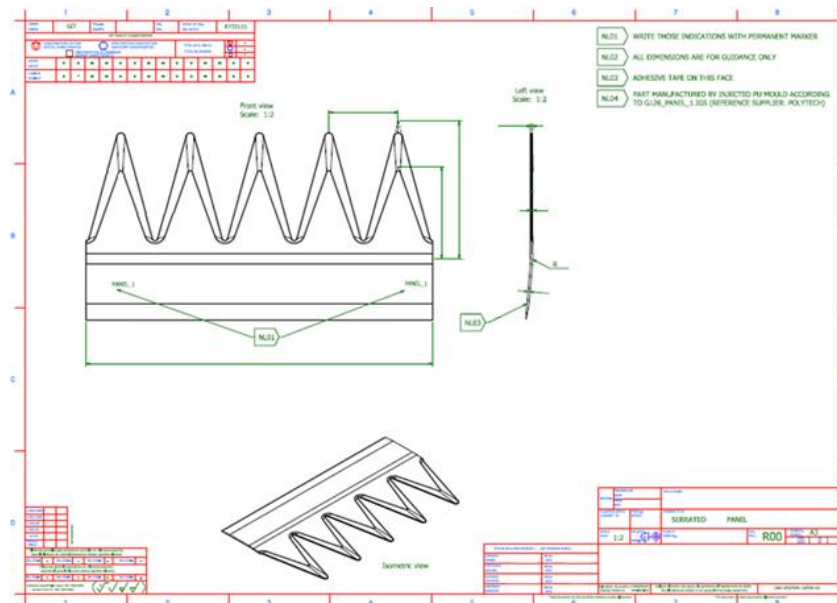


Figure 68 - Design of the airfoil serrations

## 3 Work Package 3 – Validation tests

### 3.1 Coating & metallic insert small scale tests: Material & subcomponent tests

Leader: Siemens Gamesa

Siemens Gamesa has collaborated with ODSL and Aerox in order to define the test specification for each solution based on requirements defined for leading edge solutions and coatings of blades for wind turbines.

#### 3.1.1 Aerox coating

Regarding Aerox coating solution, test specification and validation criteria in each case has been closed taking into account not only functional requirements but also application requirements in factory and field. Thus, a test specification table has been agreed in order to validate different requirements defined.

PROPERTY	Requirement	Method
Density	Reported by the supplier	ISO2811
Viscosity	Reported by the supplier	ISO 2431, DIN 53211-6 or ISO 2555 or ISO2884
Mixing ratio (by volume)	Reported by the supplier; including tolerance	N/A
Mixing ratio (by weight)	Reported by the supplier; including tolerance	N/A
Color	dE<1 and dE<2 (beaconing colors) according to GPR15001	ISO7724 and ASTM D2244
VOC content	H&S, Environment SGRE	ISO11890
NCO content hardener	Reported by the supplier	ASTM D5155
Solid content (by volume) By weight	100% by volume	ISO3251
Gloss	Reported by the supplier	ISO2813
Opacity	Visual Inspection	ISO2814 or ISO6504-1
Hiding power/Layer thickness	Hiding power 100% (layer thickness $\mu\text{m}$ )	N/A
UV-Visible blocking performance	0% transmittance at all layer thicknesses	N/A
Glass transition temperature	NA	N/A
Hardness(SHORE D)	N/A	N/A
Rain erosion resistance	5h	DNVGL-RP-0171
Adhesion (pull-offs)	min. 5MPa for individual measurements	ISO 4624
Adhesion (X-cuts)	Level $\leq 1$	ISO 2409 &/or ISO 16276-2
Repairs	Repair procedure needs to be reported by supplier	N/A
Sagging resistance	Min 150 $\mu\text{m}$	DIN EN ISO 16862 or ASTM D4400
Workable life/Working time	3- 5 min at 15 - 35 °C and 20 - 85% RH	N/A
Drying time	Reported by supplier - short drying time preferable	DIN 53150
Pot life	Min. 30 min at 15 - 35 °C and 20 - 85% RH	N/A
Gel Time	Reported by supplier	Gel timer
Application conditions	15 - 35 °C and 20 - 85 % RH	N/A
Curing charts/Curing time	Reported by supplier	N/A
Sanding charts	N/A	N/A
Flexibility	no damage, no cracks using $\varnothing$ ; 23 °C - 25mm mandrel; -40 °C - 48mm mandrel; coating thickness report	ISO1519
Particle erosion	erosion curve (mass loss vs. Mass load); max. Slope 1.5 ( $\text{mg}/(\text{g}/\text{cm}^2)$ )	ASTM G76
Thermal conditioning	Pull-off test. min. -5 MPa (thermal)	ISO 6270
Thermal at low temperature	Pull-off test. min. -5 MPa (thermal at low T)	Table 5.3.5 GMS17020
UV conditioning	Color change max. 4.5 dE; Gloss change report; Flexibility: no damage, no cracks using $\varnothing$ 25mm mandrel	ISO 11507-B or ASTM G151
Resistance to water	Report by supplier	ASTM D570
Hazardous Constituents	PBE-1-016	PBE-1-016
Shelf Life	Not less than 1 year	
Defects	The product should be homogenous and free of foreign objects, lumps and the like	N/A

Table: requirements from Siemens Gamesa of Aerox LEP

Pull-off adhesion tests done by Aerox previously showed values below Siemens Gamesa (SGRE) specification of 5Mpa. Therefore, tests have been repeated using the Siemens Gamesa configuration regarding filler and using 3 different Aerox configurations from Aerox: Primer 202, LEP 920 y Primer 202+ LEP 920 according to this figure:

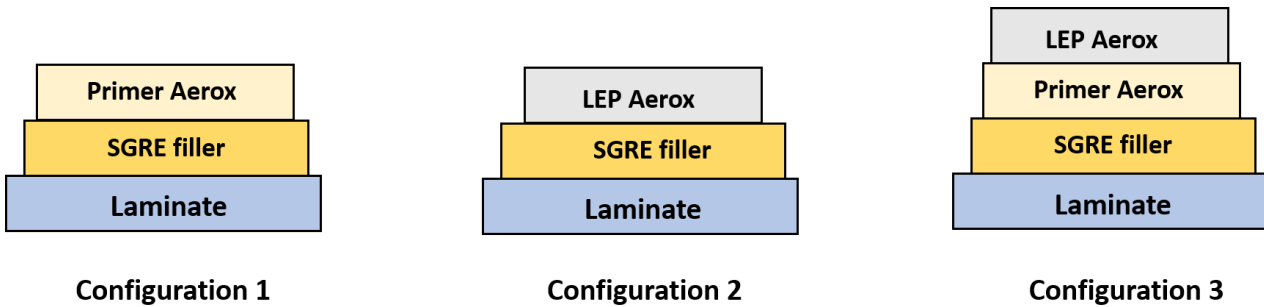


Figure: pull-off configurations tested

Obtained results indicated that adhesion between filler and primer (configuration 1) and between LEP and filler/primer (configuration 3) is above specification. However, adhesion between LEP and filler (configuration 2) is not so good and some values are not above specification (see figure below).

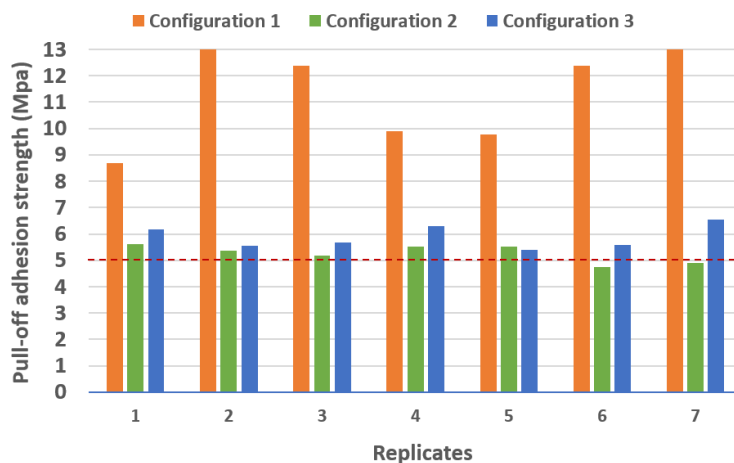


Figure. Pull-off adhesion results for different configurations

Taking into account these results, it was decided to coat the SGRE panels including filler for rain erosion tests and other characterization techniques using Aerox primer and LEP. Pull-off adhesion tests done by Siemens Gamesa confirms that most of values are above the specification of 5Mpa, although one individual value is below specification as can be observed in the picture below.

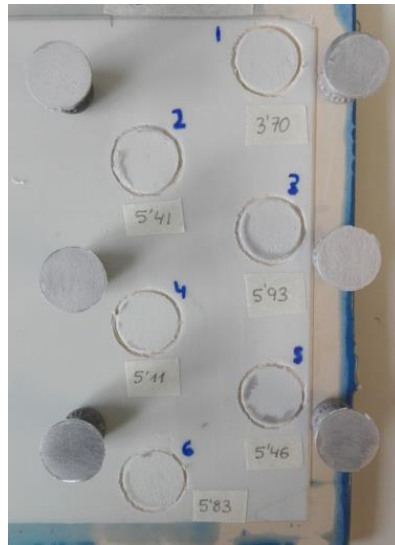


Figure: pull-off adhesion tests done by Siemens Gamesa with Aerox LEP

### 3.1.2 Metallic Insert Solution (ODSL)

Before closing a test specification, a preliminary study of the metallic insert solution based on the material technical data and the design selected was carried out by the structural and design section of Siemens Gamesa in order to ensure that the solution could be feasible from the structural point of view.

Once ensured of the preliminary feasibility, Siemens Gamesa and ORE-Catapult agreed the test specification in order to evaluate not only the functional characteristics of the solution but also the possible impact in the structure design of the blade and the integrity of other elements such as the adhesive used, etc. For the DP 490 adhesive selected, a mixture of shear and peel tests, as defined in Section 2 of Milestone 8, were performed in relevant temperature and humidity environments to prove the capability of the selected adhesive and bonding solution to retain the nickel tiles on the blades during WTG demonstration. Adhesion to the blade composite averaged 23MPa with failure occurring in the composite which is the ideal solution. Adhesion to the nickel was lower at 16MPa when used with a standard aerospace primer and showed some adhesive failure. To determine if 16Mpa is sufficient for the WTG installation, Flexural Test Rig tests were performed. Durability of the nickel solution was also assessed using rain erosion, sand erosion and corrosion tests. The rain erosion results are described in 3.3.2.

## 3.2 Wind Tunnel Test for Low Drag VGs and Metallic Leading Edge Protection

Leader: ODSL / CENER

Wind tunnel tests were performed in the WindGuard wind tunnel for a thick airfoil with VGs mounted on its surface.

This test campaign is complementary to the wind tunnel tests performed by ODSL with vortex generators and the leading edge protection system. The aim of ODSL is to test the VGs working with the leading edge protection system while the aim of CENER is to test the performance of vortex generators.

The test campaign was performed on September 2018. The airfoil measured in the campaign is the S839 airfoil, a 30% thickness airfoil designed by CENER. The Reynolds number was  $4e6$ . The VGs tested were located at 30% of the airfoil chord and they had a height of 2.25mm. Some pictures of the VGs manufactured for the campaign are shown next.

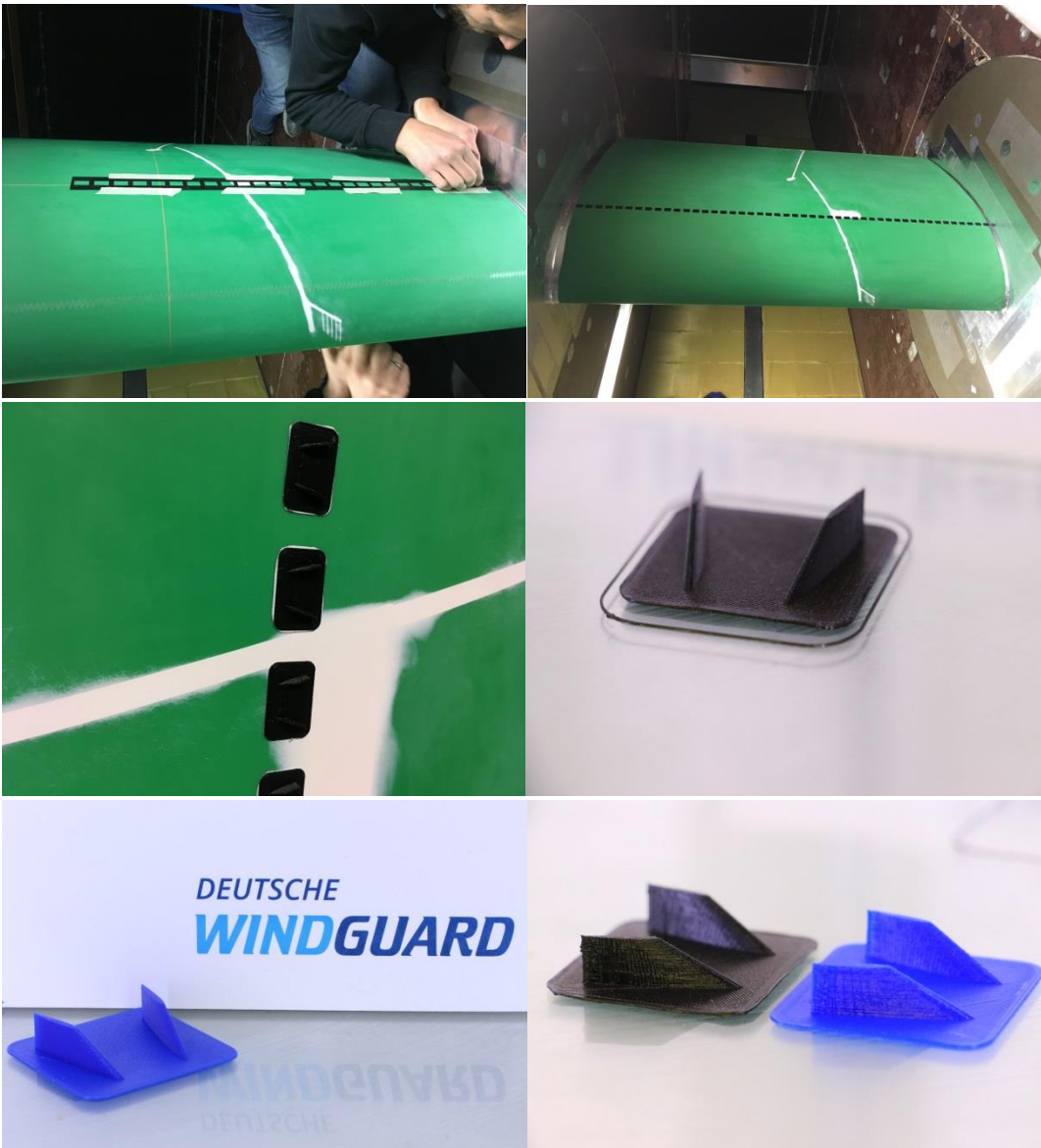


Figure 69 – Pictures of CENER’s Low Drag VGs during the tests in the Windguard wind tunnel.

In the following figures the aerodynamic polar curves measured in the wind tunnel are shown: to measurements were done for the nominal airfoil in clean conditions (marked as Windguard Re=4e6 and Windguard Re=4e6 B), one measurement with ZZ tape (Windguard Re=4e6 ZZTape) and with the VGs mounted on their surface (Windguard Re=4e6 VG).

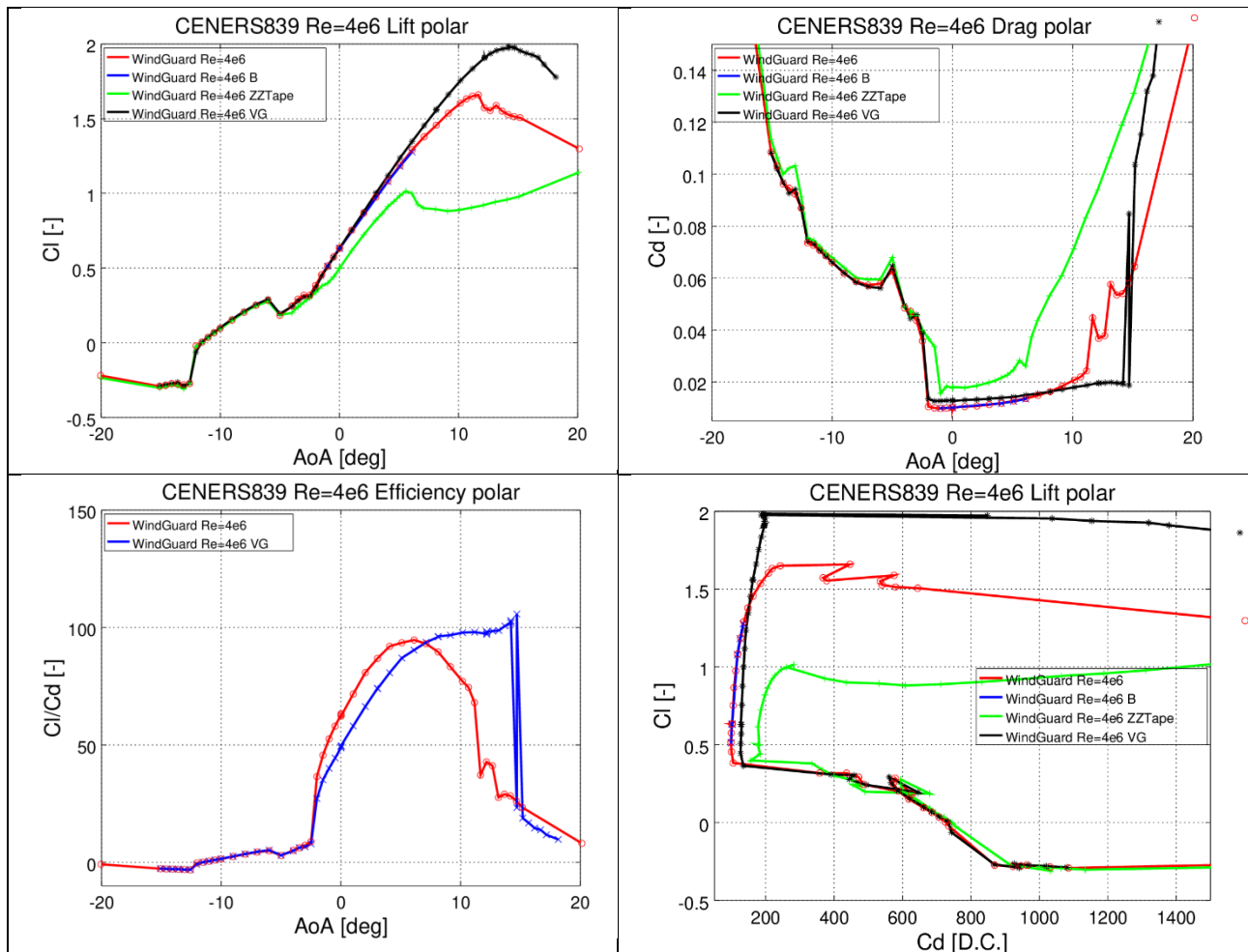


Figure 70 – Measurement of aerodynamic curves of the S839 airfoil in the Windguard wind tunnel.

As can be observed in the measurements, the use of Vortex Generators lead to an increase in lift coefficient, a slight increase in drag and an increase in efficiency. The angle of attack of maximum efficiency increases when installing VGs in the wind tunnel.

The measurements were compared with CFD computations and with XFOIL (panel code) calculations and both numerical and experimental results matched.

### 3.3 Erosion tests

Leader: ODSL

#### 3.3.1 AEROX AHP Solution

AEROX, as part of their development of the AHP system, performed a series of rain erosion testing at the ORE Catapult. This was supplementary to the rain erosion testing performed in the WARER rain erosion test rig at the University of Limerick, as the ORE Catapult rain erosion test rig uses aerofoil shaped samples rather than the WARER flat samples used for the product development tests. The aerofoil shape introduces challenges for the coating application process on the rain erosion samples for testing, and also on wind turbine blades. The rain erosion results on aerofoil samples are therefore much more representative of a product's performance on a blade.

The ORE Catapult R&D AS rain erosion test rig is also compliant with the draft DNV GL Guideline: DNVGL-RP-0171 Testing of rotor blade erosion protection systems. This standard, soon to be published, is used by the major wind turbine manufacturers, Vestas, LM Wind Power and Siemens-Gamesa who all have the same R&D AS test rig. Therefore, the application process developed in ORE Catapult rain erosion testing on the APH coating will be applicable to final qualification OEM rain erosion tests.

In total, ten sets of rain erosion testing were performed for AEROX in Phase 1, with each set testing three samples, one for each of the three blades on the ORE Catapult test rig. These tests reviewed various configurations of the AHP coating solution but showed significant variability and shorter than expected lifetimes, the latter thought to be due to the larger droplet diameter in the ORE Catapult test rig. The test rig can be seen in Figure 71. In Phase 2 a further six samples were tested of the same coating configuration to reduce variability. To further analyze any variation in test results, the coating thickness was mapped before test and showed significant variation along the length of the samples due to the application procedure. With this coating configuration, rain erosion lifetimes were doubled, and no correlation could be identified between erosion initiation points and thin/thick areas of the coating.



*Figure 71 - ORE Catapult Rain Erosion Test Rig*

### 3.3.2 Metallic Leading Edge Solution

As described in Section 2 of the report 'Baseline Report of Metallic Leading Edge Erosion Protection Solution' (Rev 00, dated 30 Nov 2018) nickel shields have been used in the aerospace, helicopter and defense industries for approximately 50 years due to their excellent resistance to rain erosion.

The current industry best performing benchmark products are all Polyurethane-based. Certain types of polyurethane polymers are well-known for their excellent rain erosion resistance up to tip speeds of 85m/s. However, at higher tip speeds, polyurethanes can initiate erosion and breakdown rapidly. The best performing products currently on the market for both production and repair are 3M's W8750 tape and the Polytech ELLE softshell. The nickel shield was therefore benchmarked against the 3M W8750 tape and Siemens-Gamesa's current leading leading edge coating solution. The erosion test results are reported in Section 3 M8 Coating and Metallic Inserts Small Scale Tests. The nickel shields didn't show any erosion visible by eye after testing for 85 hours under standard test conditions of 1000RPM, compared to lifetimes of 17 hours for the 3M W8750 tape and 8 hours for the Siemens-Gamesa coating system. This was roughly estimated as a wind turbine lifetime of over 30 years. To study the effects of increased tip speed, the nickel shields were also tested at 1200 and 1386 RPM, the latter of which is the maximum capable in the test rig. Some microscopic features were observed on the surface of the nickel shields, and the test operator thought that he could feel a slight roughening, but no mass loss was observed. To clarify if erosion had occurred or not, a 3D optical microscope was procured.

The results of the 3D microscopy are described in Milestone 20 WP3: Nickel erosion performance analysis including purchase of 3D microscope. At the tip end of the 1386RPM samples, equivalent to tip speeds of 173m/s, the maximum depth of feature was 160 $\mu$ m and width 1.6mm. As the width is less than the droplet size of 2.4mm, it was concluded that the features observed were pre-erosion cracks and that the samples were still in their erosion phase known as incubation i.e. pre- active erosion. A theoretical approach was taken to look at effects of changing the nickel thickness on erosion performance which concluded that theoretically the damage rate should be the same but due to the depth of feature being over half that of the shield thickness, thinner shields should not be used unless the consequence of cracks penetrating the shield were determined as acceptable. A review was also made of nickel shields in the aerospace and helicopter industry. It was noted that nickel shields with a 25 year rotational life at a tip speed of 120m/s, still do less 43% less rotations than helicopters at tip speeds of 220m/s. Therefore it was concluded that less effective helicopter shield solutions, such as titanium or stainless steel, used further away from the tip of the blades, may be sufficient for offshore wind turbines.

### 3.4 Blade shear deformation measurements

Leader: TNO

The measurement of the blade shear deformation at the LDT with and without the X-Stiffeners installed are planned to be performed using the cross sectional shear distortion sensor (CSSDS), TNO developed for this project.

Cross Sectional Shear Distortion (CSSD) is an indicator for the deformations a wind turbine blade experiences during operation. In the context of this project it is measured as the length change of the two diagonals of the rear box of one (specific) blade at certain distances from the blade root of the LD). The diagonal length change is expected to be less than 30 mm by the work package partners.

For illustration a cross section (at R14) is depicted in Figure 37 below.

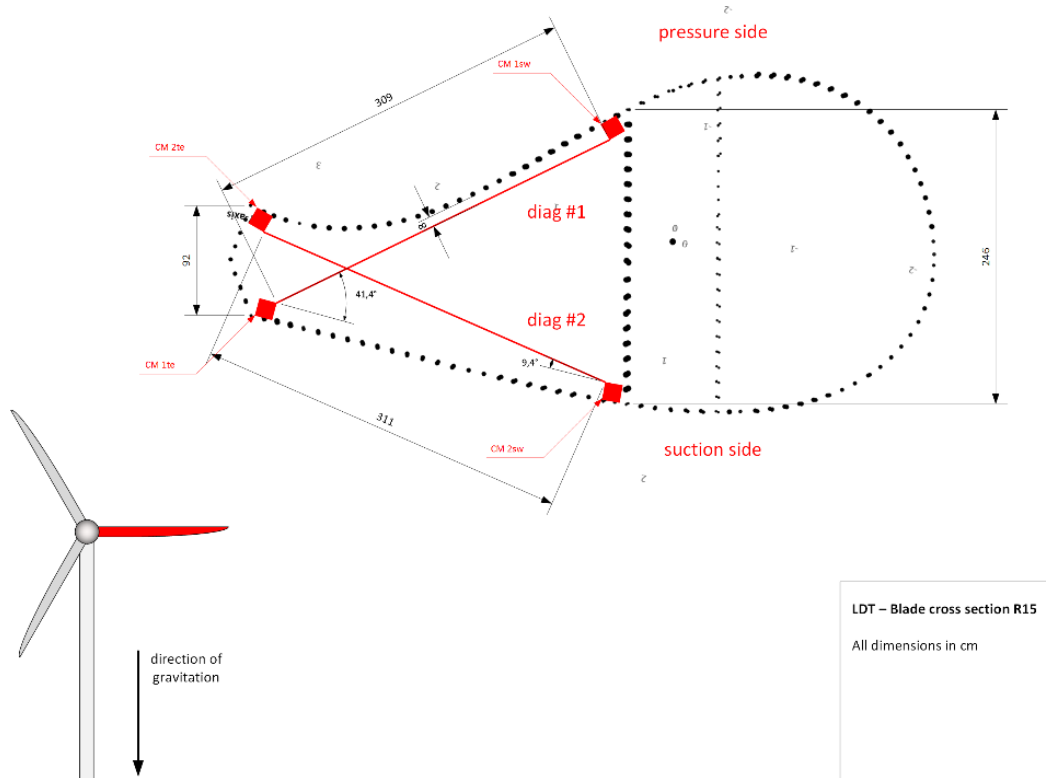


Figure 72 - Cross section R14 of LDT

To determine the length of the cross sectional diagonals, TNO developed the CSSDS based on its Fibre Bragg Grating (FBG) technology and is designed such, that it can measure the diagonal length change of the specified cross sections with an accuracy and precision of below 0.5 mm over a period of operation of 12 months. Also it has to be able to be installed and decommissioned by trained technicians and comply to the requirements of the LDT.

The two most complex components that had to be developed for the CSSDS are the Fibre Corner Mount (FCM) and the Hub Cabinet (HC) and are therefore briefly discussed subsequently.

The main purpose of the FCM is to transfer rear box deformation into the sensing optical fibre to pick up upon the strain along the diagonals. Therefore it has to:

- Provide a robust and rigid interface to the blade surface;
- Clamp the sensing optical fibre without slip and not exceeding the minimal bend radius of 15 mm;
- Apply a well-defined pre tension to the fibre, such that the fibre can also measure compression of the rear box diagonals;
- Be able to be installed simply and safely by dedicated wind turbine technicians (project partner).

One FCM is placed in each of the 4 corners of the 3 designated cross sections of the rear box as depicted in Figure 72 symbolized by red cubes. Although the CSSDS sensor is developed by TNO, it had to be installed by dedicated trained wind turbine technicians in a wind turbine that is managed by ORE Catapult and its contractors.

The separation of tasks and responsibilities inherent to this construction and the fact that it will be a first time right installation form a risk for the installation and operation of the CSSDS that is mitigated by a test integration of the CSSDS into the blade test rig at DTU.

There the complete CSSDS system was installed with two cross sections of the blade equipped in November 2017. The test integration (see Figure 73) resulted in an improved installation manual, training the offshore technicians and confidence to be able to integrate the CSSDS successfully into LDT with the estimated effort.



*Figure 73 - CSSDS test integration at DTU, installed FCMs inside the blade (left) and test rig (right)*

The complete CSSDS system was installed with two cross sections in August 2018.

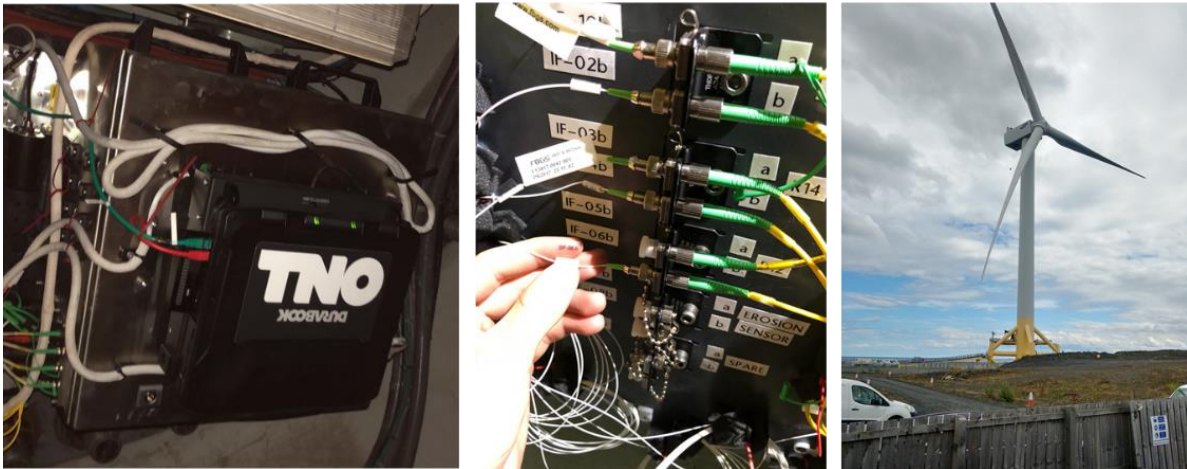


Figure 74 – Overview sensor components during integration of the CSSDS in the Levenmouth turbine

In the figures below the output is shown of the CSSDS. The first picture, Figure 75 is a zoom-in of the wavelength shift during start-up. The wavelength shift can be translated into strain and this is shown in **Fejl! Henvisningskilde ikke fundet.** for two diagonals at two cross sections.

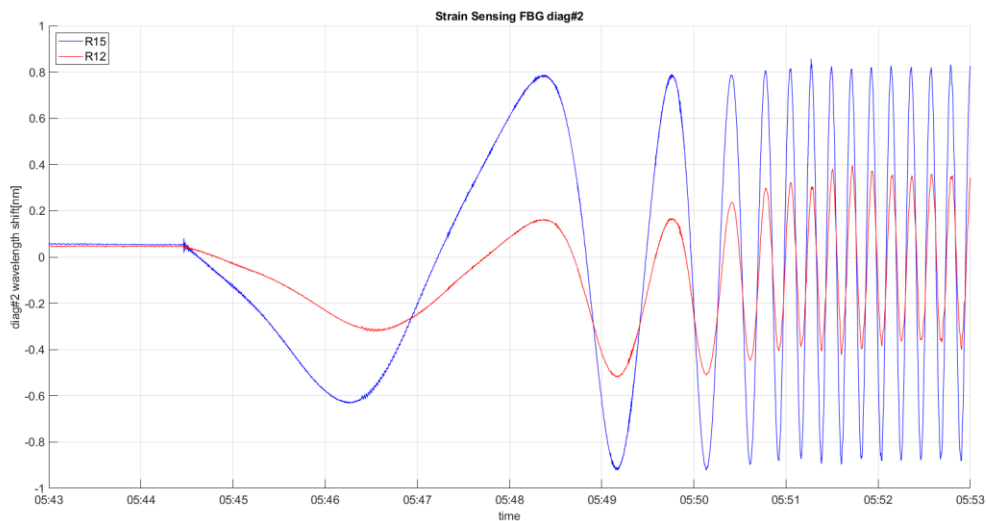


Figure 75 - Zoom into above example data for turbine start up at about 5:45 on 31.07.2018

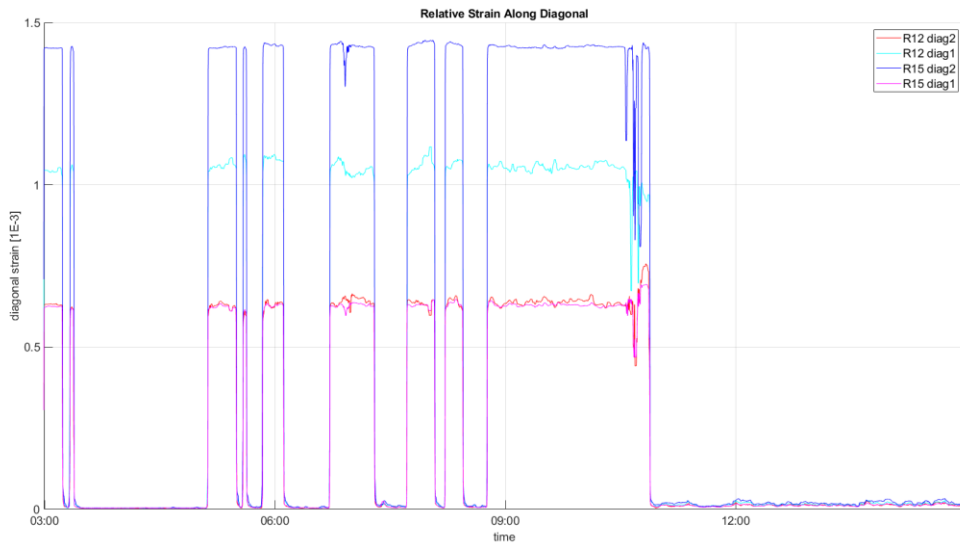


Figure 76 - Derived strain data for above example data for all diagonals on 31.07.2018

In the figure below the diagonal strain is shown for diagonal 2 at location R15, for wind speeds varying from 5 up to 14 m/s.

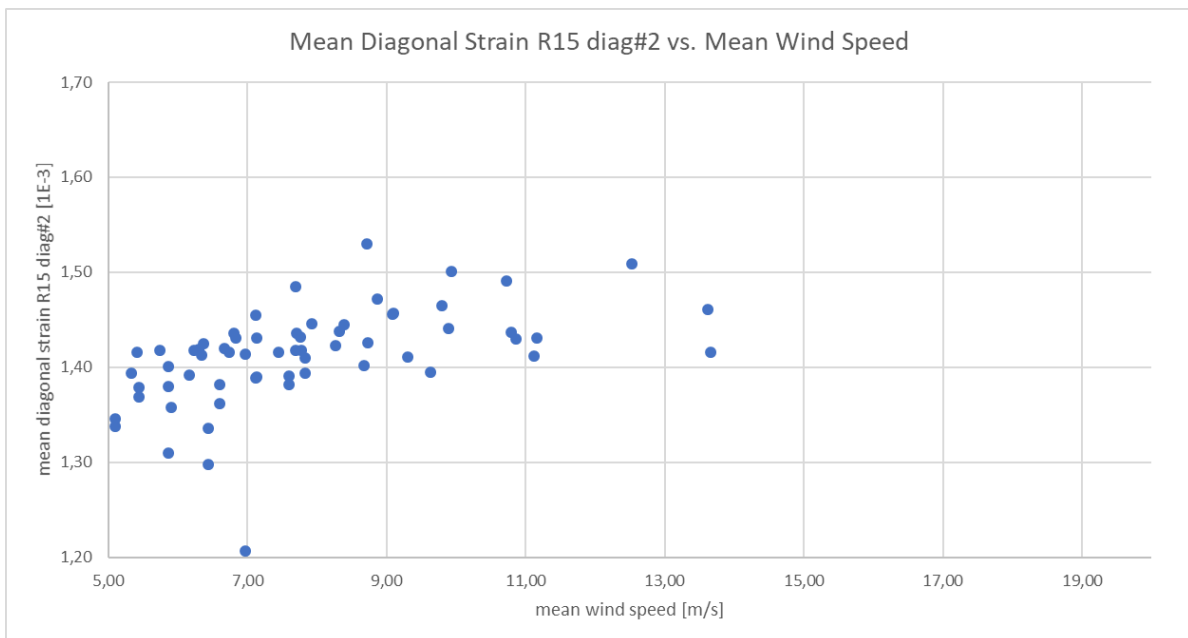


Figure 77 - Measured mean diagonal strain of diagonal #2 at R15 vs. mean wind speed

### 3.5 Planning and construction of test rigs

Leader: DTU

Coupon specimens for evaluation of normal and shear strength of the adhesive joint of the X-Stiffener are designed and under construction. Glass fibre plates on which the adhesive joint interface for both the normal and shear test are still outstanding.

The test rig for strength evaluation of the adhesive joint in pure tension are designed and ready for use.

Strength evaluation of the adhesive joint will be conducted in a double lap shear configuration. The test rig is a standard configuration, which is available at the DTU structural lab.

### 3.6 Sub-component testing of the X-Stiffener

Leader: Bladena

#### Mechanical testing of the X-stiffener™ and others

Product development of the X-stiffener™ solution is among others supported through mechanical testing at coupon and sub-component scale level performed at the Technical University of Denmark (DTU), Mechanical Engineering department.

##### Mechanical testing at coupon scale level

Coupon specimens for normal and shear strength evaluation of the adhesive interface between the corner mount and glass fibre material within the X-stiffener™ solution is undertaken by Bladena in corporation with DIS and DTU. Both tests are planned to be executed in a uniaxial test machine of the type Instron 8872 including an axial servo hydraulic actuator with a stroke and load capacity of  $\pm 50\text{mm}$  and  $\pm 25\text{kN}$  respectively. Two feedback transducers are mounted in conjunction with the actuator: an internally mounted linear variable displacement transducer (LVDT) and load cell (LC) with a capacity of  $\pm 25\text{kN}$ . The adhesive interface in the normal direction is evaluated in tension according to the ASTM standard. The adhesive interface in the shear direction is handled as double lap shear adhesive joints by tension loading according to the ASTM D3528-96 standard. However due to the specimens being compromised during manufacturing no testing were executed and the test campaign were terminated for these specific specimens.

Mechanical testing of the rope and lock within the X-stiffener™ solution is undertaken by Bladena in cooperation with DTU. The specimen is loaded in a uniaxial test machine of the type Instron 8502 including an axial servo hydraulic actuator with a stroke and load capacity of  $\pm 125\text{mm}$  and  $\pm 100\text{kN}$  respectively. Two feedback transducers are mounted in conjunction with the actuator: an internally mounted LVDT and LC with a capacity of  $\pm 25\text{kN}$ . With the load train and test setup represented in *Figure 78*, the rope and lock are quasi-statically loaded from 0.5kN (initial pre-tensioning level at installation) to failure with a fixed deformation rate of 2.0mm/min.

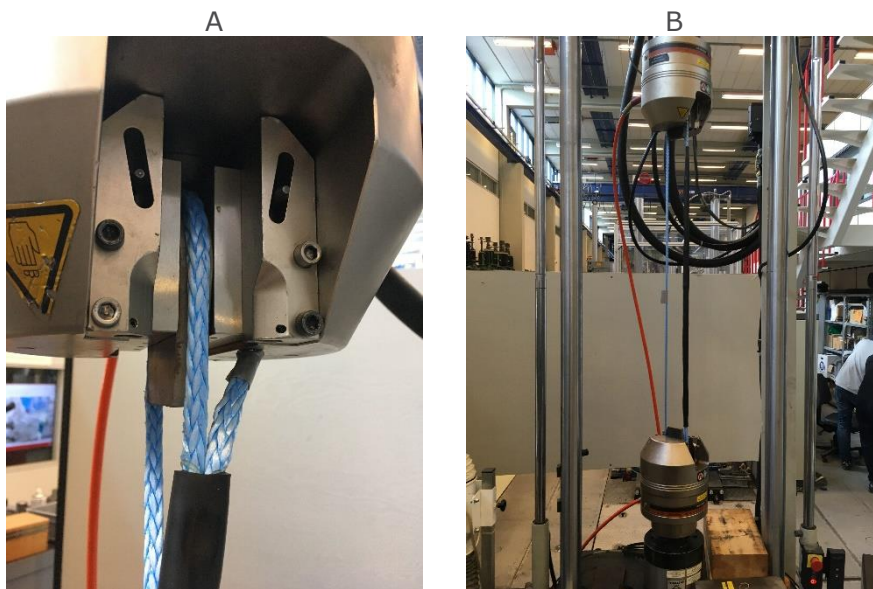


Figure 78 - Test setup: A) boundary conditions and B) overall setup

A number of nine specimens were tested including three different length of overlapping within the friction lock. Test was stopped when the friction lock started to fail. Key results including specimen elongation (compliance), max static load and corresponding overlap are given in [Table 10](#).

Table 10 - key results from rope and locker test

Test specimen [-]	1	2	3	4	5	6	7	8	9
Max. static load [kN]	21.6	22.2	22.7	26.6	28.5	17.5	14.0	14.1	9.88
Elongation, 1-10kN [mm]	6.45	5.89	5.5	4.01	3.94	4.49	4.56	4.37	4.87
Elongation 1.5-10kN [mm]	5.84	5.29	5.03	3.62	3.55	3.86	4.16	4.00	4.42
Overlap [m]	1	1	1	0.5	0.5	0.5	0.25	0.25	0.25

For comparison of the max static load between the individual test specimens, please use the column diagram provided in [Figure 79](#). For precise failure mode at 600 kg multiple other similar

tests was performed resulting in an overlap of 0,11 m used for the X-Stiffener™ final installation.

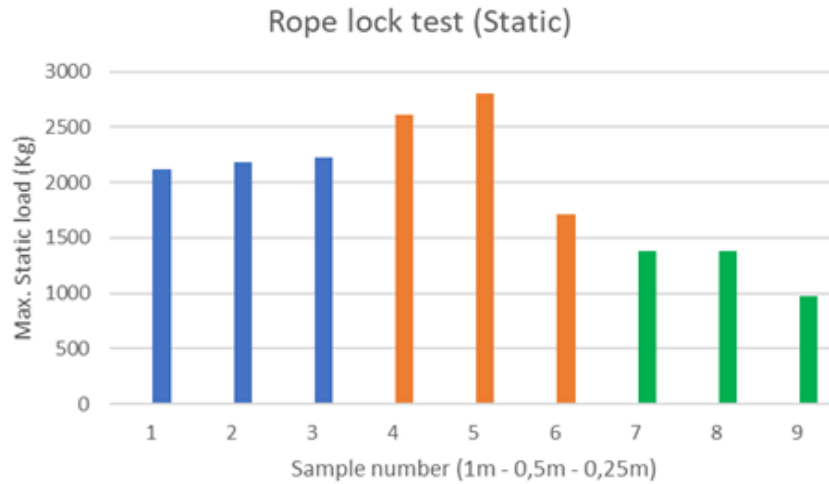


Figure 79 - Column diagram representing the max static load for each test

In addition, the normal strength of the adhesive interface between the corner mount for the FBG sensor and glass fibre material were evaluated, undertaken by TNO in corporation with DTU. The specimen (see [Figure 80 A](#)) is loaded in a uniaxial test machine of the type: Instron 8872 with a T-slot strong table and an axial servo hydraulic actuator with a stroke and load capacity of  $\pm 50\text{mm}$  and  $\pm 25\text{kN}$  respectively. Two feedback transducers are mounted in conjunction with the actuator: an internally mounted LVDT and LC with a capacity of  $\pm 10\text{kN}$ . With the load train represented in [Figure 80 B](#), the specimen is quasi-statically loaded from 0,10kN-8kN with a fixed loading rate of 2.0 kN/min.

A

B

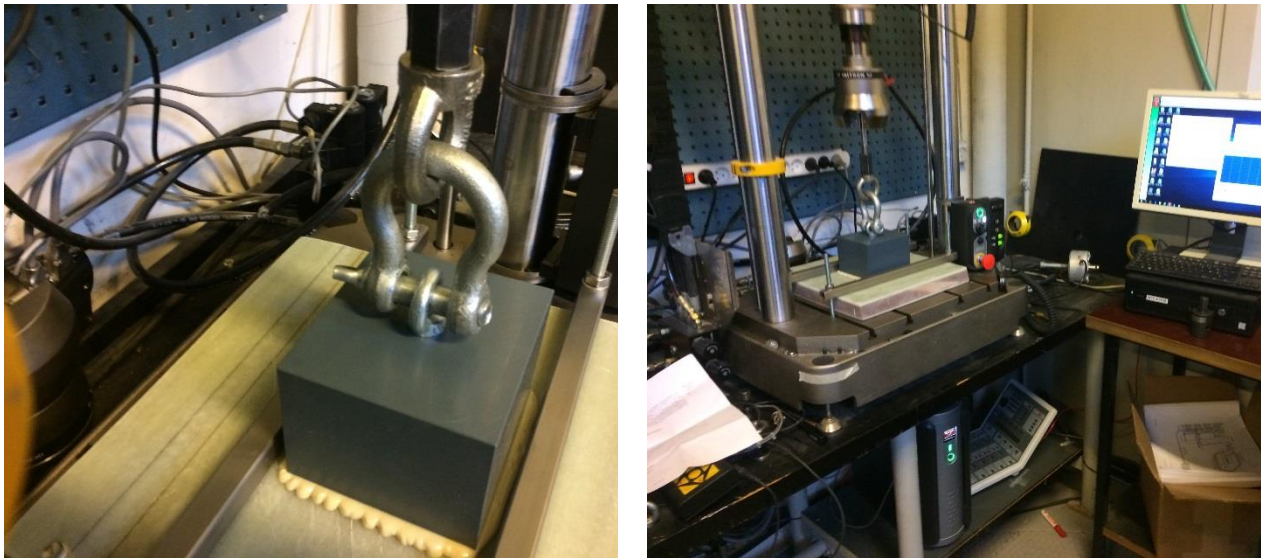


Figure 80 - Test setup: A) interface detail and B) overall setup

A number of three specimens were tested and specimen compliance is represented in Figure 81. The non-linear response in the load interval 0.1kN – 1kN is governed by slack in the load train.

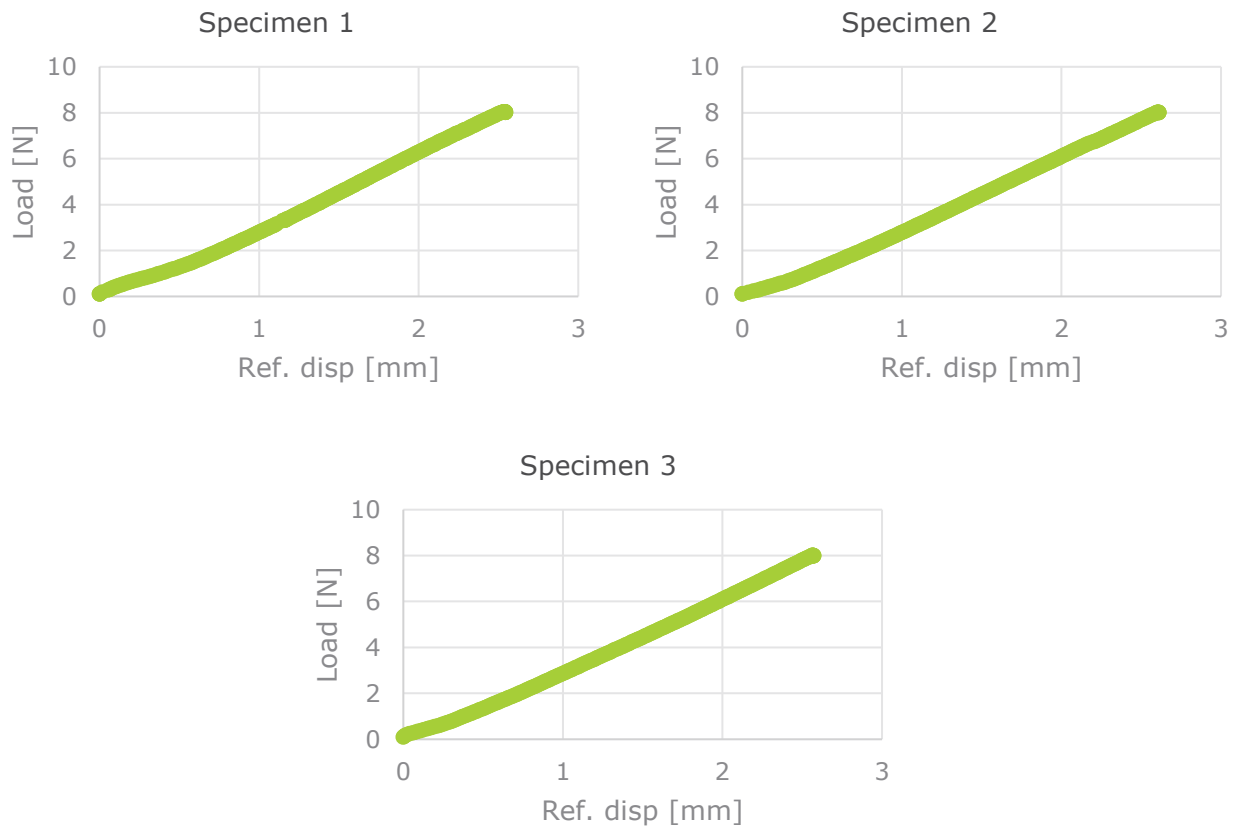


Figure 81 - Compliance of specimen 1, 2 and 3

All specimens were undamaged throughout the test program. A picture of each specimen is represented in *Figure 82*. According to the data and on-sight observations no sign of imminent mechanical failure is observed at the given load level.



*Figure 82 - Specimens after testing*

### Mechanical testing at sub-component level

An X-stiffener™ corner mount in combination with rope and locker is mechanically tested at subcomponent scale level in a uniaxial test machine. The corner mount is glued into a glass fibre corner referred to here as a bracket (see *Figure 83 A*). The test specimen is loaded in a four-column MTS 810 test machine with a T-slot strong table and an axial servo hydraulic actuator with a stroke of  $\pm 33.00\text{mm}$  and load capacity of  $\pm 100\text{kN}$ . Two feedback transducers are mounted in conjunction with the actuator: an internally mounted LVDT and load cell model MTS 661.19E-04 with a capacity of  $\pm 25\text{kN}$ . With the load train represented in *Figure 83 B*, the specimen is quasi-statically loaded from 0.5kN (initial pre-tensioning level at installation) to failure with a fixed deformation rate of 2.0 mm/min.



*Figure 83 - Test setup: A) details of bracket and corner mount and B) overall setup*

Three different types of corner mounts are investigated in the following, capable of accommodating angles in the interval 60 through 80 degrees, 80 through 110 degrees and 110 through 140 degrees. Given that an acute angle of the bracket is the dimensional configuration, the bracket angle is chosen lowest possible for the given corner mount. A parametrical study is conducted including three different corner mounts with the key results given in table 2.

*Table 11 - key results from bracket and corner mount loaded in combination with rope*

Test specimen [-]	1	2	3	4	5	6	7	8	9
Max. static load [kN]	14.9	14.7	15.1	21.6	14.9	16.1	23.9	16.7	18.8

---

Corner mount [degrees]	60- 80	60- 80	60- 80	60- 80	60- 80	80- 110	110- 140	110- 140	110- 140
Bracket [degress]	60	60	60	80	80	80	110	110	110



## 4 Work Package 4 – Wind turbine integration

### 4.1 Manufacturing & installation instruction: Low drag vortex generators

Leader: CENER

In this work package CENER has worked in the definition of the materials and procedures to install the vortex generators in the wind turbine. The activities focus on the primer, the adhesive and protective coating characteristics. The location of the VGs is also specified in this chapter.

#### 4.1.1 Primer

Type: W9910 TAPE ADH. PROMOTER 1 PINT / 3M Wind Tape Adhesion Promoter

- The bonding surface must be smooth, clean and dry. If applying 3M Wind Protection Tape, the surface should be sanded smooth with 320 grit sandpaper. Clean the surface with isopropyl alcohol and a clean, lint-free towel or cloth. Allow the surface to dry completely.
- The surface should be wiped with the pre-saturated 3M Wind Tape Adhesion Promoter W9910 wipe or with a clean, lint-free cloth wetted with 3M Wind Tape Adhesion Promoter W9910, using the minimum amount that will coat desired surface. More is not better. Promoter should be allowed to dry for 10 minutes. For best results, apply 3M Wind Protection Tape to the promoter covered surface within two hours.

#### 4.1.2 Adhesive

Type: FITA AD. SAFT VHB 4110 84MMX33M / 3M™ Solar Acrylic Foam Tape

- To obtain optimum adhesion, the bonding surfaces must be stable or unified, clean and dry. A common surface cleaning solvent is IPA/water mixture.
- As a pressure-sensitive adhesive, bond strength is dependent upon the amount of adhesive-to-surface contact developed. Firm application pressure develops better adhesive contact and helps improve bond strength. Generally, this means that the tape should experience >15 psi (>100 kPa) in roll down or platen pressure.
- After application, the bond strength will increase as the adhesive flows onto the surface. At room temperature, approximately 50% of the ultimate strength will be achieved after 20 minutes, 90% after 24 hours and 100% after 72 hours. Handling Strength is typically achieved immediately after application of pressure to the bonded components. In some cases, bond strength can be increased and ultimate bond strength can be achieved more quickly by exposure of the bond to elevated temperatures (e.g. 150 °F (66 °C) for 1 hour).
- Cut the tape with the same dimensions as the base of the VGs. So it must be one piece of tape for each VG. Paste each piece to its respective VG and later to its position on the blade.

#### 4.1.3 Protective Coating

- Air-dries in 1 hour at +75°F (+24°C). Do not apply subsequent protective coatings for at least 2 hours from time of application. Normal cure takes about 24 hours at room temperature. Further improve chemical resistance with 1 hour bake at +200°F (+95°C).

- The protective coating must cover the leading edge face of the adhesive for each VG.

#### 4.1.4 Location

- 18-19 Vgs (for each blade) with a pair distance of 0.05292m~52.9mm on the same span (1m) as the LEPS, 74m from the root. The Vgs leading edge is at the 50% of the chordwise position.
- 17 Vgs (for each blade) with a pair distance of 0.18515m~18.5cm since 23m to 25m distance from the root (the 3m span where are localized the airfoil profile DU00-W2-350). The Vgs leading edge is at the 30% of the chordwise position.
- A cardboard template can be used to do a properly position and spaced for VGs.

## 4.2 Manufacturing & installation instruction: metallic protective insert kit

Leader: ODSL

The metallic protective insert technology will be comprised of two 0.5m tiles to be installed on each of the three blades (making six tiles in total). The tiles are custom manufactured in nickel using an electroforming process which grows the part to the required geometry and thickness.

For ease of incorporating the metallic tiles into the Levenmouth Demonstration Turbine (“LDT”) earthing system, the metallic tiles will be installed either side of the blade lightning receptor, located 74 m along the blade from the hub. Details of the installation procedure will be documented in the End of Project Report, however key risks that the installation will address include consideration of rope access, installation of redundant attachment mechanisms, and suitable protection for the operative from the plates (as thickness is only 0.3 mm).

## 4.3 Manufacturing & installation instruction: Shear distortion measurement

Leader: Bladena

The measurement of the blade shear deformation at the LDT with and without the X-Stiffeners installed are planned to be performed using the Cross Sectional Shear Distortion Sensor (“CSSDS”) TNO developed for this project (see section 2.6).

For the installation of the CSSDS a Risk Assessment and Method Statement (RAMS) together with a Hazard and Operability Study and the instruction manual for the CSSDS (D4.3) had to be delivered to ODSL in order to get approval for the installation of the CSSDS. The documents have been delivered by TotalWind and TNO and the CSSDS has been approved for installation on the LDT by ODSL.

## 4.4 Manufacturing & installation instruction: X-Stiffener

Leader: Bladena

The final production of the X-Stiffener™ solution is divided into different suppliers for each component used for the full assembly.

- Tinby Danmark A/S  
Tinby have supplied the moulds and mouldings of the PUR 1150 Solid corner mount brackets. They have been chosen as they have the relevant experience for complex high strength non-metallic mouldings.
- Dynamica Ropes ApS  
Dynamica have supplied the pre-heated, pre-stretched high strength dyneema® rope. They have many years of experience with extreme loading on various rope types and sizes and have helped with the specifications of what was needed for this specific application.
- 3M Danmark  
For the lock of the X-Stiffener™, 3M have supplied their heavy-duty glue-lined shrink wrap. They have the necessary products for these high load applications in harsh environment.
- Würth Danmark  
All tools and ancillaries needed to perform the installation is acquired mainly through Würth.

Installation was based on information from the report: "X-Stiffener™ Structural Enhancement for large blades" (October 2018) and "X-Stiffener Installation info\_V1.pdf" (16-11-2018).

Based on these reports the GEV team were trained by Bladena technician. During the training it was emphasized that a proper bond between the bracket and blade panel was crucial. Cleanliness and sanding of surfaces, both on the blade and the brackets is necessary to achieve this. Also, the equal distance between brackets is more important than exact position of the brackets in relation to the root (radial position).

Due to limitation from security rules for confined spaces the supervisor from Bladena did not have access to the internal part of blade, but full procedure was documented by GEV.

Below in Table 12 is shown the precise positions for the installed X-Stiffener™ connections together with the bracket type used in each blade corner.

*Table 12 – Positions from X-Stiffener™ installation, May 2019*

#	Radius (mm) (Centre of bracket)	TE/PS Bracket type	Shear web /SS Bracket type
1	12250	60-80°	80-110°
2	12450	60-80°	80-110°
3	12650	60-80°	80-110°
4	12850	60-80°	80-110°
5	13050	60-80°	80-110°
6	13250	60-80°	80-110°
7	13450	60-80°	80-110°
8	13650	60-80°	80-110°

9	13850	60-80°	80-110°
10	14050	60-80°	80-110°

To assist the installation of the brackets in the correct position on the blade, Bladena delivered a tool with a laser point, which is mounted into the bracket to help alignment between connecting brackets see Figure 84.



Figure 84 – Photo showing the specially made corner mount insert for laser alignment of brackets

This helps with the rotational position of the bracket during bonding and also provide the radial position for the opposing bracket. The bracket close to the web was placed according to measurements of the radial position and the opposing bracket was located with the laser. All other brackets were positioned in relation to this pair (#10 – as alignment was most straight). After the position was measured and marked, the areas for sanding was marked on the blade. After sanding, the brackets close to the web was bonded to the blade. The chosen pitch of the blade meant the bracket close to web could be held in place by gravity while adhesive was curing. The blade could not be held in a safe pitch position 180° opposite of the position used for measuring and installing the bracket close to the web. This meant the brackets close to the TE had to be held in place until enough cure of the adhesive was obtained. In the installation in May a small amount of fast curing Sikaforce 7800 BLUE was used strategically to secure the bracket until the main adhesive was cured. This proved to be viable solution if the operators took care not to disturb the already glued brackets when installing the following ones. This meant that only every second bracket was installed in the first step and after the primary adhesive was cured the bracket in between the others was installed in the second step.

The brackets were left to cure for more than 3 days before the ropes was installed with a pre-tension of approx. 50 kg. The rope was cut to a length of twice the distance between the brackets and adding 1.5 m for overlapping. The rope was cut to length in the nacelle, leaving the rope on the drum as long as possible to keep the rope in the pre-stretched condition.

Step by step procedure (Blade position horizontal 90° pitch):

Step 1 – Mark positions close to web according to specification.

Step 2 – Chose reference pair and mark reference position on TE using tool with laser pointer.

Step 3 – Mark other positions on TE in relations to reference pair.

Step 4 – Sand the blade at the positions for the brackets in preparation for bonding. Keep sanding area clean and use within short time to ensure proper adhesion.

Step 5 – Sand faces on bracket which comes in to contact with adhesive. Remember to sand the area where fillet is covering bracket.

Step 6 – Insert rope guide into bracket. It is advised the guide is preinstalled and bonded to the bracket before delivery.

Step 7 – Apply adhesive to the blade in the corner where bracket must be placed. Apply adhesive to backside of bracket and place into corner. Adjust rotation of bracket for best direction for rope.

Step 8 – If applicable, fill gap behind bracket. Create a generous fillet around the bracket.

Step 9 – If bracket cannot be held in place by gravity – apply a minor amount of fast curing SikaForce 7800 BLUE adhesive on the middle of bracket side as shown in Figure 85 **Fejl!** **Henvisningskilde ikke fundet.** and keep the bracket in place until strength to hold the bracket is obtained.



*Figure 85 – Photo showing the 60 to 80-degree bracket installed in the PS/TE corner, being held in position by very fast curing SikaForce 7800 BLUE while primary adhesive is curing*

Step 10 – Leave brackets to cure for at least 24 hours. Turbine can be running after few hours of curing at 15°C.

Step 11 – Measure distance between opposing brackets. Multiply distance by 2 and add approx. 1.5 m. Cut rope to length. Use tape around rope to secure ends before cutting.

Step 12 – Using a stiff wire to thread through bracket. An eye on the one end of the wire can be used to catch the other end of the wire inside the bracket. Tape the wire to the rope and pull through bracket as shown in Figure 86.

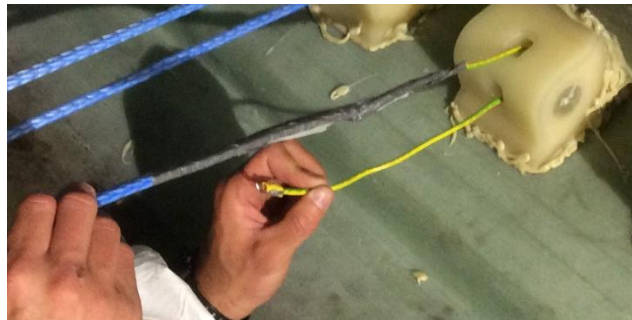


Figure 86 – Photo showing the threading of the rope through corner mount procedure

Step 13 – Mark on ropes where the heat shrink tube can be mounted. Clean rope with IPA degreasing wipes thoroughly.

Step 14 – Connect ropes with plastic ties on each side of the heat shrink tube. Rope must be able to slide in plastic ties. Tie a simple half knot in the appropriate places and mount ropes in clamp on quick grip.

Step 15 – Tighten rope with quick grip as shown in Figure 87. Pull in rope to ensure that the rope is not binding in brackets. Tighten quick grip one more time.

Step 16 – Cover adjoining rope with a piece of alutape to prevent damage from heat gun when applying heat to heat shrink tube. Heat up heat shrink tube. Heat rope and heat shrink tube thoroughly to ensure that hot glue is adhering to ropes. Heat until hot glue is squeezed out at the ends of heat shrink tube as seen in Figure 87.

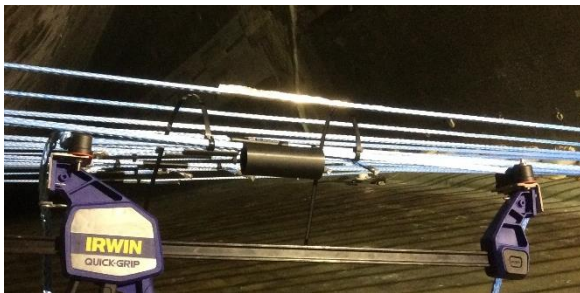


Figure 87 – Photo showing the rope tensioning and locking procedure

Step 17 – Leave the quick grip on until rope and heat shrink tube is cooled sufficiently (around 45°C) .

Step 18 – Remove alutape and adjust length of rope ends. See full installation in Figure 32.

## 4.5 Manufacturing & installation instruction: Erosion Sensor

Leader: TNO

Due to a lack of certainty of the mechanical stability of the fibre based sensor in the LEP coating (see section 2.5), installation in the turbine is not recommended. In the remainder of the project alternatives were screened together with CEU and Aerox in the form of different fibre materials to be implemented at the AHP primer, layer number two, shown in **Fejl! Henvisningskilde**

**ikke fundet.** Several polymer optical fibres (POFs) were investigated, since these materials show a better match, in terms of mechanical properties, with the flexible LEP coating. Specifically, PMMA, perfluorinated polymer and PUR materials were simulated. Although a slight improvement in mechanical stress distribution was predicted, the use of POFs would probably not prevent the acceleration of the erosion. In addition, few commercial POFs were available with sufficiently small diameter. In contrast with glass fibres (125  $\mu\text{m}$ ), the standard POFs have a much larger diameter (800 - 1000  $\mu\text{m}$ ). This would imply that integration of the POFs would be more challenging, since they have to be imbedded deeper into the substrate (puty) layer, underneath the LEP and primer layer (c.f. **Fejl! Henvisningskilde ikke fundet.**). Hence, for both glass fibre and POFs, the only possible solution would be to place the sensor much deeper in the coating system of the blade. Unfortunately earlier studies in the project made clear that sensor response is insufficient when it is embedded in the substrate layer (c.f. Section **Fejl! Henvisningskilde ikke fundet.**). In addition, the installation of such fibres on existing windmill blades would become very challenging, since part of the substrate (puty) layer has to be removed and reshaped under field conditions. Because of these reasons the Aerox LEP coating has been put on the offshore wind turbine blade in May 2019, but without TNO's fibre optic erosion sensor.

#### **4.6 Manufacturing & installation instruction: Cross Sectional Shear Distortion Sensor for the X-stiffener (CSSDS)**

Leader: TNO

The measurement of the blade shear deformation at the LDT (both with and without the X-Stiffeners installed) are planned to be performed using the cross sectional shear distortion sensor (CSSDS) TNO developed for this project, see section 4.3. Due to several delays in the project the CSSDS has been gathering data without the X-stiffener only. Prior to installation of the X-stiffener in May 2019 one of the lead fibres of the CSSDS got loose and damaged the sensing fibres. An inspection will be carried out in July 2019 and based on that it will be decided if the CSSDS will be repaired.

#### **4.7 Manufacturing & repair instruction: Aerox coating O&M solution**

Leader: Aerox

##### **4.7.1 Repair Method With Aerox AHP LEP**

The Aerox AHP LEP has been developed to protect the leading edge of wind turbine rotor blades from rain, sand, and particles suspended in the air. A technical instruction has been developed which describes a systematic procedure for the right application of the Leading Edge Protection (LEP) system in service conditions with access by rope or platform. A full description of the repair method is detailed in Annex A. This has been designed & approved by Aerox for all climatic conditions.

#### **4.8 Manufacturing & work instruction: Aerox coating O&M solution**

Leader: TNO

#### 4.8.1 Application Method of the Aerox AHP LEP in Factory Conditions

AEROX AHP LEP has been developed to protect the leading edge of wind turbine rotor blades from rain, sand, erosion and particles suspended in the air. The aim of this technical instruction is to describe a systematic procedure for the right application of the Leading Edge Protection (LEP) system in factory conditions where the blade is placed in horizontal position. A full description of the application method is detailed in Annex A. This has been designed & approved by Aerox for all climatic conditions.

### 4.9 Manufacturing & installation instruction: Aerodynamic add-ons for Siemens Gamesa turbine

Leader: Siemens Gamesa

Once the designs were selected (i.e. the ones which gave the best results in tunnel validation phase) the next phase of the project consisted of testing those designs in the field. The purpose of this was to finally validate the technological solution. For these field tests, a wind turbine was selected, located in the wind farm of Alaiz.

In parallel, a complete design was done for the devices that would be installed in the rotor of the selected wind turbines. The 4 different designs that were selected for turbines G132 and G126 were the following:

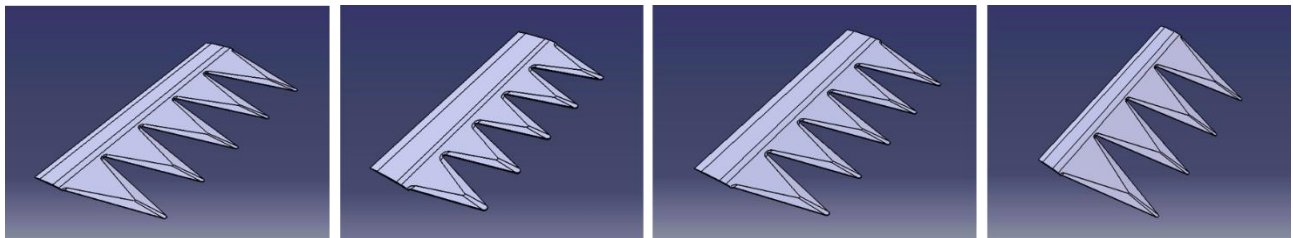


*Figure – Selected serrations design*

When the scaling was finished and the drawings had been prepared, a purchase order was created to manufacture the devices for the field test.

For the assembly of the devices in the wind turbine, instructions were prepared. The devices must be placed in order (Set 1 ⇒ Set 2 ⇒ Set 3), from tip to root and in the Trailing Edge, as shown in the **Fejl! Henvisningskilde ikke fundet.**

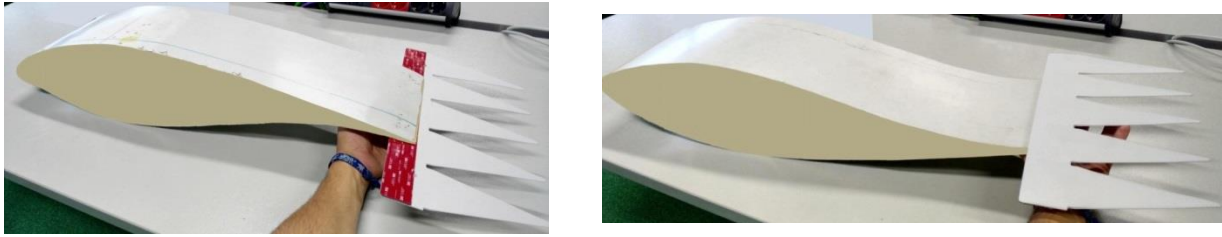


*Figure 88 - Installation Method Development*

The sets will be clearly identified, using the nomenclature shown in **Fejl! Henvisningskilde ikke fundet.**, to avoid mistakes on assembly process:

Set	Name	No. of Sets
P1	Panel 1	3
P2	Panel 2	8
P3	Panel 3	10

*Table 13 - Serration Panel Sets*

For assembling the devices, the blade must also be cleaned prior to installation.

#### 4.10 Installation procedure definition & review

Leader: GEV Windpower

GEV Windpower attended a project brief in June 2018 whereby we were presented with the background to the project and the technical details of each of the technologies. Though some work had been carried out by the previous blade partner, a full overhaul of the Risk Assessment and Method Statement were required for the first technology to be addressed (TNO CSSDS). Training had also been undertaken with the previously assigned technicians, so it was vital that the same level of training be provided to the GEV technicians to ensure a successful installation.

A similar process was followed for subsequent technologies, with task specific RAMS developed around the installation instruction for each ODB technology. Each technology and document pack were then briefed to the installation team prior to works to ensure roles and responsibilities were clearly understood between work parties. Toolbox talks were undertaken each day prior to works to establish all key risks and ensure all parties were happy with the mitigations in place to manage them.

Images were captured throughout the stages of the installations via GEV Windpowers' IRIS reporting system allowing quick synchronisation to the server and distribution to end client.

## 5 Work Package 5 – Installation, service and decommissioning

### 5.1 Product installation: Low drag vortex generators

Leader: GEV Windpower

CENER Low drag vortex generators (VG's) were designed to work in conjunction with the metallic protective insert kit for which the decision was made not to progress the installation (see notes below).

At this point the decision was made that there was little perceived benefit to installing the VG's in their current design. Additional work was undertaken to look at an alternative VG design, however, there was insufficient time during the project to undertake wind tunnel testing, etc with a view to subsequent installation.

### 5.2 Product installation: metallic protective insert kit

Leader: GEV Windpower

The planning discussion for the installation of the metallic protective insert raised some interesting discussion points regarding the risks of detachment and also the requirement for decommissioning. There was the risk that should any part of the installation detach, the rotational speed would throw the component a considerable distance and present a potential risk to the general public. The other consideration was the difficulty that decommissioning would present, particularly when undertaken via rope access.

The decision was made to suspend the installation of the component.

### 5.3 Product installation: X-Stiffener

Leader: GEV Windpower

GEV initially visited site in December 2018 to undertake the X-Stiffener installation, however, the ambient conditions created a difficult working environment in which the adhesives could not cure sufficiently during the working windows. A decision was made to decamp until improved conditions presented themselves.

In May 2019 the team returned to site to perform the installation with a slightly adapted procedure which proved far more effective, with the support of the Bladena engineer the brackets were all mounted successfully. Once left to cure overnight the ropes were fitted, tensioned and secured as per the work instruction. The system was fitted without any issues and all involved parties were satisfied with the works undertaken.

### 5.4 Product installation: Cross Sectional Shear Distortion Sensor for the X-Stiffener

Leader: GEV Windpower

To achieve a first time right installation of the CSSDS, close cooperation between the work package partners took place. The main goals were to ensure that the rather complex and delicate CSSDS lends itself to be installed by trained blade technicians, and that the installation complies with the requirements for safe and robust installation and operation at the LDT. This was formalized in the Risk Assessment and Method Statement (RAMS) together with a Hazard and Operability Study and the instruction manual of the CSSDS that had to be delivered to ODSL in order to get approval for the installation of the CSSDS. The documents have been delivered by TotalWind and TNO and the CSSDS has been approved for installation into LDT by ODSL.

One of the first steps towards the sensor installation at the LDT was the review of the hub and blade design data provided by ODSL and the inspection of the blade interior by TotalWind in May 2017. During a site visit valuable information was gathered on the actual physical environment and constraints as well as the operational. For example, by inspecting different cabling routes inside the hub (see Figure 89) an ideal fibre path was identified that reduces the required cable length from 10.5 m to 5.6 m, while minimizing the mechanical stress on the fibre at the same time.



*Figure 89 – Technician inspecting cabling inside hub of LDT*

GEV Windpower were selected as the preferred blade partner following the withdrawal of Totalwind in late June 2018. In early meetings, the ODB team took the opportunity to present the different technologies along with anticipated timeframes. Most critical of these initially was the TNO Cross Sectional Shear Distortion Sensor, though draft RAMS were in place they required further review and amendment. Training (which had already been carried out by TNO) had to be rearranged with the GEV technicians to ensure the team were competent to execute

the works safely and successfully. A timeline was agreed for successful approval of RAMS within 2 weeks, ground level training in Blythe within 3 weeks and the successful installation of the TNO technology at LDT within 4 weeks.

RAMS were reworked and signed off by local site management within the agreed timeframe, adapted RAMS were also submitted for the onshore training within a stored blade. The training was executed successfully with a strong team leader nominated to lead the works on the back of the skills demonstrated. The team then progressed to Levenmouth site to carry out the installation proper. There were some learnings through the course of the installation, critically some measurements taken in the early stages by Totalwind were incorrect, but all involved parties collaborated to see the LDT installation operational.

## **5.5 Product installation: Erosion Sensor**

Leader: GEV Windpower

Following the results of the development process it is no longer proposed to install the erosion sensor on the LDT, as described in section 4.5.

## **5.6 Application of Aerox coating**

Leader: GEV Windpower

Originally planned to be carried out in October alongside the Bladena X-Stiffener, the environmental conditions were not aligned with the manufacturers requirements and so the decision was made to wait upon a more suitable weather window in 2019. During this time there was some revision to the material and the new material was provided ready for installation in May 2019.

RAMS & COSHH information were updated to reflect the change in materials and approved in advance of the works. The Aerox coating was applied by means of rope access to an area of the leading edge that had previously had a repair to some minor lightning damage.

The installation was carried out in May 2019 and was executed to the work instruction without any reported issues. The involved technicians had previous experience of liquid applied LEP solutions and their feedback regarding the application properties of the material was positive.

## **5.7 Support to on-site installation activities**

Leader: ODSL

ODSL have been working with TNO and Total Wind in preparation of the first ODB installation at Levenmouth (the CSSDS, see section 5.4). ODSL have reviewed the TNO Hazard and Operability Study ("HAZOP"), installation manual, and RAMS. Following the ODSL review the Project Approval Committee formally granted permission for the installation to proceed.

To facilitate the on-site installation activities ODSL have been working with TNO and Total Wind to define suitable interface for the CSSDS Hub Cabinet. A bespoke mounting plate has been designed and is scheduled to be installed immediately prior to the installation of the CSSDS

Hub Cabinet. Furthermore electrical and communication connections have been designed and installed in the LDT hub and are awaiting commissioning.

## 5.8 Installation of aerodynamic add-ons at the Siemens Gamesa turbine

Leader: Siemens Gamesa

For the field tests an operational Siemens Gamesa wind turbine was selected, located in the wind farm of Alaiz, and two of the optimised serrations designs were tested.



Figure Siemens Gamesa wind farm of Alaiz in Spain All the logistics related to the trial were appropriately managed. Resources were put in place to carry out the assembly in field, including the provision of a lifting crane and liaising with the management of the park to be able to carry out all the scheduled tasks.

And finally, the methodology for noise measurement was defined, according to the IEC standard IEC 61400:11 – Edition 3.

**Fejl! Henvisningskilde ikke fundet.** shows a picture of the assembly process:



*Figure 90 - Siemens Gamesa Field Test Turbine*

Panels were mounted at airfoil trailing edge and suction side. For better evaluation of the designs, each of the two designs were assembled on two of the blades of the aerogenerator leaving the third one without noise reduction device. Operating this way comparative results are obtained for distinguishing the performance of the two designs.

The assembly process, although conceptually simple, was a challenging site operation and required ensuring that the assembly was correct and there were no installation failures that might impact the noise measurements.

The field test is a noise measurement campaign in accordance with IEC 61400:11 – Edition 3. The time to finish the test depends on the weather conditions and test campaign has to be performed when there is no rain and with wind conditions according to the specifications described in the IEC Standard.

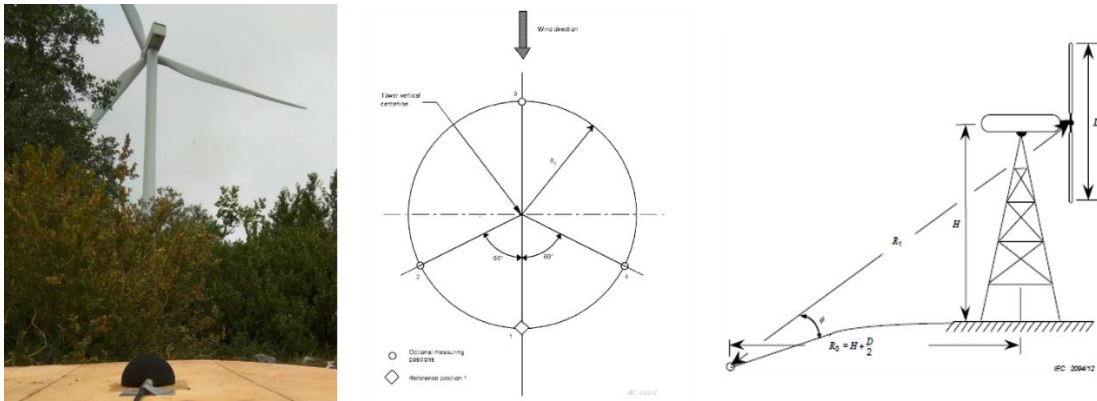


Figure: Noise field test in accordance with IEC 61400:11

## 5.9 Decommissioning of system

Leader: GEV Windpower

Decommissioning of all systems is scheduled for September 2019 although many technologies may remain if there is no risk to turbine safety or performance.

## 6 Work Package 6 – Data analysis

### 6.1 Power curve analyses

Leader: ODSL

Both the metallic leading edge protection systems and the low drag vortex generators will change the performance of the real wind turbine somehow. In order to evaluate their influence, results from the wind tunnel will be simulated with all foreseeable wind conditions in order to make a loads assessment and evaluate possible performance losses. Some previous work has already been done using a preliminary set of polar curves (which typically describe aerodynamic blade performance). Methodology and results regarding loads and aerodynamic losses caused by the metallic LEEP, will be summarized as follows.

First, the effect of these changes to the aerodynamic profile of the blade has been assessed.

Modified polars (the lookup tables for the coefficient of lift, drag and pitching moment which are used by aero-elastic codes to calculate aerodynamic loading) for the NACA 63618 aerofoil profile used on this blade towards the tip have been created by performing 2D CFD. A Reynolds number of 6,000,000 was chosen as typical of the turbine operation (and equivalent to the other aerofoil polars used on this part of the blade), and the SST K- $\omega$  turbulence model was used.

The polar data was only generated from  $-20^\circ$  to  $+20^\circ$  because the CFD solution does not converge in the deep stall region, so the aerofoil polars were extrapolated from  $-180^\circ$  to  $+180^\circ$  using the method of Montgomerie (Montgomerie, 2004) in the software package QBlade. The polars were then faired into the existing unmodified polars where the lines crossed. This is because in deep stall the plates should not make a huge amount of difference to lift and drag coefficients.

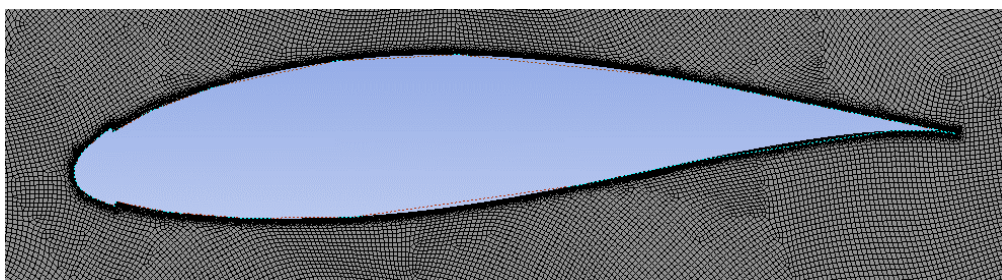


*Figure 91 - CFD mesh of blade with 5mm offset on leading edge*

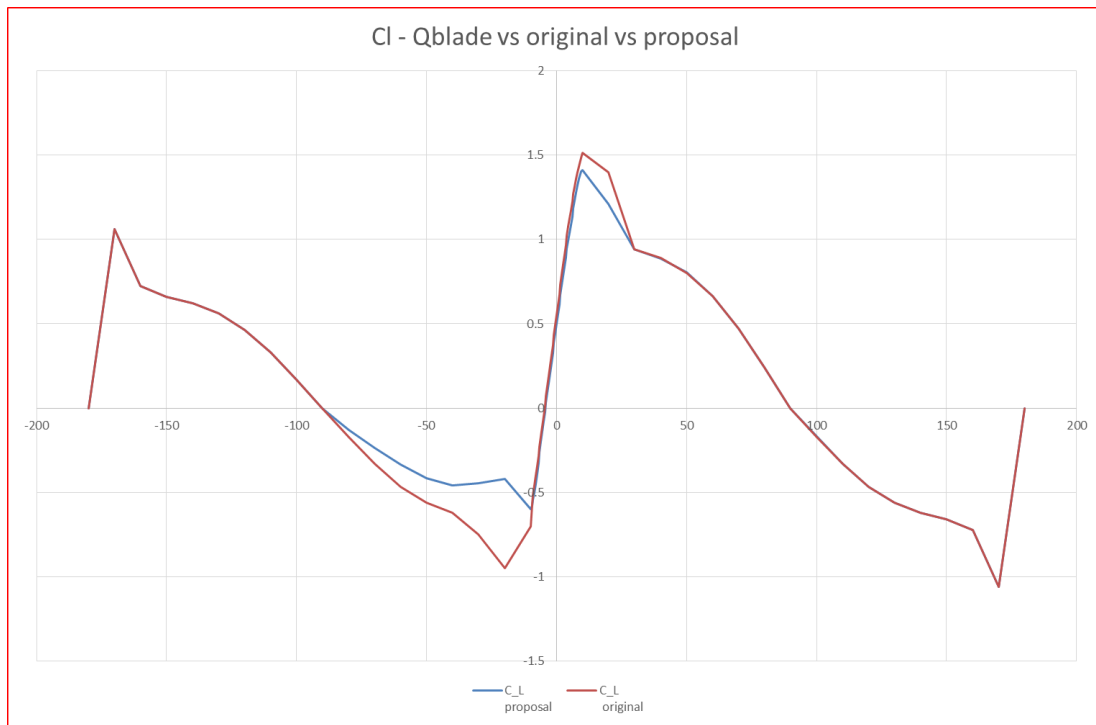


Figure 92 - Plot of lift coefficient for unmodified and modified aerofoils

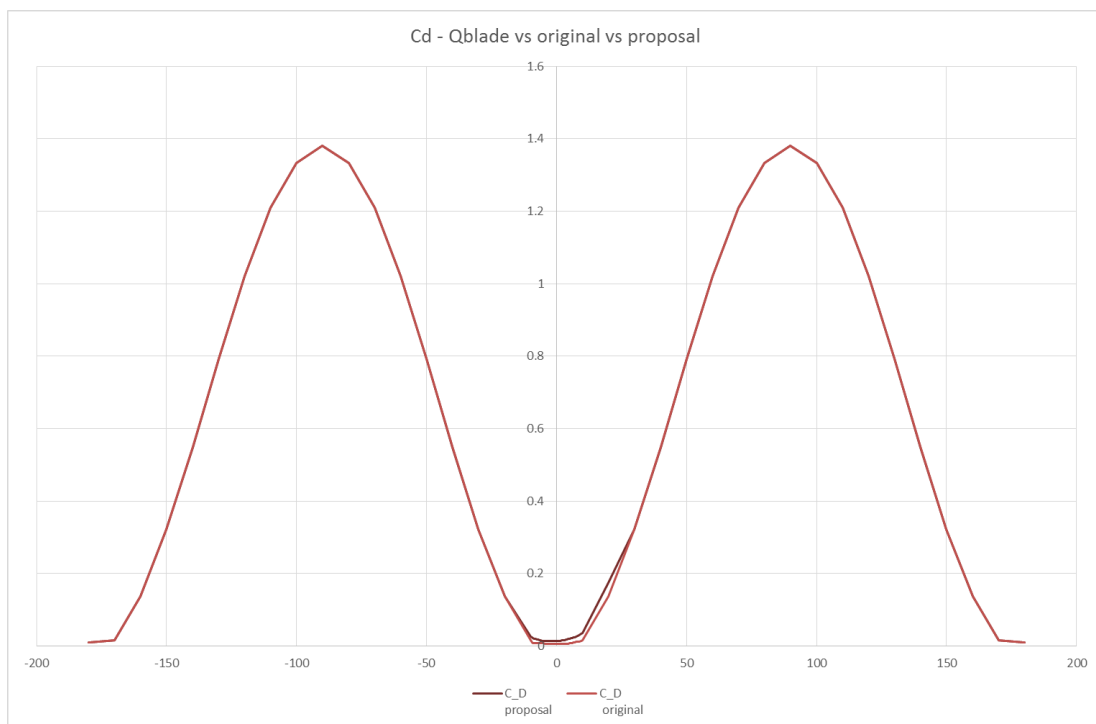


Figure 93 - Plot of drag coefficient for unmodified and modified aerofoils

The aero-elastic model in the Bladed software was modified to create new blade sections at 73.5m and 74.5m, and the aerofoil lookup table for this section was changed to the modified polars as shown in Figure 94.

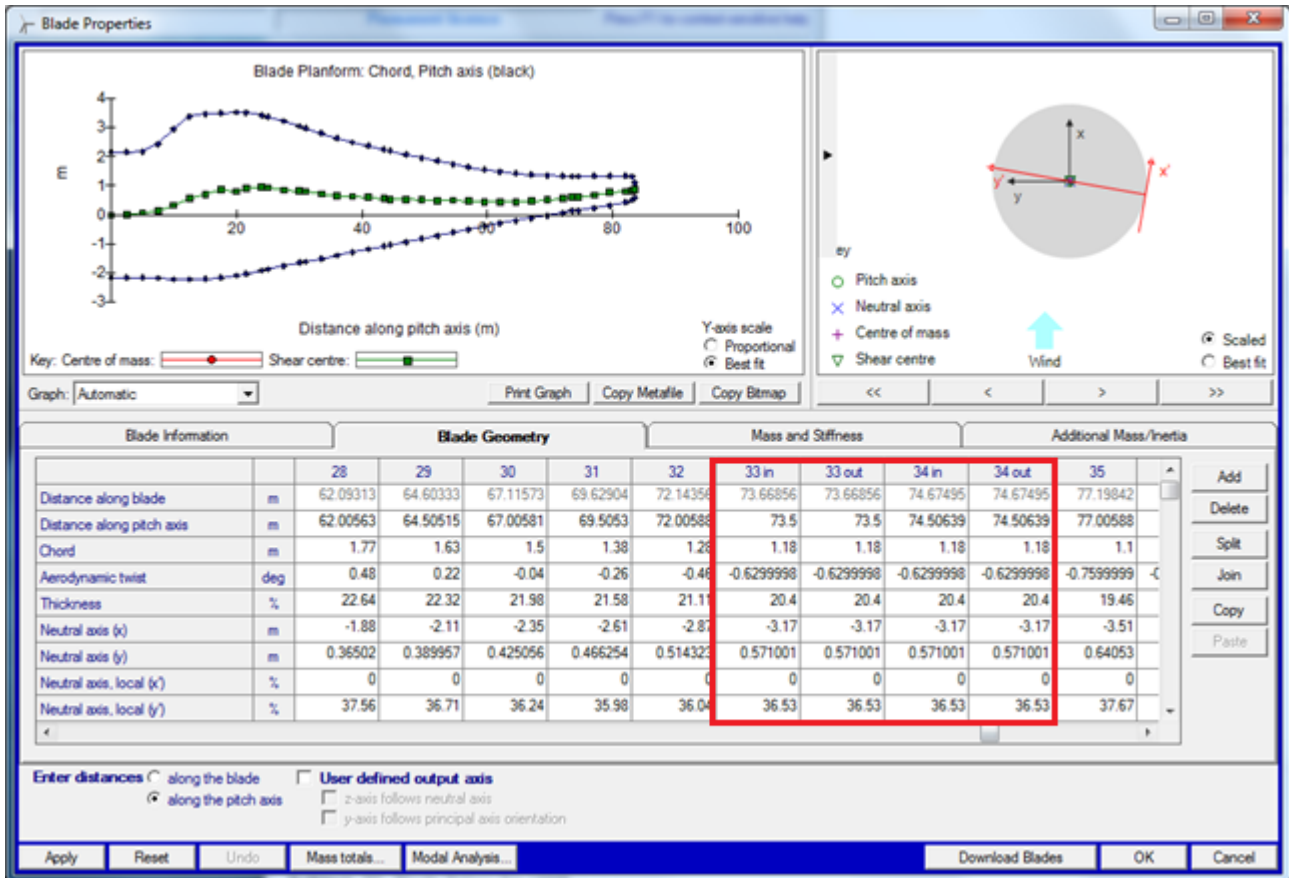


Figure 94 - Modified blade in Bladed

The effects on the extreme loads was compared at several key locations – the blade root, the tower top, and the tower bottom in Table 14, Table 15 and Table 16.

	Original Blade		LEEP at 74m		Percentage (Max)	Percentage (Min)
	Maximum	Minimum	Maximum	Minimum		
<b>M<sub>x</sub></b>	3.076E+07	-2.751E+07	3.175E+07	- 2.753E+07	3.11%	0.08%
<b>M<sub>y</sub></b>	4.127E+07	-2.925E+07	3.981E+07	- 2.903E+07	-3.65%	-0.76%
<b>M<sub>xy</sub></b>	4.215E+07	1.000E-01	4.209E+07	1.000E-01	-0.15%	0.00%
<b>M<sub>z</sub></b>	6.612E+05	-1.036E+06	6.629E+05	- 1.033E+06	0.25%	-0.36%
<b>F<sub>x</sub></b>	8.933E+05	-7.483E+05	8.814E+05	- 7.594E+05	-1.35%	1.46%
<b>F<sub>y</sub></b>	9.084E+05	-9.285E+05	9.221E+05	- 9.310E+05	1.48%	0.26%
<b>F<sub>xy</sub></b>	1.045E+06	1.000E-01	1.041E+06	1.000E-01	-0.32%	0.00%
<b>F<sub>z</sub></b>	2.669E+06	-5.432E+05	2.669E+06	- 5.433E+05	-0.02%	0.02%

Table 14 - Blade root extreme loads comparison

	Original Blade		LEEP at 74m		Percentage (Max)	Percentage (Min)
	Maximum	Minimum	Maximum	Minimum		
<b>M<sub>x</sub></b>	2.748E+07	-2.766E+07	2.636E+07	- 2.728E+07	-4.22%	-1.37%
<b>M<sub>y</sub></b>	1.972E+08	-1.890E+08	1.976E+08	- 1.892E+08	0.21%	0.13%
<b>M<sub>z</sub></b>	1.816E+08	-2.221E+08	1.768E+08	- 2.196E+08	-2.70%	-1.14%
<b>M<sub>yz</sub></b>	2.224E+08	1.000E-01	2.199E+08	1.000E-01	-1.15%	0.00%
<b>F<sub>x</sub></b>	-9.851E+06	-1.461E+07	- 9.835E+06	- 1.461E+07	-0.16%	0.00%
<b>F<sub>y</sub></b>	2.468E+06	-2.334E+06	2.446E+06	- 2.298E+06	-0.90%	-1.53%
<b>F<sub>z</sub></b>	2.574E+06	-2.557E+06	2.573E+06	- 2.541E+06	-0.03%	-0.61%
<b>F<sub>yz</sub></b>	2.582E+06	1.000E-01	2.581E+06	1.000E-01	-0.03%	0.00%

Table 15 - Tower base extreme loads comparison

	Original Blade		LEEP at 74m		Percentage (Max)	Percentage (Min)
	Maximum	Minimum	Maximum	Minimum		
<b>M<sub>x</sub></b>	2.734E+07	-2.717E+07	2.609E+07	2.710E+07	-4.79%	-0.25%
<b>M<sub>y</sub></b>	1.404E+07	-1.118E+07	1.381E+07	1.128E+07	-1.64%	0.90%
<b>M<sub>z</sub></b>	1.042E+07	-5.495E+07	9.893E+06	5.558E+07	-5.32%	1.14%
<b>M<sub>yz</sub></b>	5.495E+07	1.000E-01	5.565E+07	1.000E-01	1.26%	0.00%
<b>F<sub>x</sub></b>	-5.182E+06	-8.248E+06	5.165E+06	8.248E+06	-0.32%	0.00%
<b>F<sub>y</sub></b>	2.297E+06	-2.142E+06	2.191E+06	2.110E+06	-4.82%	-1.50%
<b>F<sub>z</sub></b>	1.860E+06	-2.015E+06	1.854E+06	1.973E+06	-0.32%	-2.13%
<b>F<sub>yz</sub></b>	2.298E+06	1.000E-01	2.192E+06	1.000E-01	-4.86%	0.00%

Table 16 - Tower top extreme loads comparison

The fatigue loads were also compared at the same locations. The results are in Table 17, Table 18, and Table 19. For the blade root, slope factors of 3 (relevant for the pitch bearing) and 10 (relevant for fibre reinforced fabric) are given.

	Slope Factor	Design Equivalent Load (Original)	Design Equivalent Load (LEEP)	Percentage Change
<b>M<sub>x</sub></b>	3	4.103E+07	4.096E+07	-0.18%
<b>M<sub>y</sub></b>	3	1.951E+07	1.979E+07	1.44%
<b>M<sub>z</sub></b>	3	3.483E+05	3.428E+05	-1.62%
<b>F<sub>x</sub></b>	3	5.484E+05	5.520E+05	0.65%
<b>F<sub>y</sub></b>	3	1.658E+06	1.648E+06	-0.57%
<b>F<sub>z</sub></b>	3	1.565E+06	1.559E+06	-0.37%
<b>M<sub>x</sub></b>	10	2.408E+07	2.416E+07	0.33%
<b>M<sub>y</sub></b>	10	1.745E+07	1.741E+07	-0.25%
<b>M<sub>z</sub></b>	10	2.786E+05	2.777E+05	-0.30%
<b>F<sub>x</sub></b>	10	4.885E+05	4.916E+05	0.62%
<b>F<sub>y</sub></b>	10	9.645E+05	9.640E+05	-0.05%
<b>F<sub>z</sub></b>	10	9.944E+05	1.030E+06	3.43%

Table 17 - Design equivalent loads at blade root for slope factor 3 and 10

	Slope Factor	Design Equivalent Load (Original)	Design Equivalent Load (LEEP)	Percentage Change
<b>M<sub>XT</sub></b>	3	2.55E+07	2.53E+07	-0.73%
<b>M<sub>YT</sub></b>	3	6.52E+07	7.80E+07	16.40%
<b>M<sub>ZT</sub></b>	3	5.51E+07	6.54E+07	15.76%
<b>F<sub>XT</sub></b>	3	6.24E+05	6.20E+05	-0.73%
<b>F<sub>YT</sub></b>	3	9.64E+05	1.05E+06	7.82%
<b>F<sub>ZT</sub></b>	3	1.14E+06	1.24E+06	7.84%

Table 18 - Tower base design equivalent loads

	Slope Factor	Design Equivalent Load (Original)	Design Equivalent Load (LEEP)	Percentage Change
<b>M<sub>XT</sub></b>	3	2.492E+07	2.475E+07	-0.73%
<b>M<sub>YT</sub></b>	3	2.016E+07	2.010E+07	16.40%
<b>M<sub>ZT</sub></b>	3	1.574E+07	1.570E+07	15.76%
<b>F<sub>XT</sub></b>	3	6.243E+05	6.198E+05	-0.73%
<b>F<sub>YT</sub></b>	3	6.437E+05	7.246E+05	7.82%
<b>F<sub>ZT</sub></b>	3	7.618E+05	8.604E+05	7.84%

Table 19 - Tower top design equivalent loads

The increase in the tower design equivalent loads is slightly concerning, but given that the tiles will only be installed for a year it is not unduly concerning, particularly when considering that the extreme loads do not increase substantially in these locations.

A better evaluation of performance loss will be possible once the wind tunnel testing has been conducted, but some previous work has been done in advance to account for baseline performance of the actual wind turbine, comparing theoretical and actual power curves. Results can be seen in Figure 95, where blue line is the ideal power curve, calculated with an ideal steady and uniform wind. Grey dots represent actual measurements of 10 minutes mean power production for a given 10-minute mean wind speed. The orange curve is the foreseeable trend of those measurements.

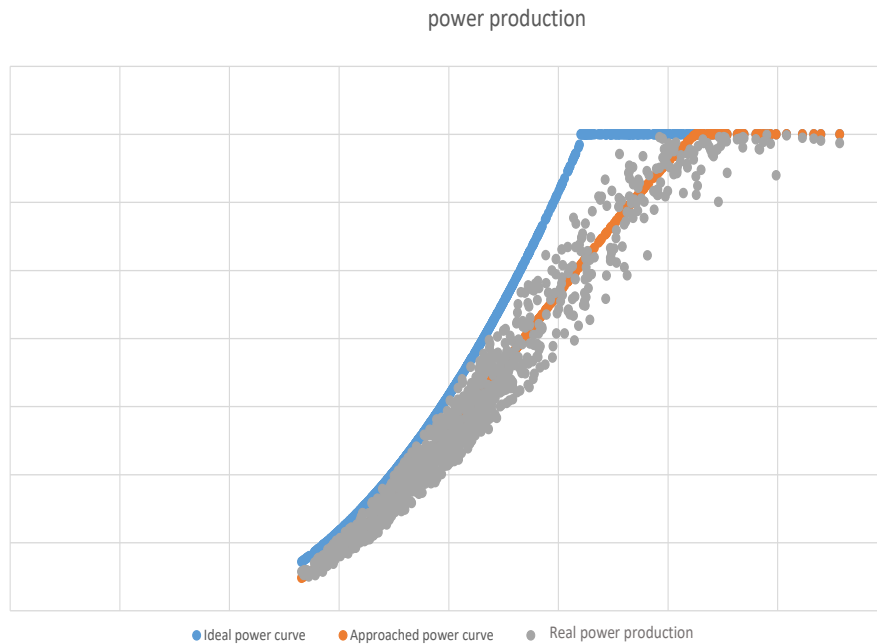


*Figure 95 – power curve: ideal vs actual performance*

We expect our results to look similar to those shown in Figure 96, where orange and blue lines are the same that in previous figure, and brown line would describe the expected behaviour of the turbine once the metallic LEEP and low drag VGs are installed. The latter would be calculated using wind tunnel results. This is only a very rough approximation, as it is too soon to accurately evaluate aerodynamic behaviour of the modified blade without the wind tunnel test results.

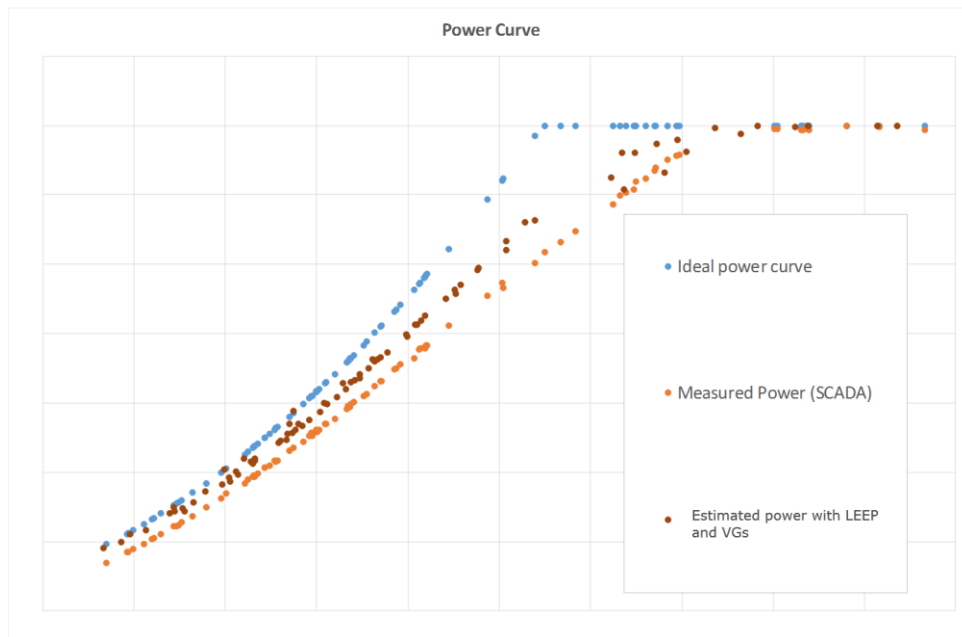


Figure 96 – power curve: *ideal vs actual vs estimated performance*

## 6.2 Blade shear distortion data analysis (pre X-stiffener installation)

Leader: Bladena

Bladena has extensive experience with understanding structural failures of wind turbines. Shear distortion is one of the main root causes of failures of bondlines in large wind turbine blades. Magnitude and shape of the specific shear distortion data will be analysed before the installation of X-Stiffener™, hence the blade will be understood.

The Finite Element Modelling (“FEM”) work was split in three main phases:

1. Pre-processing phase, where the model and necessary additional tools were developed and upgraded in order to accommodate the specific needs.

In this phase, the large flatback, found in the Levenmouth turbine, was incorporated in the pre-processor used to build more traditional design blades with a sharp edge, see Figure 97.

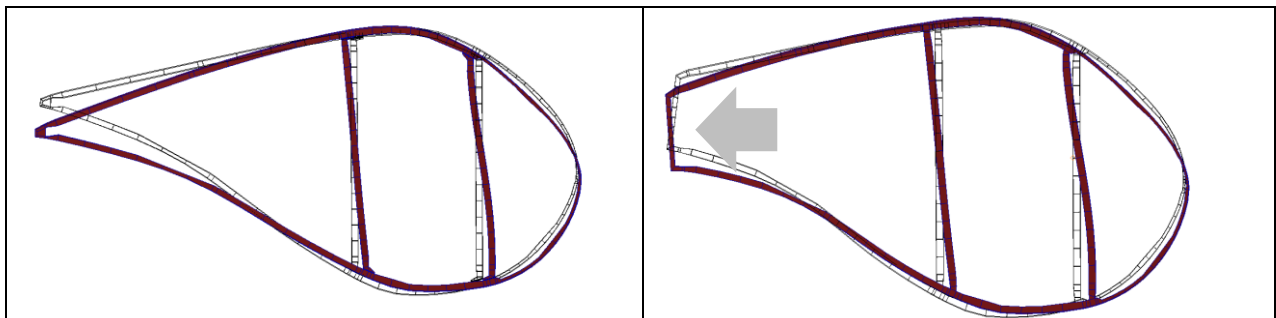
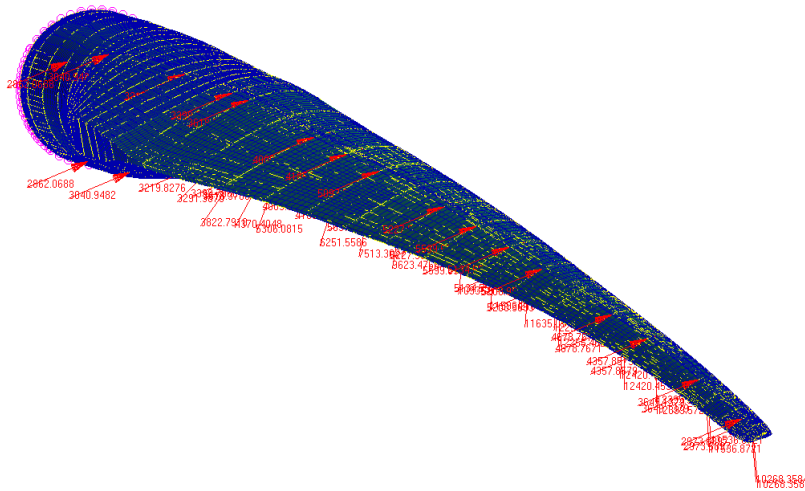


Figure 97: Comparison of a normal sharp trailing edge blade with a modern flatback construction

2. Verification / validation / calibration part. Work was carried out on the FEM blade model in order to ensure the deformation results are similar to the real blade.

Measurements performed by TNO were used to calibrate the model in the area of interest. Cross-sectional shear distortion magnitude was measured during turbine field operation in a combined loading scenario (both aerodynamic flapwise loads as well as edgewise are taken into consideration in the same time).

Similar load conditions were used in the FEA (flapwise + edgewise) where the edgewise loads are applied in the shear centre and aerodynamic loads in the aerodynamic centre, assumed to be at  $\frac{1}{4}$  distance from the leading edge.



*Figure 98: Combined loading methodology*

The model was assessed in the area where measurements were taken, once the calibration procedure was performed. In the end the model was ready to install the X-Stiffeners.

3. Post-processing part. FEM results were extracted, and conclusions were made once the validity of the model is accepted.

Different loading configurations were used to assess the model response, e.g. pure edgewise, pure flapwise and combined. This parameter study have indicated the model response in terms of cross sectional shear distortion to the loading, see Figure 99, Figure 100 and Figure 101.

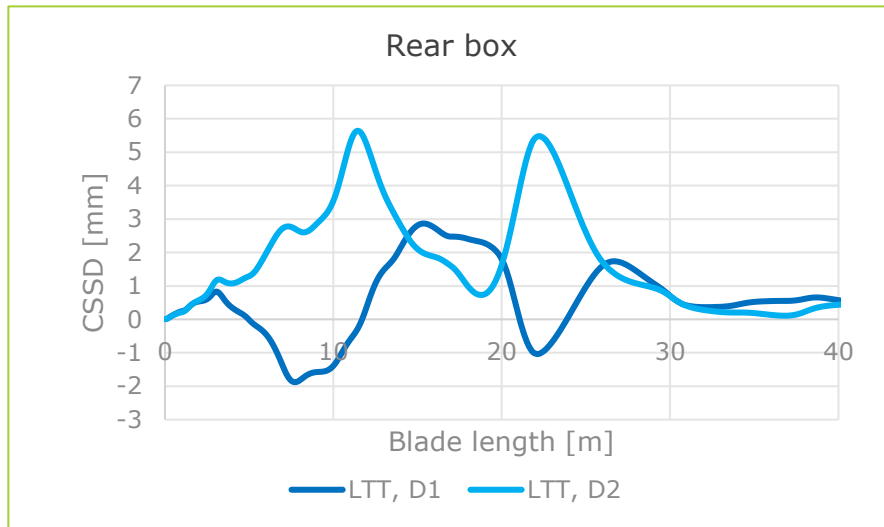


Figure 99: Edgewise loading (Leading towards trailing edge - LTT)

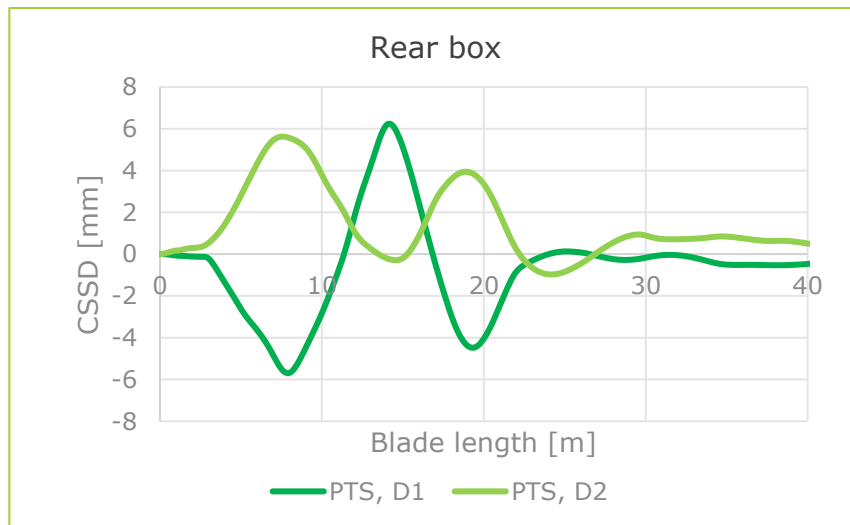


Figure 100: Flapwise loading (Pressure side towards suction side - PTS)

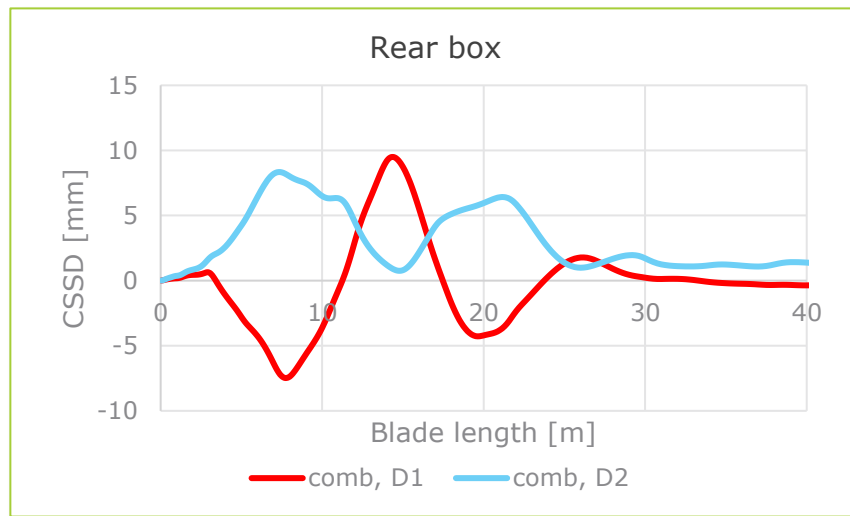


Figure 101: Combined loading

From the three graphs above, Figure 99, Figure 100 and Figure 101, the influence of the combined loading scenario is noted on the magnitude of the cross-sectional shear distortion in the rear box being larger in the combined loading scenario. The reason why the magnitude is increased is, when both edgewise and flapwise loads are applied in the same time, a twisting moment is created in the blade, see Figure 102.



Figure 102: Torsional moment created by the twisting of blade when the blade is subjected to combined loading.

This twisting component is split in two main components: pure torsion and pure distortion(cross-sectional shear distortion), see Figure 103.

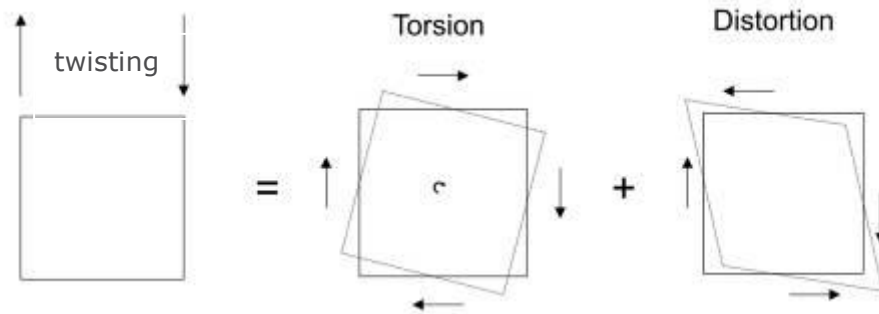


Figure 103: Twisting components: Torsion and Distortion (Cross-sectional shear distortion)

### 6.3 Blade shear distortion data analysis (post X-stiffener installation)

Leader: Bladena

Once the X-Stiffener is installed in the blade, the FEM model was calibrated, with the field measurement being post processed. At this stage the comparison before and after the X-Stiffener installation was made, see Figure 104.

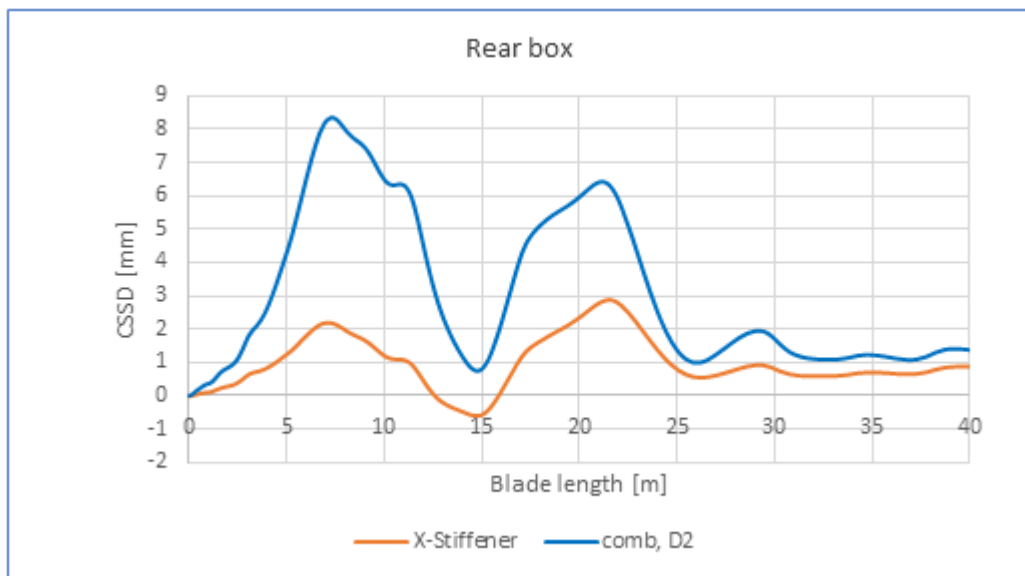


Figure 104: Comparison of cross-sectional shear distortion with and without X-Stiffener. With red with X-Stiffener, with blue without X-Stiffener.

The main impact of the X-Stiffeners presented in Chapter 2.3 is the reduction of the cross-sectional shear distortion magnitude. In terms of blade structural integrity, avoiding local deformations, such as the cross-sectional shear distortion will prologue the blade lifetime. Composite materials are able to withstand high number and magnitude of loads, as long as no local out-of-plane deformations occurs. The X-Stiffener does just this: limits the local deformations, hence it ensures the blade lifetime.

Furthermore, in case extreme loading scenarios occurs, such as vibrations or extreme flap due to e.g. yaw misalignment or extreme turbulence, the X-Stiffener will limit the local deformation magnitude. It is known that composite material lifetime is affected by high peak loading, in a greater manner than low magnitude cyclic loading. Therefore, when the peak loading is avoided, the lifetime of the structure is assured

## 6.4 Blade CSSDS data analysis

Leader: TNO

The sensor data of the CSSDS will be generated and stored inside the CSSDS Hub Cabinet, to be located in the hub of the LDT. The CSSDS samples the shear strain of each diagonal at 20 Hz, which corresponds to one sample every 3° of rotation at the maximum rotor speed of 10.6 rpm. The recorded data is stored in text files at an interval of 30 min with a size of 3Mb. This results in 48 files and 144Mb of data every day. They are processed per day automatically and since only the maximum length change of the diagonals is relevant for the project the data gets reduced significantly. The data product of the CSSDS is the maximum length change per diagonal and cross section per day.

## 6.5 Erosion sensor measurement analyses

Leader: TNO

This analysis of the erosion sensor measurement is now limited to those determined in the development testing of the erosion sensor, see section 4.5.

## 6.6 Coating performance analysis

Leader: Aerox

AEROX AHP LEP system was finally installed on the Levenmouth Wind Turbine in late May 2019. Due to the late installation, no analysis of the performance of the coating have been done yet. However, after the end of the project the coating performance will continue being assessed by means of observation during the maintenance and review tasks regularly carried out by ORE Catapult.

Within the Task 6.6, AEROX has performed an analysis of the data obtained during the project, with the aim of better understand the properties required for the coating system in order to protect effectively the leading edge.

Starting from the numerical method simulations of the effect of the impact of the rain droplets on the leading edge coated system, some aspects were observed to have high influence on the expected results of the erosion tests:

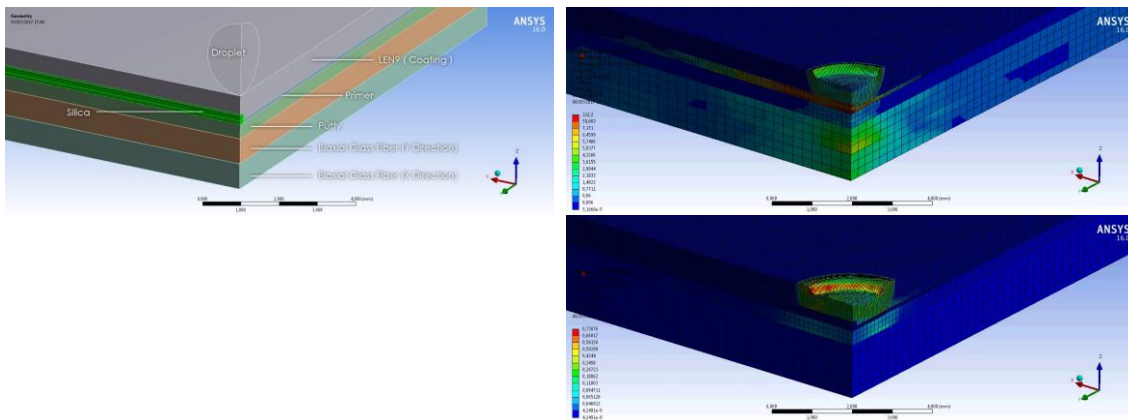


Figure 105. Simulation of the impact of a rain droplet on a wind blade leading edge.

- The configuration of the different layers of the coated leading edge, including the composite material, putties and fillers, primers and topcoats as well as the LEP itself affects the result of the RET. The ability to transmit and reflect the shock waves caused by the impact of the droplets along the different materials determine the ability of the system to dissipate the stresses caused on the materials.

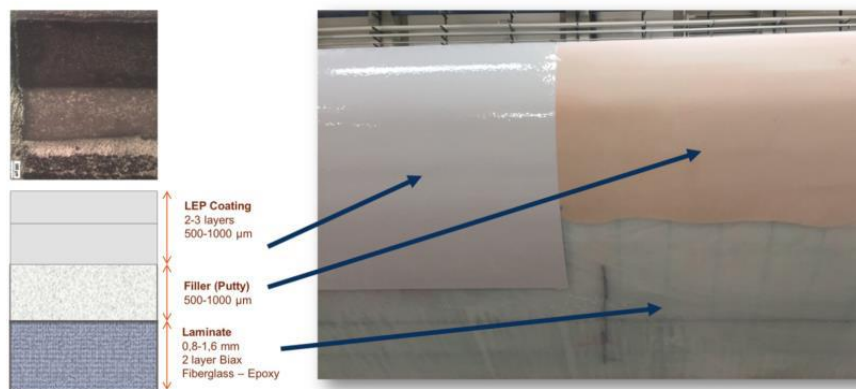


Figure 106. Different layers forming the system wind blade-LEP.

- The homogeneity of each one of the layers which form the LEP system is essential to obtain high erosion resistance. Imperfections such as pores, bubbles or particles act as stress concentrators where the failure of the material starts at short time.

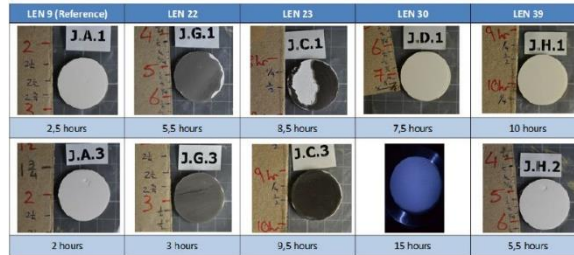
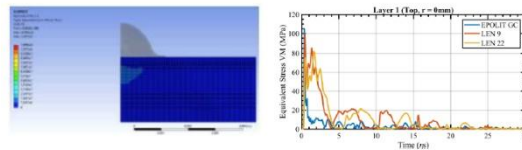


Figure 107. Simulation of the erosion resistance of the LEP.

Based in the conclusions obtained in the simulations, an analysis of the results of the tests performed during the project was carried out.

Sample Information							RET Resistance (h)						Average	Desv	Failure
Week	Batch	Substrate	Cannula	Sanding	LEP PR	LEP Thickness av	Specimen #1	Specimen #2	Specimen #3	Specimen #4	Specimen #5	Specimen #6			
1	S445 - 113_500	Clipcarbano MS Scratch	MFH 13-24	P1000	AHP LEP 920 2,5A NO PR	879	0,5	-	0,75	0,5	-	0,25	<b>0,50</b>	0,204	Delamination Damage
	S445 - 113_1000	Clipcarbano MS Scratch	MFH 13-24	P1000	AHP LEP 920 2,5A NO PR	968	0,5	0,5	0,5	0,75	-	-	<b>0,56</b>	0,125	Damage
	S445 - 114_500	MAGMA MS Scratch	MBLT 14-12	P1000	AHP LEP 920 2,5A NO PR	465	-	0,5	1	0,25	0,5	-	<b>0,56</b>	0,315	Delamination
	S445 - 114_1000	MAGMA MS Scratch	MBLT 14-12	P1000	AHP LEP 920 2,5A NO PR	885	-	0,5	0,25	0,25	-	0,5	<b>0,38</b>	0,144	Delamination Damage
2	S445 - 118_500	Clipcarbano MS Scratch	MFH 13-24	P600	AHP LEP 920 2,5A NO PR	445	-	2	2	0,5	-	-	<b>1,50</b>	0,866	Delamination Damage
	S445 - 119_500	MAGMA MS Scratch	MFH 13-24	P600	AHP LEP 920 2,5A NO PR	435	-	0,75	1	0,25	-	-	<b>0,67</b>	0,382	Damage
	S445 - 119_1000	MAGMA MS Scratch	MFH 13-24	P600	AHP LEP 920 2,5A NO PR	622	-	1	0,75	0,5	-	-	<b>0,75</b>	0,250	Damage
5	S445 - 121_500	MAGMA MS Scratch	MFH 13-24	P120	AHP LEP 920 2,5A NO PR	260	5	5	17	43	-	-	<b>17,50</b>	17,916	Delamination Damage
	S445 - 121_1000	MAGMA MS Scratch	MFH 13-24	P120	AHP LEP 920 2,5A NO PR	772	0,25	4	0,25	-	-	-	<b>1,50</b>	2,165	Damage
	S445 - 122_500	MAGMA MS Scratch	MFH 13-24	P120	AHP LEP 920 2,5A NO PR	310	-	1	-	1,5	-	-	<b>1,25</b>	0,354	Damage
	S445 - 122_1000	MAGMA MS Scratch	MFH 13-24	P120	AHP LEP 920 2,5A NO PR	788	-	2	2	-	-	-	<b>2,00</b>	0,000	Damage
9	S445 - 135	MAGMA MS Scratch	By Hand	P120	AHP LEP 920 2,5A NO PR	669	-	0,25	-	0,25	-	-	<b>0,25</b>	0,000	Damage
	S445 - 136	MAGMA MS Scratch	By Hand	P120	AHP LEP 920 2,5A AHP PR 302	457	-	0,75	-	0,75	-	-	<b>0,75</b>	0,000	Damage

Table 20. Results of different samples tested in a RET rig.

Complementary to specific single impact simulations, CEU developed a model that was computationally evaluated and implemented as a model to carry out studies in the optimization of the mechanical parameters involved on the LEP material erosion performance criteria. The methodology proposed to link Springer modelling with modulation of coatings properties is based on the analysis of the induced effects of variation for a given material property (density, impedance, endurance limit, etc) on the Lifetime performance predicted by the model. Regarding of the testing conditions and materials properties to be analysed on erosion performance, a complete map of the input parameters of the modelling is proposed in Figure 63.

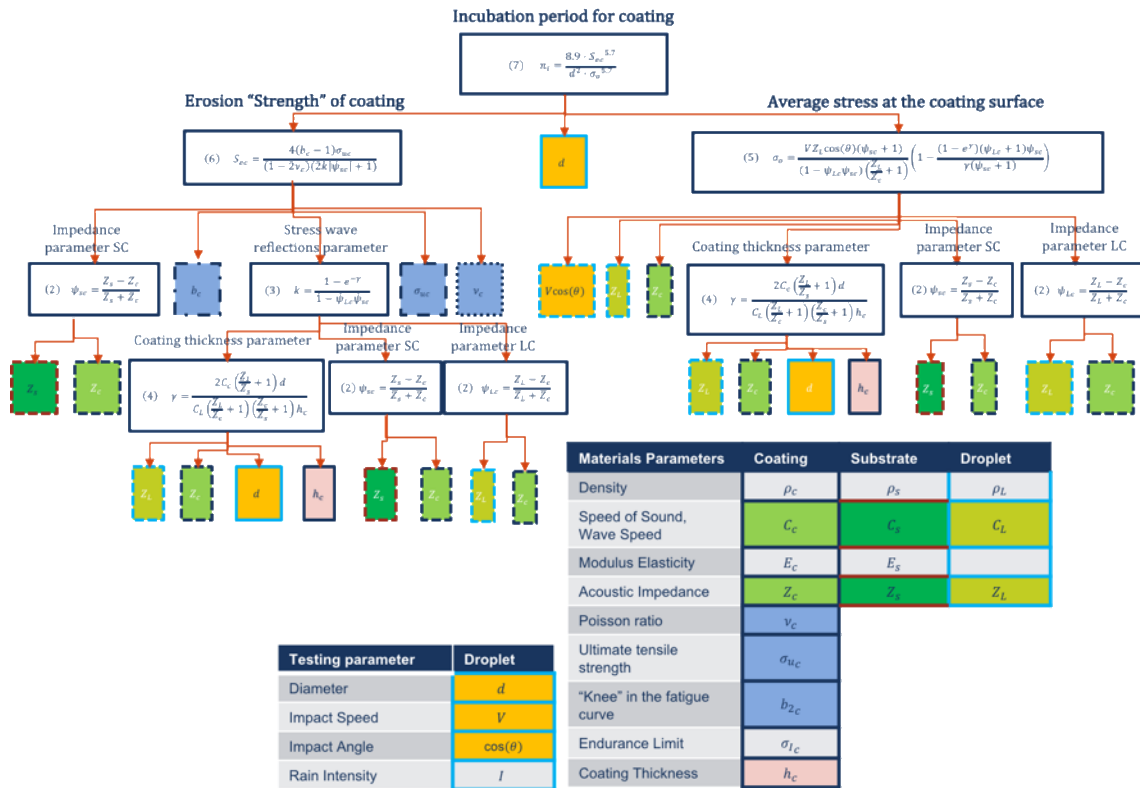


Figure 108. Diagram of material and testing parameters affecting rain erosion performance.

This modelling framework allowed us to specify a procedure to use the fatigue properties, the material safety factors, the loads and the calculation model to design and predict the useful life of a system. The erosion performance depends on the interaction of the coating layers of the system and the impact / load conditions, as such, a parametric analysis was performed to examine the impact of the selected coating properties on the erosion performance. This provides guidance in the selection and modulation of coating properties and should reduce the scope of testing to verify the rain erosion resistance of coating systems.

Figure 64 shows the simulated analysis and the testing results tested at the U.Limerick WARER for two experimental batches of given top coating material prototypes. On the left vertical axes one can observe the mass loss measured of the RET tested coupons (in marked points) and the mass loss for the simulated estimated results (in straight lines). On the right vertical axes, the box and whiskers plots are shown for each batch experimental RET tested coupons (over five coupons size batches). Horizontal axes define the incubation time for the experimental and simulated coupons.

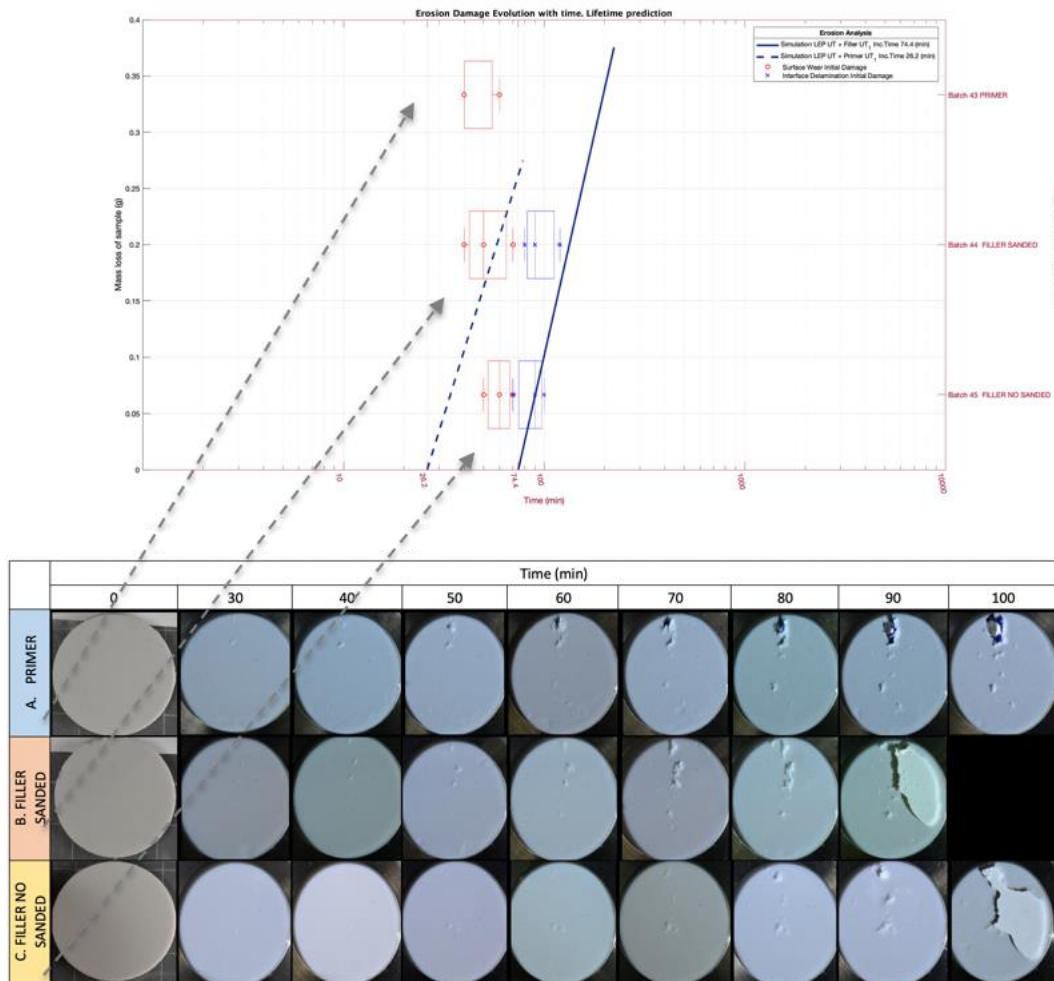


Figure 109. Rain erosion testing analysis for experimental tested (box and whisker plots for wear in red and delamination in blue) and simulated material prototypes. Incubation time for wear failure with primer layer (- -) and without primer (-) on interface.

The establishment of numerical guidelines for the design and correlation of variables, validated in this phase of the project, was developed for the different configurations selected.

The erosion performance analysis confirmed also what had been observed in the previous single impact simulations, obtaining some conclusions regarding several aspects of the LEP system:

#### LEP manufacturing process

During the manufacturing and packaging processes a considerable amount of air bubbles are introduced in the material. When a deaeration step is not included in the process, some bubbles are still in the material.

The effect of the bubbles has been studied and confirms that they reduce drastically the performance of the LEP in the RET.

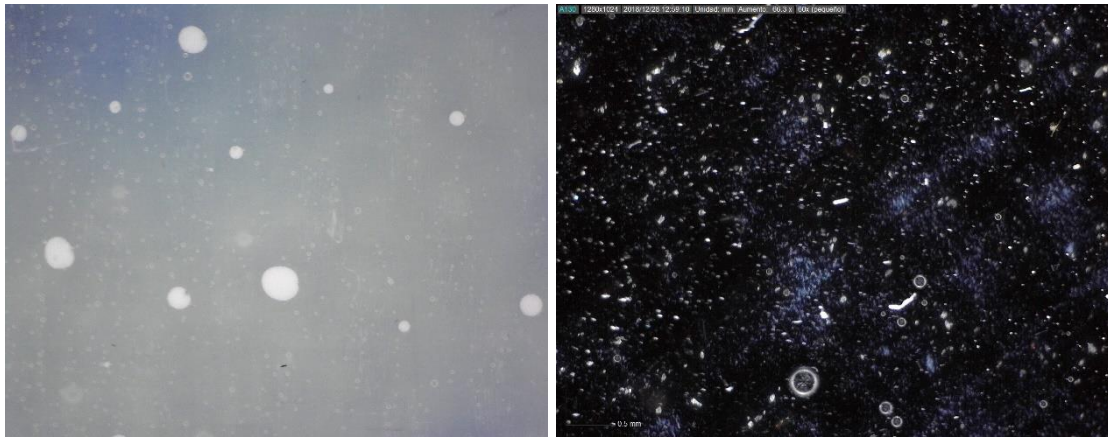


Figure 110. Microscopy images of air bubbles in the LEP.

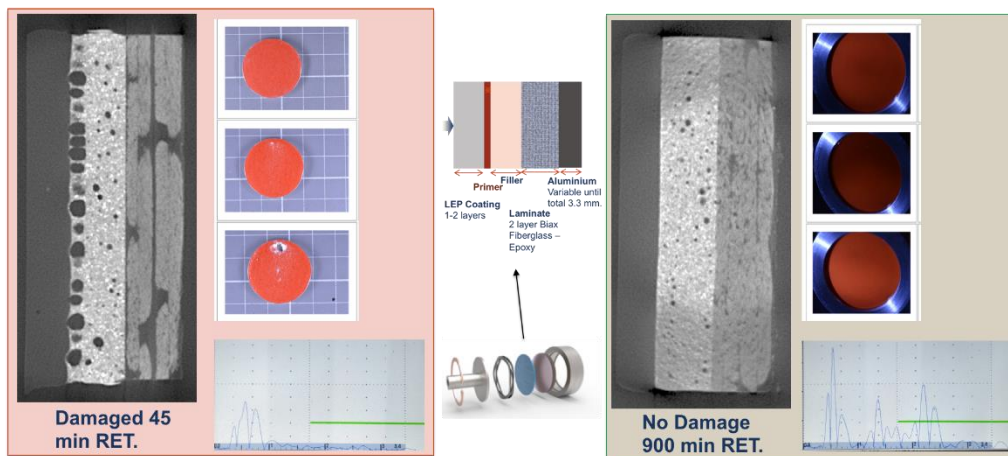


Figure 111. Influence of air bubbles in the RET resistance.

### Material application:

The method and application processes are extremely important to reach a good performance of the material. On the one hand, the mixture of the two components is decisive to reach the expected mechanical properties after its curing. A defective mixture results in low adherence and low elastic modulus. This defect could be identified by performing adherence tests, when values are under 5-6 MPa and high dispersion of values is observed.

On the other hand, the surface finish of each layer forming the LEP system affects directly in the results of the erosion tests. The existence of pores or imperfections reduces drastically the ability to resist the impacts of the rain droplets. This was observed clearly when the erosion sensors were embedded in the LEP system.

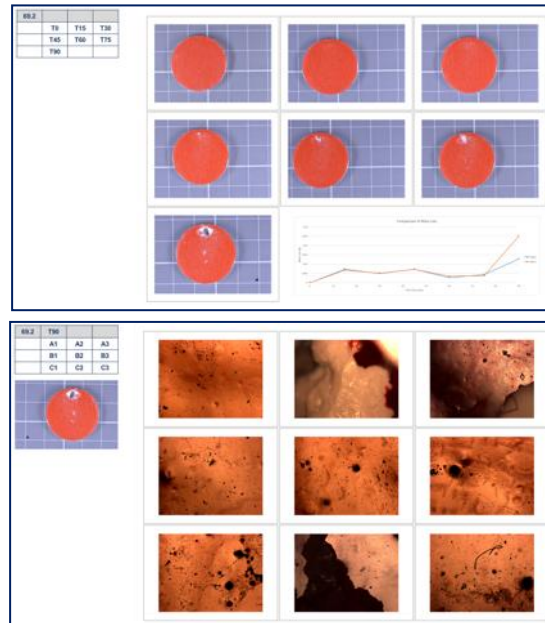


Figure 112. Influence of surface defects in RET resistance.

#### Adherence between layers.

The adherence between the layers of the LEP system as well as between the LEP and the substrate of the leading edge plays an important role in terms of the way the failure is generated. When low adhesion is registered (pull-off below 5MPa), the LEP fails by delamination. When the adhesion is above 5 MPa, the failure is produced by erosion and higher resistance is observed.

Figure 113 shows the difference observed between the failure produced by delamination (left) and the failure produced by erosion (right).

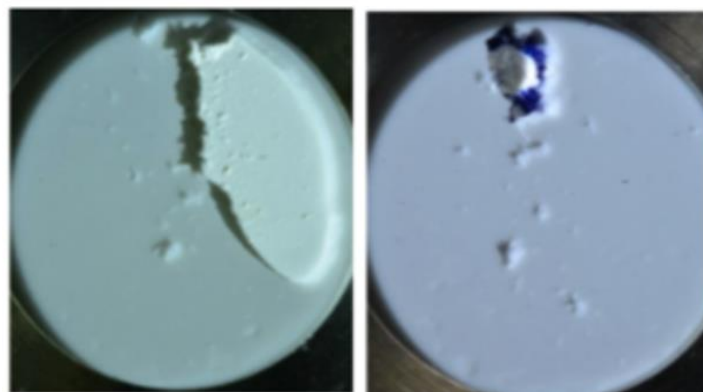


Figure 113. Delamination failure (left) and erosion failure (right).

#### Configuration of the leading edge + LEP system

As predicted by the numerical models, the erosion resistance of the leading edge is affected not only by the LEP but by the complex system composed by the laminate, gel coat, filler, topcoat and the LEP.

Different resistance was observed between samples with different materials configuration protected with the same LEP system.

RET results varied from 15 horas when applying the LEP directly on the laminate to 3 hours with more complex configurations including fillers and pore fillers.

Figure 114 and Figure 115 show an example of the different results observer in RET between samples with different configurations protected with the same LEP system.

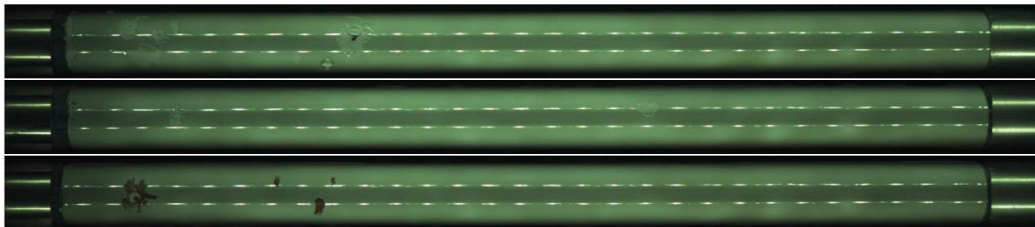


*Figure 114. Specimens after 9 hours in RET. Some spots of erosion*

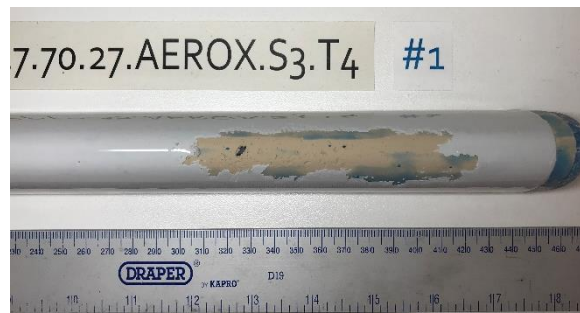


*Figure 115. Specimens after 2 hours in RET. Large zone eroded.*

This influence makes necessary to carry out a study of each configuration and a modulation of the LEP system properties in order to reach an optimal compatibility to optimise the erosion resistance.

## 6.7 Add-ons performance analysis

Leader: Siemens Gamesa

The two designs selected and installed on the Siemens Gamesa blades behave similarly concerning noise reduction. They are both capable of reducing noise level considerably as compared to a blade without any add-on. In the figures below we can see that both designs installed on blades A and C decrease the noise level as compared the blade B where no add-on was installed at different blade position angles at a constant wind speed.

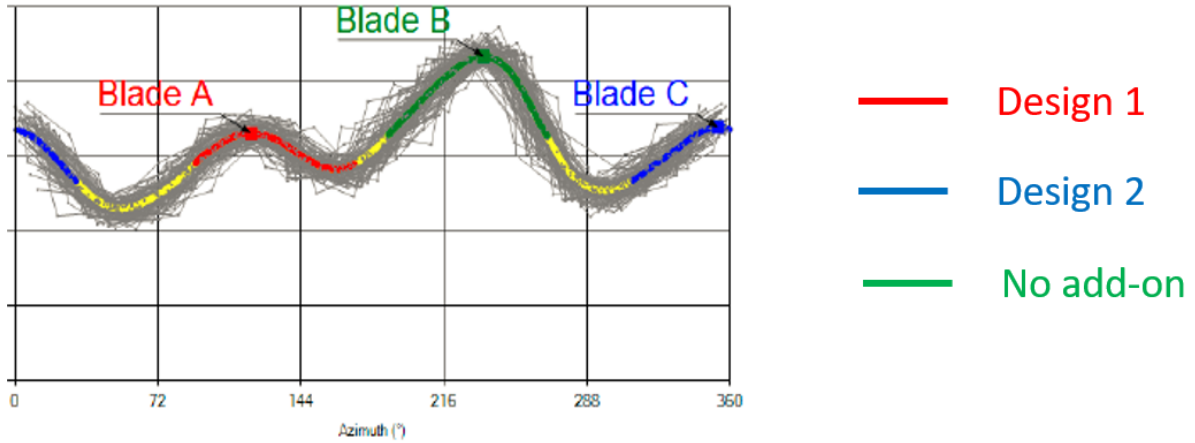


Figure: sound pressure / noise level at different blade position angles at 8.6m/s of wind speed

Moreover, similar behaviour is observed independent of the wind speed. Both designs decrease the noise level considerably and similarly as compared to the blade without any add-on, as can be observed in the figure below.

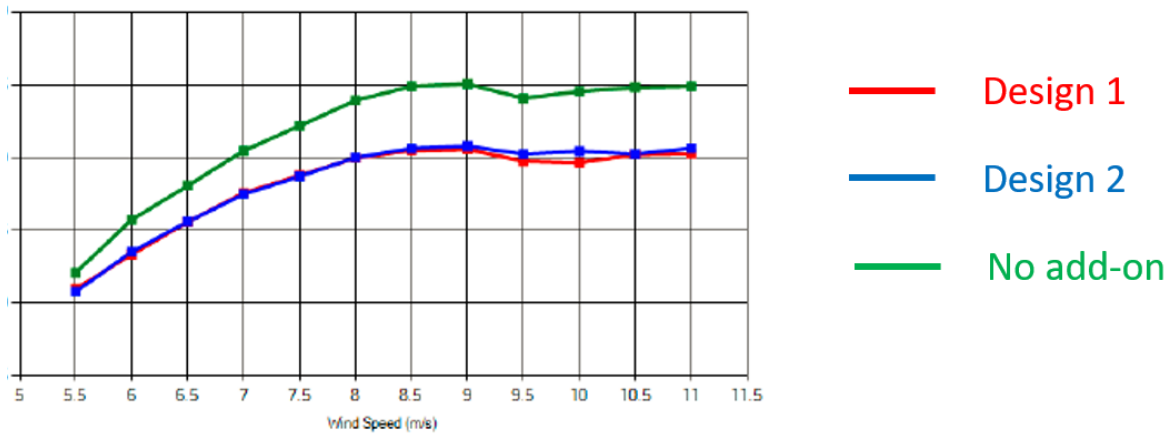


Figure: sound pressure / noise level at different wind speeds

## 7 Work Package 7 – Dissemination and exploitation

### 7.1 Kick-off seminar

Leader: DIS

The kick-off seminar was held the 1<sup>st</sup> and 2<sup>nd</sup> of February 2017 in Denmark. The event was held at DIS in Stilling on the first day and the second day was hosted by Total Wind in Brande.

Attendance from all project partners in person and via Skype.

The first day focused on the communication plan, work package and the consortium agreement. The second day focused on the different technologies.

### 7.2 Mid-term Seminar and Report

Leader: DIS

The mid-term seminar was held at the CEU facility in Valencia, Spain on 14<sup>th</sup> March 2018. This was held to coincide with the next General Assembly held the following day in March 2018.

A summary video from the mid-term event can be seen using the link below, and the presentations from the day will be made available on the project website.

**Project Website:**

<http://odb-project.com/>

**Summary Video:**

[https://www.youtube.com/watch?v=VZ7\\_biPg5ww&feature=youtu.be](https://www.youtube.com/watch?v=VZ7_biPg5ww&feature=youtu.be)

### 7.3 Final Dissemination Event

Leader: DIS

The Final Dissemination Event was held by ORE Catapult in London, United Kingdom on 18<sup>th</sup> June 2019. This was held to coincide with the next General Assembly held the following day in June 2019.

This final report is the summary of what was presented in London.

### 7.4 Closing and final reporting to national funding bodies

Leader: DIS

This will be delivered at the close of the ODB Project on request by the relevant funding bodies.